Graduate School ETD Form 9
(Revised 12/07)

PURDUE UNIVERSITY
GRADUATE SCHOOL
Thesis/Dissertation Acceptance

This is to certify that the thesis/dissertation prepared

By Kevin Alton Mauser

Entitled
A Digitally Invertible Universal Amplifier for Recording and Processing of Bioelectric Signals

For the degree of Master of Science in Biomedical Engineering

Is approved by the final examining committee:

Ken Yoshida
Chair

Edward Berbari

Paul Salama

To the best of my knowledge and as understood by the student in the *Research Integrity and Copyright Disclaimer (Graduate School Form 20)*, this thesis/dissertation adheres to the provisions of Purdue University's "Policy on Integrity in Research" and the use of copyrighted material.

Approved by Major Professor(s): Ken Yoshida

Approved by: Edward Berbari 11/21/2012
Head of the Graduate Program Date

Graduate School Form 20
(Revised 9/10)

PURDUE UNIVERSITY
GRADUATE SCHOOL

Research Integrity and Copyright Disclaimer

Title of Thesis/Dissertation:

A Digitally Invertible Universal Amplifier for Recording and Processing of Bioelectric Signals

For the degree of Master of Science in Biomedical Engineering

I certify that in the preparation of this thesis, I have observed the provisions of *Purdue University Executive Memorandum No. C-22,* September 6, 1991, *Policy on Integrity in Research.**

Further, I certify that this work is free of plagiarism and all materials appearing in this thesis/dissertation have been properly quoted and attributed.

I certify that all copyrighted material incorporated into this thesis/dissertation is in compliance with the United States' copyright law and that I have received written permission from the copyright owners for my use of their work, which is beyond the scope of the law. I agree to indemnify and save harmless Purdue University from any and all claims that may be asserted or that may arise from any copyright violation.

Kevin Alton Mauser

Printed Name and Signature of Candidate

12/4/2012

Date (month/day/year)

*Located at http://www.purdue.edu/policies/pages/teach_res_outreach/c_22.html

A DIGITALLY INVERTIBLE UNIVERSAL AMPLIFIER FOR RECORDING AND PROCESSING OF BIOELECTRIC SIGNALS

A Thesis

Submitted to the Faculty

of

Purdue University

by

Kevin Alton Mauser

In Partial Fulfillment of the

Requirements for the Degree

of

Master of Science in Biomedical Engineering

December 2012

Purdue University

Indianapolis, Indiana

In all your ways acknowledge Him and He shall direct your paths.

–Proverbs 3:6

ACKNOWLEDGMENTS

I would like to first acknowledge, thank, and give praise to Jesus Christ, my LORD and Savior, for giving me the physical and emotional strength, mental ability, perseverance, and commitment to be able to start and complete this research.

Next, I would like to acknowledge and thank my thesis advisor, Dr. Ken Yoshida, for welcoming me into his lab family and giving me the great experience of working in the area of bioinstrumention and neuro-stimulation and recording. Through this opportunity and this research he has deepened my love of biomedical engineering, especially in his area of research, and both broadened and strengthened many of my skills as an engineer and scientist. I would also like to express my sincere gratitude to him for his steady patience, insights, assistance, and guidance during the prolonged work and writing of this thesis.

With working as a teaching assistant initially and then working full-time later on while working on this thesis I could not have maintained my sanity without the love, care, and support of my wife, Bethany. I am grateful for her presence in my life, love her with all my heart, and hope that the LORD blesses us with life together until we are old and gray.

I am grateful for my parents, siblings, and extended family for being supportive, encouraging, and being understanding of my situation during this time. I would also like to thank the people at church for the various encouragements and prayers during this time.

I would like to thank my other advisory committee members, Dr. Edward Berbari and Dr. Paul Salama, for their time and attention during the completion and defense of this work.

TABLE OF CONTENTS

Page

LIST OF FIGURES

Figure Page

Figure Page

ABSTRACT

Mauser, Kevin A. M.S.B.M.E., Purdue University, December 2012. A Digitally Invertible Universal Amplifier for Recording and Processing of Bioelectric Signals. Major Professor: Ken Yoshida.

The recording and processing of bioelectric signals over the decades has led to the development of many different types of analog filtering and amplification techniques. Meanwhile, there have also been many advancements in the realm of digital signal processing that allow for more powerful analysis of these collected signals. The issues with present acquisition schemes are that (1) they introduce irreversible distortion to the signals and may ultimately hinder analyses that rely on the unique morphological differences between bioelectric signal events and (2) they do not allow the collection of frequencies in the signal from direct-current (DC) to high-frequencies. The project put forth aims to overcome these two issues and present a new scheme for bioelectric signal acquisition and processing.

In this thesis, a system has been developed, verified, and validated with experimental data to demonstrate the ability to build an invertible universal amplifier and digital restoration scheme. The thesis is primarily divided into four sections which focus on (1) the introduction and background information, (2) theory and development, (3) verification implementation and testing, and (4) validation implementation and testing.

The introduction and background provides pertinent information regarding bioelectric signals and recording practices for bioelectric signals. It also begins to address some of the issues with the classical and present methods for data acquisition and make the case for why an invertible universal amplifier would be better. The universal amplifier transfer function and architecture are discussed and presented along with the development and optimization of the characterization and the inversion, or restoration, filter process. The developed universal amplifier, referred to as the invertible universal amplifier (IUA), while the universal

amplifier and the digital restoration scheme together are referred to as the IUA system. The IUA system is then verified on the bench using typical square, sine, and triangle waveforms with varying offsets and the results are presented and discussed. The validation is done with in-vivo experiments showing that the IUA system may be used to acquire and process bioelectric signals with percent error less than to 6% when post-processed using estimated characteristics of and when compared to a standard flat bandwidth high-pass cutoff amplifier.

1. INTRODUCTION

1.1 Problem Statement

Bioelectric signal recording and processing rely on classical techniques for analog filtering, amplification, and digital signal processing techniques. These analog and digital techniques are often thought of as separate domains but the quality or successfulness of any digital signal processing is in some ways dependent on the quality of the signal that has been filtered with the analog amplifier. Thus, they are irrefutably linked. Moreover, analog filtering amplifiers are designed to intentionally attenuate and distort the signal in an attempt to eliminate noise and create a window around the frequency content of the desired signal in order to improve the starting point for the digital signal processing; however, this approach can cause two problems:

First, the attenuation and distortion by analog filtering amplifiers creates a problem for high-resolution recordings or for neural spike separation. High-resolution recordings are typically event-triggered averaged to negate random events in the signal, but high frequency components of the signal may be forever lost due to the low-pass filtering options applied. Neural spike separation today relies on the ability to collect large numbers of neural spikes with the idea that with a large database some spikes may be distinguished based on differences between them. Often the techniques involved in the separation that are discussed in the literature are correlation-based. However, such correlation-based approaches may be ignoring more minute morphological differences. Yet even if better processes were applied, these differences are still masked by any analog filtering applied prior to acquisition.

Second, due to the understanding of the frequency characteristics of the signals coming from the human body the common practice is to create different filtering amplifier setups for each type of signal. Due to this numerous different styles of analog filtering amplifiers have been created in order to capture specific signals. Attempting to collect a different signal

requires the selection and the use of a different set of analog filtering and amplification parameters. Although integrated circuits have lowered the time and cost associated with creating these amplifiers in large numbers, having to make numerous different ones can be tedious or purchasing them separately or in small quantities can still be costly.

1.2 Objectives

The objectives or aims of this thesis are to develop a method to (Aim 1) design and implement a new high-impedance input, low-noise, low-bias current amplifier that provides an invertible universal amplifier for bioelectric recordings with appropriate bioelectric-oriented analog filtering that is easily and accurately estimated and inverted through digital processing, and (Aim 2) leverage the power of digital signal processing to invert the amplifier transfer function and restore the recorded signal to an accurate representation of the original signal, which may then be digitally processed in ways that minimize distortion of morphological characteristics. Together these two objectives will overcome the two problems identified. These objectives are achieved throughout the course of this work by successfully designing and implementing an analog filtering amplifier that relies on digital signal processing to restore the recorded signal.

1.3 About This Thesis

In order to achieve both aims of this thesis a system has to be created that works both in the analog and digital domains. The system is thus comprised of two different components that together are called the invertible universal amplifier (IUA) system. The component that operates in the analog domain is the amplifier and is referred to as an invertible universal amplifier. The component that operates in the digital domain is a computer script that digitally inverts the IUA. To fully appreciate the usefulness of the IUA system, a general understanding of bioelectic signals and current signal filtering and processing techniques is important. Chapter 2 will present background information that has been the foundation for bioelectric recording and signal processing for decades. Chapter 2 will further discuss the

need for the invertible universal amplifier. From there Chapter 3 will lay the ground work for the invertible universal amplifier and digital signal processing integration and make the case for the IUA system. Chapter 4 will focus on the analog amplification scheme, introduce the criteria for ensuring the amplifier is digitally invertible, and discuss the theory used to create the Matlab program to restore the signal. Chapter 5 will discuss the realization and demonstration of the IUA and digital restoration scheme. Chapter 6 will discuss design and implementation considerations and issues associated with the new system. Chapter 7 will compare the restored input estimate produced with the IUA system to the original input of arbitrary square, sine, and triangle waves to the IUA to evaluate usefulness and success of the IUA system. Chapter 8 will present an in-vivo demonstration and comparison of the IUA system compared to a custom built low-noise headstage amplifier with a high-pass cutoff and constant gain. Lastly, the thesis will be brought to an end with a summary of the work, the key results, and final conclusions. The appendices include code used during this work.

2. BACKGROUND OF BIOELECTRIC POTENTIALS AND RECORDING TECHNIQUES

This section provides background on the origin of the bioelectric potentials, describes how they are picked up using electrodes, presents the justification and necessity for filtering and amplification, characteristics of bioelectric amplifiers, and discusses the issue of capturing noise while attempting to picking up the bioelectric phenomenon. These are all important concepts to understand and will help lead into the further development and discussion of the IUA system.

2.1 Origins of the Bioelectric Potential

The primary target of any bioelectric recording is the bioelectric potential. Ionic and chemical signaling mechanisms are the basis upon which the body creates these bioelectric biopotentials, which propagate and transmit information across electrically active tissues and between different locales. These mechanisms involve ionic gradients and voltage-gated sodium and potassium ion channels in different tissue in the body in order to portray information to different locations or tissues. This information is first portrayed at the cellular level when changes in transmembrane potentials of the cell lead to the opening of sodium and potassium channels letting ions into and out of the cell along their gradients.

The gradients are created because the concentration of sodium outside the cell is nearly 10 times higher, specifically 145 mM : 15 mM ([out] : [in]), whereas the concentration of potassium inside the cell is nearly 27 times higher, specifically 120 mM : 4.5 mM ([in] : [out]). This leads to a standing transmembrane biopotential that can be momentarily discharged to transmit information from one part of the cell to another. The momentary discharge is manifested locally through the opening of voltage-gated ion-selective chan-

nels. So as the channels open the ions move down their concentration gradients, which is sodium into the cell and potassium out of the cell. Specifically, once the transmembrane potential is raised from -90 mV to about -70 mV due to a depolarizing stimulus, the sodium ion channels are activated and begin to let sodium ions into the cell. This cause the transmembrane potential to become less negative and rapidly depolarizes the cell. As the cell depolarizes the potassium ion channels are activated and begin to release potassium ions into the interstitial space which slows the depolarization. As the depolarization slows down, the sodium ion channels close causing the depolarization to reverse since the potassium ion channels are still open and are releasing potassium ions. As the transmembrane potential returns to -90 mV, the potassium ion channels gradually close causing the resting potential to be achieved. While at rest the sodium-potassium pump actively restores the gradients for the next activation [1].

2.2 Bioelectric Potentials in Different Anatomy

When the behavior discussed so far occurs on a cell-to-cell basis it results in the propagation of what is know as the action potential. In an ideal measurement condition the amplitude of the cell action potential is up to 100 mV and it lasts for approximately 1 ms. Building from the cellular level, this behavior go on to have different effects in different anatomy [1].

To discuss the bioelectric potentials in different anatomy, the first anatomical structure selected is the nerve. Along the length of an unmyelinated nerve axon there are sodium and potassium ion channels. An unmyelinated nerve is a nerve that is not wrapped with Schwann cells and is not insulated. In the case of a myelinated axon, the action potential appears only at the nodes of Ranvier where the sodium and potassium ion channels are located in a method known as saltatory conduction. Saltatory conduction is when the action potential conducts from one node to the next because of the insulating myelin sheath between the nodes. There is extensive literature on these events and the understanding of

the axon that goes beyond the scope of this thesis; however, greater detail of these events may be found by first reviewing the Hodgkin-Huxley model and associated theory [2].

In a similar fashion to the nerve axon, the muscle fiber has a transmembrane potential of approximately -80 mV while at rest. Upon chemical activation of acetylcholine-activated channels in the neuromuscular synpase the muscle fiber transmembrane potential drops briefly and activates the voltage-gated sodium ion channels. The sarcolemma, the muscle cell membrane, will depolarize as the sodium ions enter. The sodium ion channels begin to close due to the breakdown of the acetylocholine. Once at this depolarized state, repolarization of the cell primarily occurs when potassium ion channels open and let potassium ion channels out of the cell. Continued repolarization returns the fiber to the resting transmembrane potential such that all the ion channels are closed. The action potential that is created from these events propagates across the muscle fiber and downward into the transverse tublar system leading to the release of calcium, which is necessary for the contraction of the muscle fibers [3].

Other muscle cells such as cardiac cells, specifically Purkinje fibers and pacemaker cells, participating in cardiac rhythm rely on sodium, potassium, and calcium ion characteristics in ways similar to the nerve or muscle fiber. However, they also have gap junctions that allow for instantaneous conduction resulting in synchronous activity [4, 5]. By reviewing the anatomy of excitable tissue and how these different anatomy produces the action potential it is clear that the dynamics of all these different types of cell are dominated by primarily the sodium ion and potassium ion channels.

2.3 The Extracellular Action Potential

When these physiologic mechanisms producing the action potential in the body are measured, observed, or monitored through the use of electrodes and acquisition equipment they are represented to us by various waveforms, which are generically called bioelectric signals. As these bioelectric signals first started to be observed they were classified by the tissue that originates the signal. Typically, these bioelectric signals have been classified

as electrocardiograms (ECG), electroencephalograms (EEG), electromyograms (EMG), or electronuerograms (ENG) depending on their point of origin. Each bioelectric signal has been recorded and studied over the years and is understood to have various frequency content, amplitudes, and durations.

2.3.1 The ECG

The ECG originates from heart. The ECG has frequency content that covers a wide range. The ECG is comprised of three main waveforms: the P-wave, the QRS complex, and the T-wave. The P- and T-wave are comprised of lower frequency content in the tens of Hertz (Hz) while the QRS complex is a higher-frequency event that is centered near 150 Hz. Additionally, the amplitude of the QRS is on the order of several millivolts (mV) and is larger than that of the P- or T-wave [1, 3].

2.3.2 The ENG

The origin of the ENG is from nerve axons in the peripheral body. ENG signals usually have a maximum amplitude of several microvolts and the duration is approximately 1 ms but can vary widely. Its short duration seems to coincide with its high frequency content, which ranges from a upper hundreds of Hertz to tens of kiloHertz (kHz) [2, 3].

2.3.3 The EMG

The origin of the EMG signals are from muscle fibers in the body. The EMG recorded during muscle contraction spans a frequency range of 10 Hz to 2 kHz and vary in amplitude depending on their recording location but can range from a few microvolts (V) to a few millivolts [3].

2.3.4 The EEG

The origin of EEG signals is from neurons inside the central nervous system. EEG signals generally contain low frequency information, ranging from 0.2 Hz to approximately 50 Hz and usually has a very small amplitude centered in the low microvolt range [1].

2.3.5 The EIP

Whenever an electrode is used to record the physiological mechanisms that produce the usual bioelectric signals another type of signal may result called an electrode-interface potential (EIP). While this is not typically thought of as a bioelectric signal the interface of the electrode and the surrounding tissue can cause this potential difference. This potential difference can be on the order of several millivolts to volts, which is significantly larger then other bioelectric signals and thus must be recognized [6].

2.4 Spectral Organization of Biolectric Signals and Noise

The frequency and duration characteristics of the five different types of extracellular bioelectric signals discussed could hinder the development of a filtering scheme suitable for use in recording any one of these signals with the invertible universal amplifier. Moreover, different noise sources, such as unwanted bioelectric signals as well as noise introduced by recording equipment might also present a challenge. To begin to assess the challenge, the first step is to look at the spectral organization of these bioelectric signals and at their relative magnitudes in order to gain better insight on how to go about developing an invertible universal amplifier. It is also important to understand the noise sources that the amplifier must filter out to ensure that the amplifier will be a useful tool in signal acquisition.

2.4.1 Spectral Organization of Bioelectric Signals

The five different bioelectric signals previously discussed are listed below in Table 2.1 along with their points of origin, their respective amplitude, frequency characteristics, and duration.

Table 2.1
Bioelectric signal, frequency and amplitude classifications [7]

Bioelectric Signal	**Point of Origin**	**Frequency Bandwidth (Hz)**	**Amplitude**	**Duration**
Electrointerface Potential (EIP)	Tissue-Electrode Interface	0 – 0.2 Hz	Low millivolts (mV) to volts (V)	Infinite
Electrocardiogram (ECG)	Heart	0.2 – 200 Hz	2 – 3 mV (QRS complex)	Up to 100 ms
Electroencephalogram (EEG)	Central Neurons	0.2 – 50 Hz	10 – 300 μV	5 – 10 ms
Electromyogram (EMG)	Muscles	10 Hz – 2 kHz	5 μV – 20 mV (surface); 50 – 1000 μV (invasive)	2 ms
Electroneuralgram (ENG)	Perhiperal Nerves	100 Hz – 10 kHz	Low microvolts μV	1 ms

Table 2.1 contains a wide variety of information pertaining to these bioelectric signals and as it can be difficult to fully appreciate the relationship between these signals when presented in purely a tabular form, the amplitude and frequency properties of bioelectric signals and of electrode potentials are displayed in Figure 2.1 for a visual representation of Table 2.1.

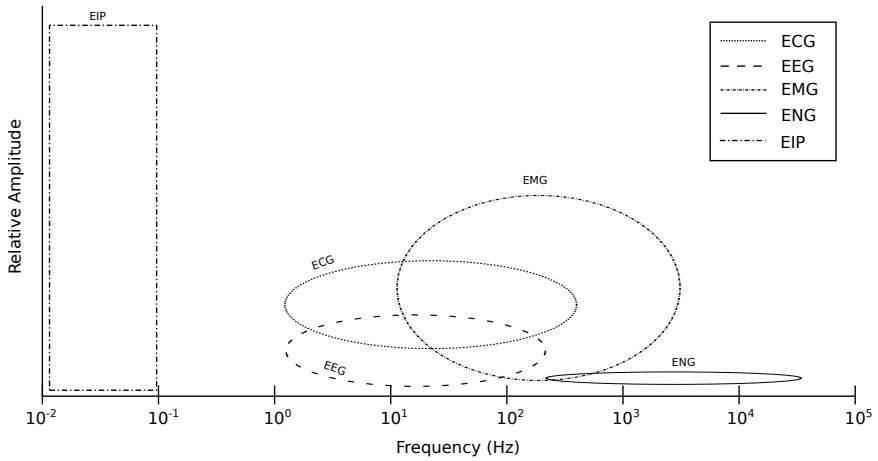

Figure 2.1. Visual representation of bioelectric amplitude-frequency relationships.

According to Figure 2.1 there are large areas of overlap of amplitude and frequency of the different bioelectric signals [7]. Due to these areas of overlap it might appear to be difficult to make a specific bioelectric recording and not also collect other bioelectric signals without the use of a specially tuned bioelectric filter. However, this illustration of the data does show that there is a trend in which the high-frequency signals tend to have lower amplitudes than the lower frequency signals. Such a trend is key to creating the invertible universal amplifier as the analog filtering amplifier in the IUA system.

2.4.2 Spectral Noise Considerations

In addition to dealing with the spectral distribution of the bioelectric signals, a universal amplifier would have to also deal with common noise sources, as would any good bioelectric amplifier, so it is important to consider them now. Unwanted bioelectric signals are often considered a type of noise source in bioelectric recordings and, as previously described, can vary widely in their spectral distribution. A more common noise source from the environment is 50 Hz or 60 Hz sine waves and their harmonic signals from power mains. These 50 Hz or 60 Hz sine wave noise sources are often much larger in amplitude than the bioelectric signals ranging from several millivolts to several volts and can completely mask bioelectric signals.

Another introducer of noise are high impedance electrodes. High impedance electrodes can introduce high frequency thermal noise into the recording. Thermal noise is the random movement of charged particles and is proportional to the resistance of the electrode. Thermal noise is often referred to as background noise. An additional source of background noise is the amplifier and filtering frontend that is used for the recordings. Since the filter frequency characteristics of an amplifier are set to match that of the desired signal any shot noise from the environment will be shaped by the filter and begin to take on characteristics of the signal. This makes it more difficult to separate signal and noise in the case of neural recordings where artifacts can be made to appear similar in shape to action potentials. This specifically, creates an issue with single unit identification and tracking in the case of an ENG recording [6]. This type of problem exemplifies that all of these potential sources of noise decrease the ability to distinguish or separate the desired signal from the noise.

2.5 The Signal-to-Noise Ratio (SNR)

The ability to separate the signal from the noise, or in other words the quality of the signal, is determined by a quantitative value called the signal-to-noise ratio (SNR). While there are different ways to determine the SNR such as comparing peak-to-peak amplitudes of the signal and noise, the best estimate is based on the standard deviations of the signal and noise and an understanding of the variances of the signal and noise. Under the statistical assumptions that the noise is stationary and is independent of the signal (i.e. uncorrelated) than the square of the variance of the signal plus noise is the sum of the independent squares of the variance of the signal and the variance of the noise such that:

$$\frac{\sigma^2_{signal+noise}}{\sigma^2_{noise}} = \frac{\sigma^2_{signal} + \sigma^2_{noise}}{\sigma^2_{noise}} = \frac{\sigma^2_{signal}}{\sigma^2_{noise}} + 1 \tag{2.1}$$

Thus, the SNR can be determined as follows:

$$SNR = \frac{\sigma_{rms,signal}}{\sigma_{rms,noise}} \approx \frac{\sigma_{signal}}{\sigma_{noise}} = \sqrt{\frac{\sigma^2_{signal} + \sigma^2_{noise}}{\sigma^2_{noise}}} - 1 \tag{2.2}$$

The only thing piece of information lacking after a bioelectric recording is σ^2_{noise}. Yet, it is possible to get an estimate of σ^2_{noise} by recording during quiescence or in the absence of the driving stimuli. The largest error in this is that it may not be possible to obtain an recording of the noise that is absolutely free of any signal, in which case the noise will be overestimated and the SNR will be decreased [6].

2.6 Considerations for Analog to Digital Conversion and Acquisition

With the ability to determine and quantify the SNR it is often desired to increase the SNR as much as possible. There are several things to consider that may help improve the SNR when recording the signal and converting the signal from analog to digital. These methods involve making the right choices in terms of amplifier impedance matching and common-mode rejection, amplification, recording configurations, minimizing external sources of noise, and analog filtering techniques.

2.6.1 High Input Impedance and CMRR For Improved SNR

It is an advantage to use an amplifier that has a very high input impedance so that it will cause the thermal noise introduced into the signal by the amplifier to be insignificant compared to the thermal noise of the electrodes and it can also overcome issues with impedance mismatch between electrodes in differential recordings. These high input impedance amplifiers are often referred to as pre-amplifiers. The method of coupling a high-impedance pre-amplifier with high-impedance electrodes is known as impedance matching. This means that the pre-amplifiers are designed with high input impedance so that they can measure voltages (the control voltage) with theoretically no current being shorted by the device, similar to an ideal voltmeter. The need for this impedance matching relates back to the origin of the action potential and basic resistor-divider theory, the former of which is not detailed in this thesis: A very small flow of ionic current is being generated whenever the cell membrane is activated. The current flows from the inside of the cell, through the membrane, outside the cell and then returns.

These small currents that flow outside the cell, in conjunction with the low resistance extracellular space, allow for transmembrane potentials to be recorded as long as the recording device has an impedance much higher than the recording electrodes so that the voltage is not dropped across the electrodes and their leads and so that the amplifier itself does not allow a current leak which would short out the small current. Such high-impedance amplifiers that meet these requirements are low-noise, low-bias current, field-effect transistor (FET) based on differential or instrumentation op-amp configurations. They require an ultra low-bias current in the picoamperes to bias the transistors in the operational amplifiers which leads to a very small output-error of the amplifier. These amplifier configurations are generally used close to the recording site with minimal recording leads in order to quickly amplify the signal before more noise can be introduced into the recording chain from external sources [6]. The SNR can be improved by using one of these high input impedance amplifiers that also has a good common-mode rejection ratio (CMRR). CMRR is the amplifiers ability to reject signals that are common on both of its inputs [8].

2.6.2 Amplification Considerations

The amplification step provided by the amplifier in the recording chain is very important for two reasons. The first is that the small transmembrane current previously discussed is very small in magnitude and the extracellular space has a very low resistance, which means that only a small potential will be detected by the electrodes. This small signal is ideally amplified before additional noise sources enter the recording chain. Secondly, the amplification of these small transmembrane potentials is also important because the act of data acquisition imposes an error in the recorded signal known as the quantization error due to the limits of its detection resolution. This quantization error is calculated as one-half the bit weight of the analog-to-digital converter (ADC). The bit weight, or the least significant bit (LSB), of the ADC is calculated as its full scale voltage divided by resolution:

$$LSB = \frac{FSV}{2^n} \tag{2.3}$$

The quantization error is then $\pm\frac{1}{2}LSB$ where LSB is found in the Equation 2.3 above [6].

2.6.3 External Noise Source Elimination

Additional methods of increasing the SNR involve minimizing external noise sources that could be introduced into the recording chain and corrupt the signal. One way of accomplishing this is to conduct recordings or place recording equipment in an isolated or shielded environment through the use of Faraday cage, which will shield the setup from external noise sources. Unfortunately, using a Faraday cage is impractical or ineffective in most recording cases as the recording equipment must be in the same space as the patient or subject and the equipment must connect to power outside the cage [9]. Other options involve ensuring that the setup is properly grounded, that there are no ground loops, and that recording equipment, leads, and cables are properly shielded. Good resouces for further discussions on eliminating external noise sources may be found in [9].

2.6.4 Electrode Configurations and Placement

The SNR is also dependent on where the recording electrodes are placed and how they are configured. Placing the recording electrode closer to or into the organ from which the bioelectric signals originate tend to increase the SNR when other appropriate recording practices previously discussed are followed. Examples of this is the difference between surface EMG recordings versus subcutaneous EMG recordings as well as nerve cuff extracellular recordings versus intrafascicular recordings, where the electrode is actually placed within the nerve fiber between the fascicles. Work by Qiao and Yoshida has demonstrated the difference in SNR that may be achieved by placing the recording electrode closer to the signals of interest [10] as may be seen in Figure 2.2 below. Figure 2.2 shows the signal-to-noise density of a cuff electrode (in green) and a longitudinal intrafascicular flat electrode (LIFE) (in blue) developed by Yoshida and Stein [6, 11].

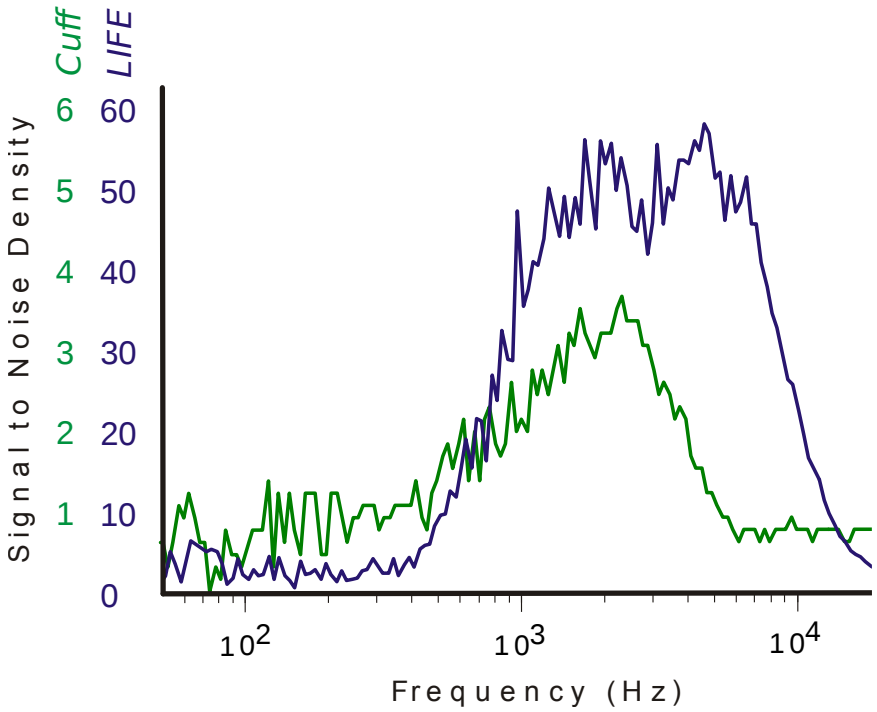

Figure 2.2. SNR difference between the cuff electrode (green) and LIFE (blue) are shown to be nearly an order of magnitude apart. Permission to reproduced requested [6].

Figure 2.2 shows that placing the recording electrode into the nerve fiber increased the SNR two to three times higher than when a nerve cuff electrode was used. These results are also dependent on more advance recording configurations other than monopolar or single active recording electrode. These configurations are differential recording configurations such as bipolar or tripolar setups [12].

As the names of the recording configurations suggest the setups involve two active recording electrodes in the bipolar case and three active recording electrodes in the tripolar case. In an example of neural recordings, the cases of bipolar and tripolar setups are presented below in Figure 2.3. The advantage of these setups is that the electrodes are in the same environment and can record the same noise, which when coupled with a pre-amplifier with high input impedance and high CMRR result in good noise cancellation and increased SNR.

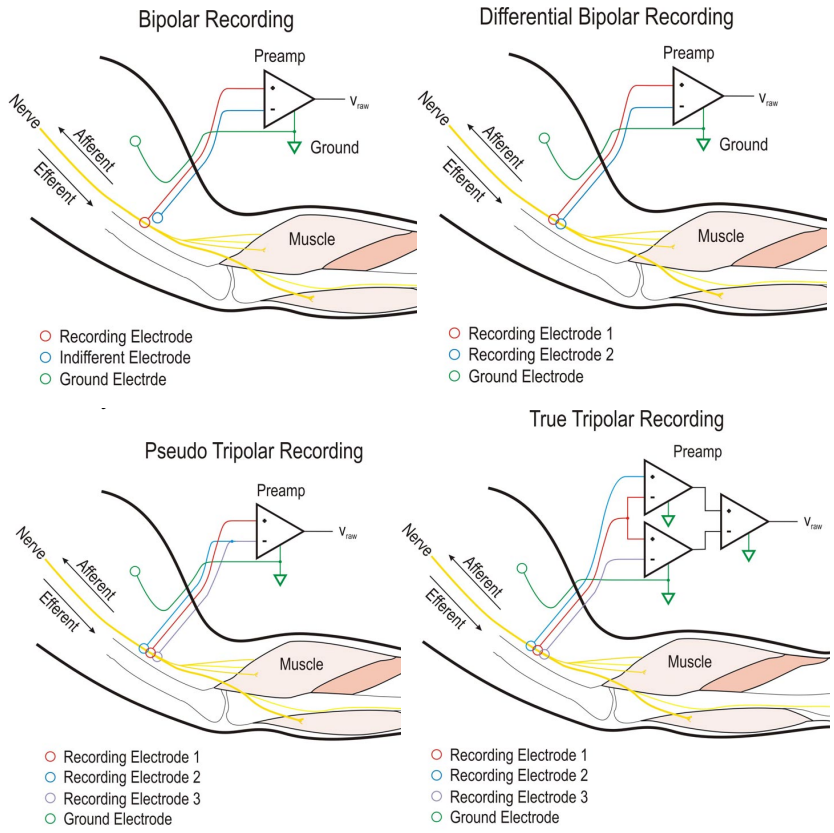

Figure 2.3. Bipolar, differential, and tripolar recording configurations for improving SNR. Permission to reproduced requested [6].

2.6.5 Filtering

Despite doing all the things mentioned previously, it might still be difficult to completely cancel out noise sources and amplify the signal more than the noise. Thus, perhaps the last method for improving the SNR before acquisition is to introduce analog filtering prior to acquisition of the signal to restrict the bandwidth of the signal to a specific region in order to block noise sources from being acquired. Digital filtering may also be implemented to improve the SNR after acquisition. Classical filtering methods such as implementing low-pass and high-pass filters, either separately or in combination, allow for reducing high frequency signals and DC to low-frequency content, respectively. Other filters such as bandpass or bandstop filters may be helpful in creating a window around a specific frequency range or to knock out a specific frequency range, respectively. The literature on filtering methods is extensive and is beyond the scope of this thesis. Ideally, the filtering would not alter the signal and thus the SNR would increase with the correct choice of filtering applied. However, it is important to select the right parameters for the filter such as filter order and cutoff frequencies. Yoshida demonstrates the effect of various filtering techniques on neural recordings in Figure 2.4 [6].

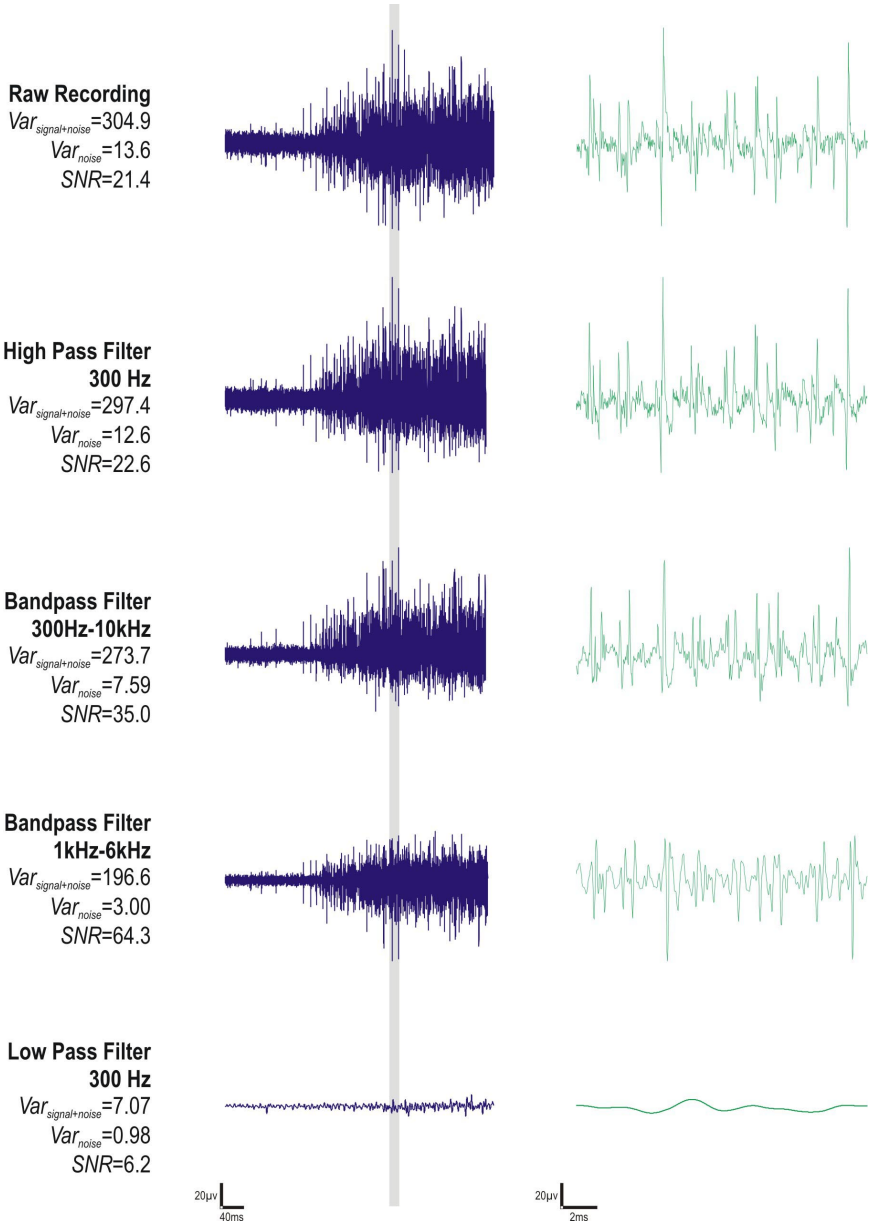

Figure 2.4. Effect on bioelectric signal from different filtering methods resulting in signal distortion and signal loss. Permission to reproduced requested [6].

In Figure 2.4 the effect of the filtering on the SNR can be seen. From the raw signal, through the progression of the different filters, and down till the low-pass filter the SNR increases with the different filtering options. However, as the SNR increases the amplitude of the neural spike begins to decrease and the shape of the spike also begins to be altered. Thus, choosing the right filtering parameters can be a delicate process and if done in analog prior to acquisition it must be done properly as not to permanently distort the signal. Restricting the bandwidth of the amplifier can cause distortion to signals of interest due to the overlapping frequency spectrum of signal and noise shown in Figure 2.1. The reality of distorting a signal when applying filters is widely discussed in the literature. Bioelectric signals such as ECG can suffer distortion that is higher than 8% in signal duration when filtering is applied. This distortion can affect the detection and estimation of morphological parameters [13]. For example, the shapes of neuronal action potentials become distorted and their uniqueness in terms of amplitude, duration, and waveform shape may be lost by using amplifiers that heavily filtering and optimizing the signal in order to eliminate noise and improve SNR [6]. This behavior was demonstrated by Qiao et al in [14] by showing how the effect of different types of filtering changed the shape of the nerve action potential. In this work, the raw signal was only filtered with a 0.1 Hz high-pass filter during acquisition and so the high frequency neural action potentials are not affected by the filter when recorded. The effects of post-acquisition filtering are shown in Figure 2.5 below and show distortion on the signal. Although in the examples shown below the signal was digitally processed after acquisition the results of the Butterworth filters would be applicable to the effect of an analog filter prior to acquisition. The Butterworth filters cause the spike to be distorted where the initial peak is decreased in amplitude and the end of the action potential overshoots the baseline significantly. Unfortunately, an analog filter would have similar effects [14].

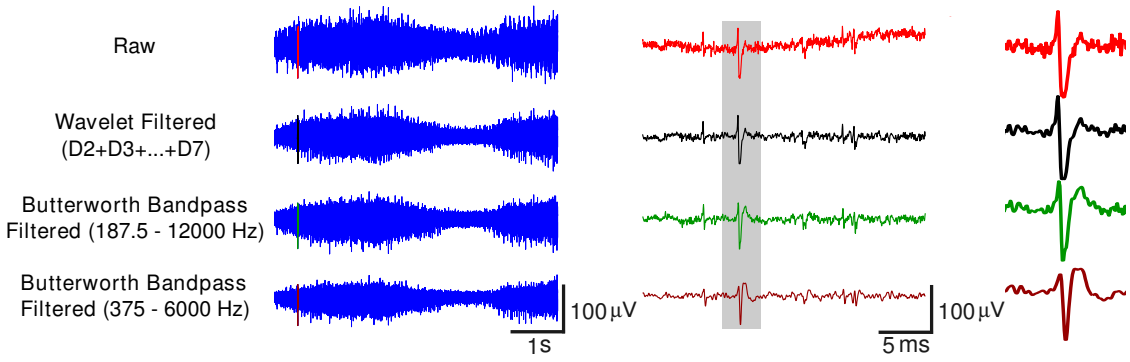

Figure 2.5. Effects of different filtering on neural action potentials. Reproduced with permission [14].

In the case of the wavelet filtered signal shown above, there appears to be very little distortion between it and the raw action potential, yet there is noticeable denoising achieved. This presents an interesting concept: if there were a way, in conjunction to the methods for increasing the SNR, to minimize any distortion of desired signal while yet capturing frequency content from DC to high-frequencies then "high powered" digital signal processing could be applied to "original" signals to denoise, separate-out desired signals, and open new analysis avenues and ways of improving the SNR.

2.7 The Usefulness of Recording from DC to High Frequencies

The concept presented above involved capturing frequency content of a signal from DC to high-frequencies but often the DC information is neglected in most bioelectric recordings. This has to do with amplification and saturation concerns pertaining to the recording equipment, which will be discussed in more detail in the next chapter. However, this section is to provide some background as to why keeping the DC information of the signal is important before moving into the next chapter. There are several applications that the DC information of the signal is used for as noted in [15–18]. It is also theorized that the DC information can be used to understand the "health" of an implanted electrode and the

immune response by monitoring the DC potential at the tissue-electrode interface. These applications are sufficient reasons to want to record the DC information along with the higher frequencies of bioelectric recordings so that the maximum amount of information may be retained and utilized for analysis and digital processing.

3. THE CASE FOR THE INVERTIBLE UNIVERSAL AMPLIFIER

Since previous work such as [14, 19–21] have shown the possibility of utilizing advanced digital signal processing to improve the ability to reduce noise and preserve the desired signal it is vitally important to design an analog frontend for this new recording scheme that can do appropriate amplification and filtering for each frequency spectrum so that the morphological characteristics may be preserved for the digital processing. The amplification and filtering must also be done in such a way that the limits of the acquisition hardware are respected, that the filtering allows for minimized, reversible distortion effects in order to preserve the morphological characteristics of the signal, and that the frequency components of the signal from DC to high frequencies may be captured by the amplifier. These topics will be discussed during this chapter and will lead into the discussion of how to develop an analog filtering amplifier that will help realize these requirements of the invertible universal amplifier.

3.1 Amplification and Filtering Working Together

While discussing methods for increasing the SNR in Chapter 2, it was mentioned that small bioelectric signals should be amplified with respect to the noise sources that may exist in the body, the surrounding environment, or the recording systems and filtered in order to improve the SNR. Amplification should be done to bring them into the dynamic range of the recording system and overcome the intrinsic noise of the recording device in order for adequate sampling and digital representation. Recording systems usually allow an acquisition of signals that range from ±10 volts with a resolution that is dependent on the voltage range and number of bits as expressed in Equation 2.3. This means that the amplification applied to the detected signals must appropriately consider the maximum and/or minimum amplitude of the signal as well as the dynamic range of the amplifier,

assuming that the signal is not to exceed the dynamic range of the amplifier. Amplification without appropriate filtering presents a particular challenge if the signal has an offset DC voltage or other low-frequency signals. If the signal at the electrode has an offset of a few hundred millivolts and is amplified, for example, with 1000x amplification without any high-pass filtering that removes this offset then the signal will saturate the amplifier and all signal information is lost since. For instance, 100 mV times 1000 equals an offset of 100 V, which well outside the rails of the amplifier as well as the dynamic range of the acquisition equipment. Despite the potential issues with this type of amplification and acquisition scheme with no filtering it may be used in limited cases where offsets caused by DC component or low-frequency signals are not an issue. This type of setup is shown in the first branch in Figure 3.1, which shows an initial representation of what the signal with DC offset should look like at the electrodes and what it looks like after amplification without any sort of high pass filtering. The result is that the signal saturates either the amplifier or the data acquisition equipment and the recorded signal loses all resemblance of the original signal.

The issue with the DC component of the signal when using amplification prior to acquisition may be overcome by utilizing a dual pre-amplifier setup in which one branch amplifies the signal preceded by a high-pass filter that removes the DC component of the signal to prevent saturation of downstream main amplifiers and the recording system and to remove any unwanted low frequency noise [12, 22, 23]. Additional downstream main amplifier usually provides further amplification to the filtered signal to ensure that the signal is within the dynamic range of the recording system. However, now that part of the signal is being removed by the high pass filter the other branch is needed to retain the low frequency/DC information. The second low-gain amplifier chain is used along with a low-pass filter to condition this spectrum of the signal for acquisition without amplifier or recording system saturation. This type of setup is shown in the second branch in Figure 3.1. The separate branches, when later recombined through digital processing, allow the collection of the wide bandwidth (i.e. DC to high frequency) components of the signal without saturating the amplifier(s) or the data acquisition equipment and recreate an amplified rep-

resentation of the original signal. The problem with this type of setup is that it effectively doubles the number of needed amplifiers and acquisition channels. This poses limitations due to manufacturing costs and size restrictions in the case where the pre-amplifier and frontend filtering need to be designed in a small package for use in implants. It can also pose limitations even for non-implant use in the same respect when the number of channels becomes large.

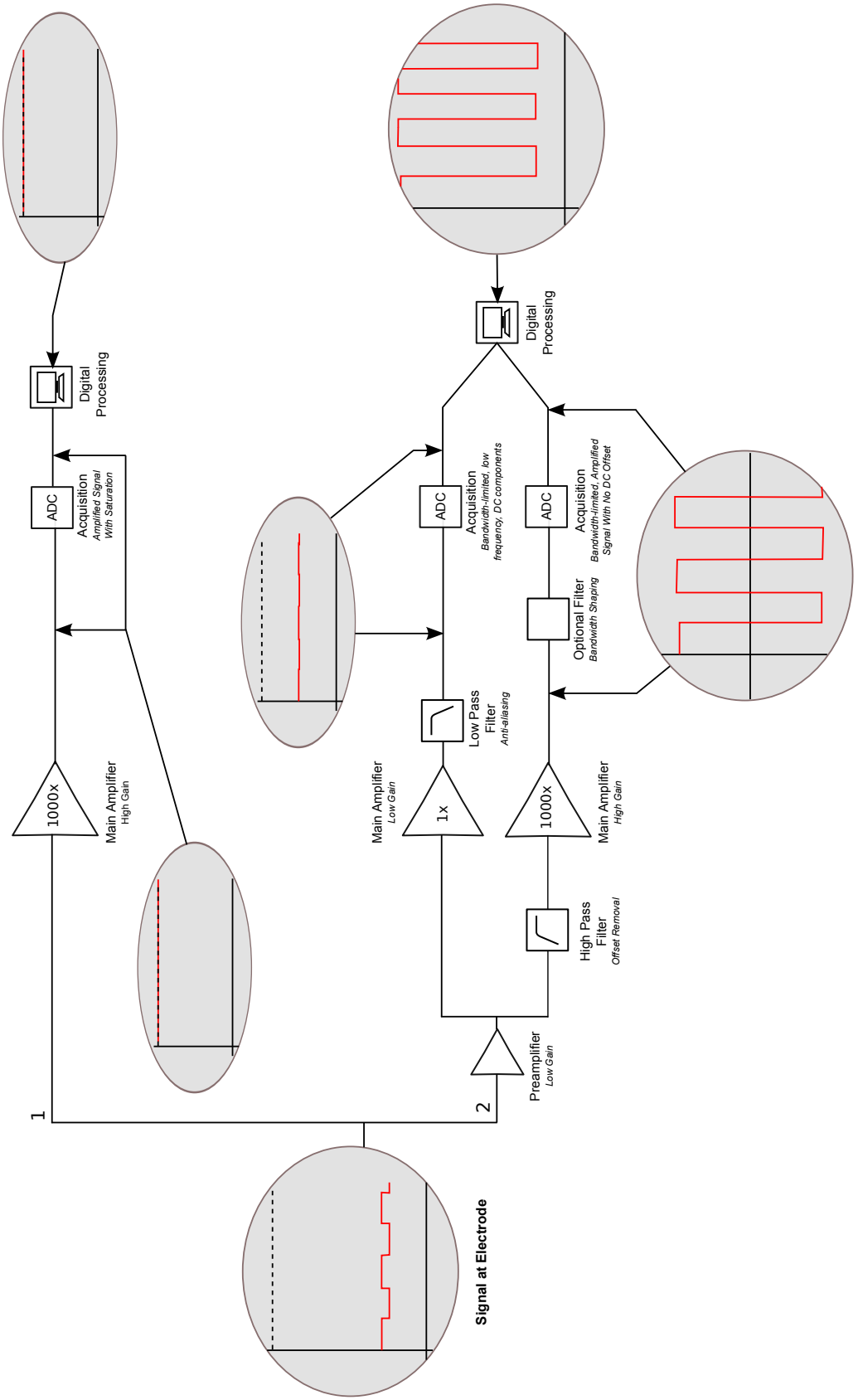

Figure 3.1. Classical amplification and filtering schemes and corresponding results.

3.2 Effects on Signal Fidelity

When it comes to the issue of preserving signal information and morphology, the recording technology, techniques, and analyses must go beyond the methods for improving the SNR previously presented such as optimal electrode placement, noise minimization techniques, and the use of the best available amplification and filtering scheme. The reason for this is that computational modeling and in-vivo verification has been completed that shows recorded bioelectric signals are effected by the electrode-signal source relationships. For example, the single fiber action potential from the nerve axon is affected by both the electrode-fiber distance as well as the conduction velocity of the single fiber action potential. This affect is not only seen in the time domain but is also seen in the frequency domain. Thus, in the time domain high-frequency information is attenuated due to a low-pass filter effect generated by increasing electrode-fiber distance and in the frequency domain the frequency bandwidth shifts downward with decreasing conduction velocity. These effects are caused by the interplay of the conduction velocity of the action potential and the electrode-fiber distance. The distance relationship and the conduction velocity confound changes in the recorded action potential [10].

In addition, Sevcencu et al in [24] showed that focal extracellular potential (FEP) recordings closely reproduced the shape of the transmembrane action potential from the same cell and that the FEP may be used as a descriptor of the transmembrane action potential. The FEPs are recorded through a pipette that is attached to the cell by suction and so there is minimal distance between the recording site and the transmembrane action potential. However, even with this minimal distance, there were still morphological differences between the transmembrane action potential and the FEP. In other words, the FEPs did not always perfectly match the simultaneously recorded transmembrane action potential. Thus, as these examples show, when the detection, amplification, and processing of morphological characteristics of bioelectric signals such as EEG, EMG, ECG, or ENG is important and when the ability to detect minute morphological differences between similar-type signals is necessary then eliminating distortion is paramount.

The elimination of this distortion has previously been limited by (1) the ability to place the recording electrode as close to the sources as possible and (2) the amplifier, filtering, and acquisition (AFA) setup as described in Chapter 2. These limitations present particular challenges in the world of neural recording and stimulation. However, work by has been completed to minimize the first limitation with respect to neural recordings through the development of specialized electrodes such as the TIME, LIFE, and tfLIFE electrodes [11, 25–27]. Yet, trying to eliminate distortion through the AFA setup and identifying specific bioelectric events during digital signal processing has two contradictory requirements: (1) SNR must be maximized through amplification and tight bandpass filtering to enable detection of the signal while (2) identification of unique events requires retention of as much of the shape as possible by minimizing the bandpass filtering. These requirements are applicable for identifying and analyzing neural signals as well as for single unit EMG recordings and ECG analysis. However, these requirements are difficult to meet because they contradict one another.

In order to find a way to deal with both of these requirements as well as solve the issue of amplifier saturation due to DC saturation, permanent morphological distortion due to analog filtering, DC component loss due to high-pass filtering, and the amplifier count doubling due to separate low- and high-frequency acquisition it is critical to develop a system that (1) is designed according to classical bioelectric amplifier specifications as to improve the SNR, (2) allows the acquisition of wide-band signals (i.e. from DC to the tens of kilohertz) without saturating the amplifier or acquisition equipment and (3) allows preserving of bioelectric signal morphology. This thesis hypothesizes that an AFA setup to meet these three requirements can be accomplished with (Aim 1) the design and implementation of a new high-impedance input, low-noise, low-bias current amplifier that provides an invertible universal amplifier for bioelectric recordings with appropriate bioelectric-oriented analog filtering that is easily and accurately estimated and inverted through digital processing, and (Aim 2) by leveraging the power of digital signal processing to invert the amplifier transfer function and restore the recorded signal to an accurate representation of the original signal, which may then be digitally processed in ways that minimize distortion of morphological

characteristics. These two aims are displayed in the recording chain illustrated in Figure 3.2 below.

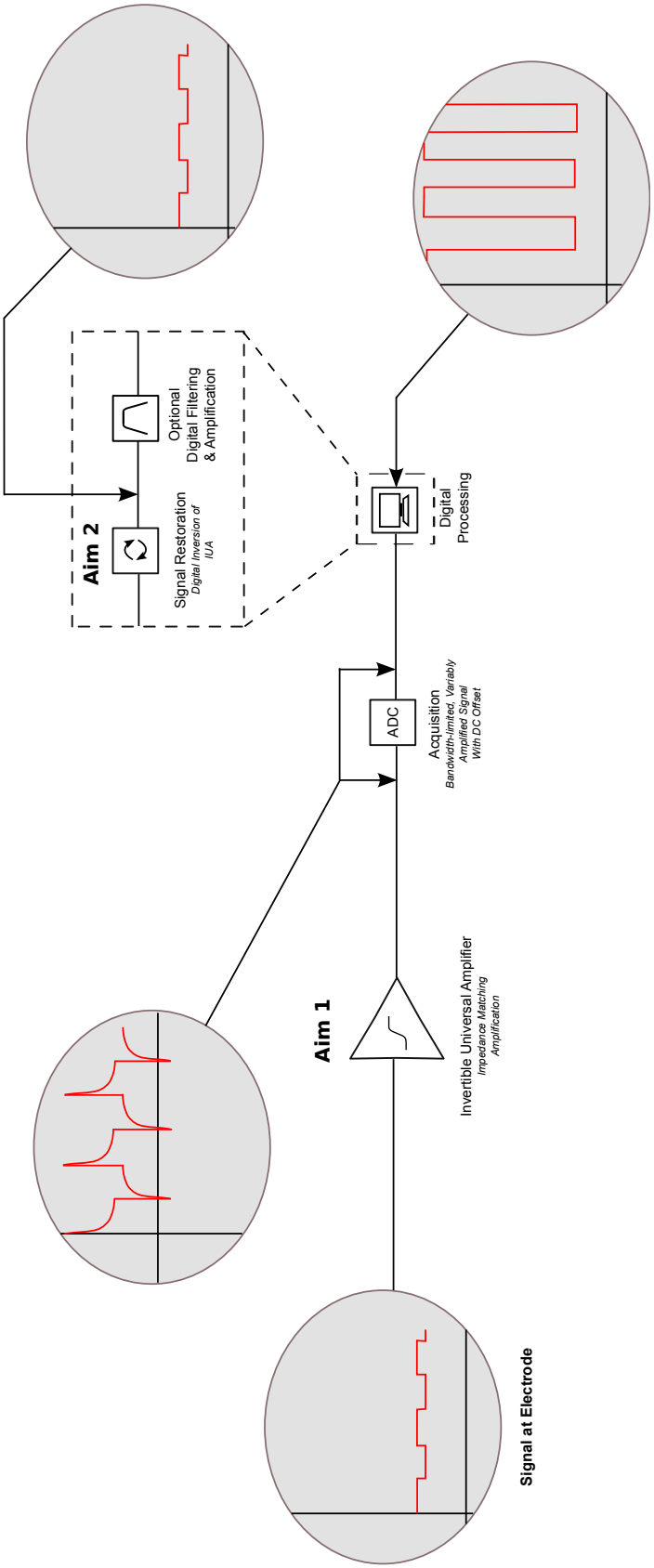

Figure 3.2. Invertible universal amplifier (IUA) system: Amplification and acquisition scheme using the IUA and digital restoration.

3.3 A New Approach: Variable Amplification, Digital Restoration

In order to implement the new method that provides the effects illustrated in Figure 3.2 and described previously, the invertible universal amplifier must take into account all the different frequency and amplitude relationships of bioelectric and electro-potentials as previously discussed. The invertible universal amplifier would need to amplify the various frequency ranges appropriately so that the signals were brought into the dynamic range of the recordings systems without saturation. While the EIPs have the largest magnitude in the bioelectric signal distribution, the relative amplitude tends to decrease as the frequency increases. This trend is displayed in Figure 3.3 below in the solid black line. The trend may be smoothed for less of a piecewise effect. This is shown in the dotted black line.

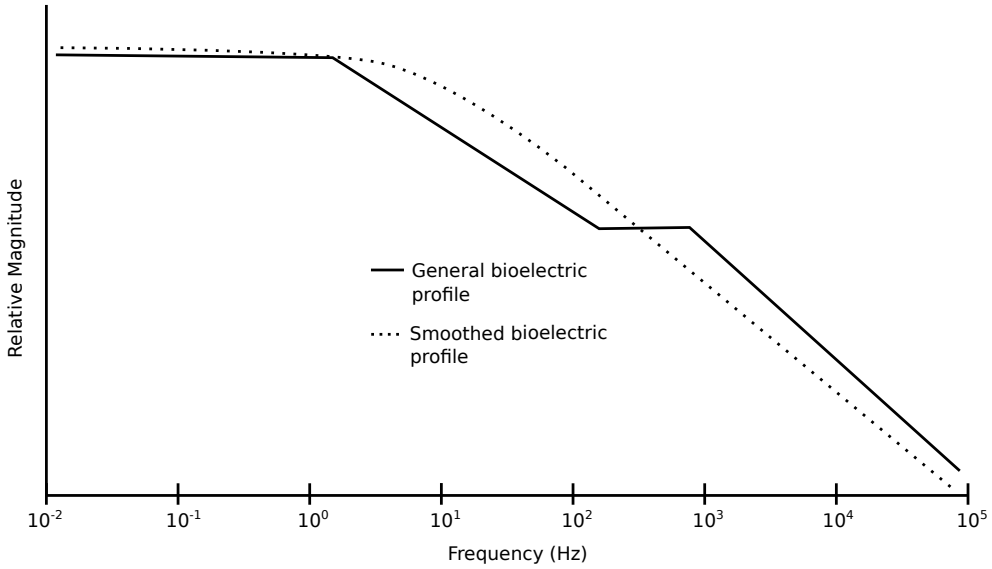

Figure 3.3. Outlined and smoothed profiles of the bioelectric signal magnitudes.

Interestingly, the smoothed magnitude behavior (dotted black line) of the various potentials resembles a low-pass filter (LPF). To achieve the first aim of this thesis the amplifier must be designed to counter balance the magnitude-frequency characteristics shown above so that signal amplitudes will remain in bounds of the amplification and recording equipment. One option is to implement an amplifier with a high-pass filter (HPF) characterstic in order to counter balance the low-pass nature of the bioelectric recording environment.

The magnitude of a HPF is shown below in Figure 3.4 as the counterbalance HPF. This could allow for a frequency-dependent attenuation of amplitude resulting in bioimpedance and bioelectric signals that are appropriately scaled, yet it does not seem to fully achieve the aims of the thesis because it neglects the DC component.

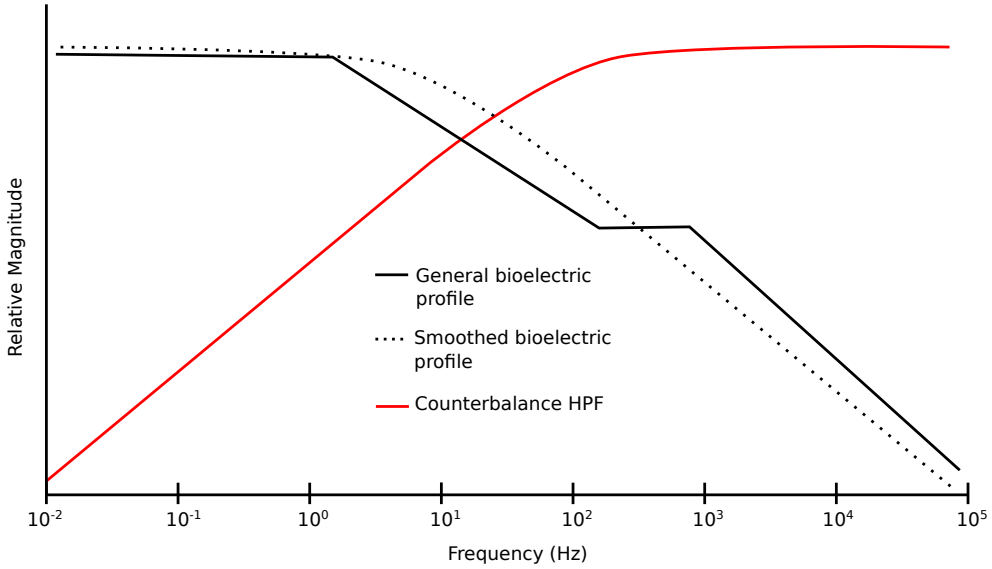

Figure 3.4. High-pass filtering compensation option.

The implementation of a HPF alone, however, would also not provide any new solution to the analog filter problems previously presented in Chapter 2 and would only lead to loss of signal and distortion of both the temporal and frequency distributions due to the attenuating effects of the filter. The latter issue of signal distortion is more difficult to address and one that the filter cannot overcome alone. However, the filter may be used to avoid the loss of signal at lower frequencies by creating a low-frequency corner that brings the attenuation in the low-frequency range to a plateau rather than a constant roll-off of -20 dB/decade or more. This allows for low-frequency (i.e. 0–1 Hz) signals to be retained without saturating the recording equipment, yet at the same time, it will ensure that the smaller amplitude, low-frequency signals are amplified enough to bring them into the dynamic range of the recording system without masking other bioelectric signals excessively. This type of implementation is conceptualized in Figure 3.5 below.

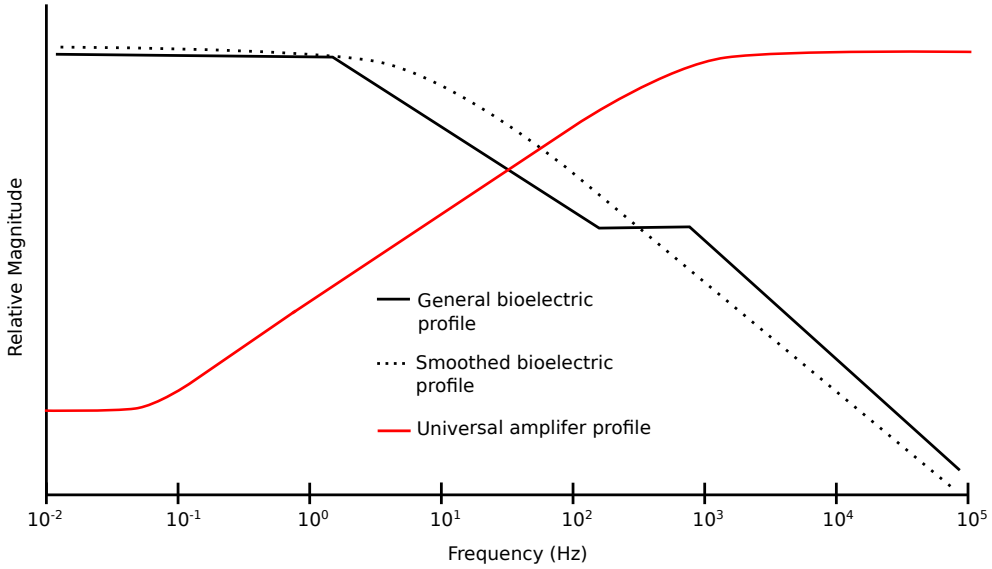

Figure 3.5. Variable gain compensation with constant DC amplification.

An amplifier designed in this way may not seem to contribute much more than other specialized amplifiers with custom frequency characteristics, however, this type of setup lays the foundation for dealing with the issues of amplifier signal (time and frequency) distortion caused by the filtering of the amplifier. The method of dealing with this distortion comes through the use of the second component of the IUA system. This second component will be a computer script that once a signal is digitally recorded with the IUA, will make use of the architecture of the invertible universal amplifier to filter the digital signal, through a process referred to as restoration, to return a bandwidth-limited version of the signal seen by the electrodes. Thus, in order to achieve an IUA system, the key components are the means to scale and capture what appears on the electrode through the use of the invertible universal amplifier and a means to reconstruct that signal in the digital domain through the use of computer software, programming, and processing power. Therefore, throughout the remainder of this thesis, a system that consists of an IUA to be used during the recording of bioelectric activity as well as a digital scheme to invert the IUA are presented.

4. THEORETICAL ANALYSIS AND DEVELOPMENT OF AN INVERTIBLE UNIVERSAL AMPLIFIER

The background theory and the theoretical development of the invertible universal amplifier discussed in the beginning chapters is key to laying out the requirements for the analog amplifier and identifying the digital method with which the signal will be restored via the inverted amplifier transfer function. The key requirements for the amplifier are that it have an architecture that follows classic bioelectric amplifier characteristics like high input impedance and that an analog amplification scheme can be adopted that accommodates the bioelectric frequency spectrum discussed early on. The amplification must be appropriate so that larger amplitude-low frequency bioelectric signals are being amplified less than small amplitude-high frequency bioelectric signals. The means to determine the transfer function of the amplifier will be discussed in this chapter as well.

4.1 Optimal Amplifier Layout

In order to physically implement an analog amplifier scheme like the one proposed, there must be an input stage amplifier that allows the frequency dependent amplification and a second stage amplifier that raises the amplification value. The input stage should be built around an op-amp structure that provides low noise and high input impedance. The second stage amplifier should also be a low noise operational amplifier. A generic analog amplification circuit constructed to allow a frequency-dependent amplification is shown below in Figure 4.1.

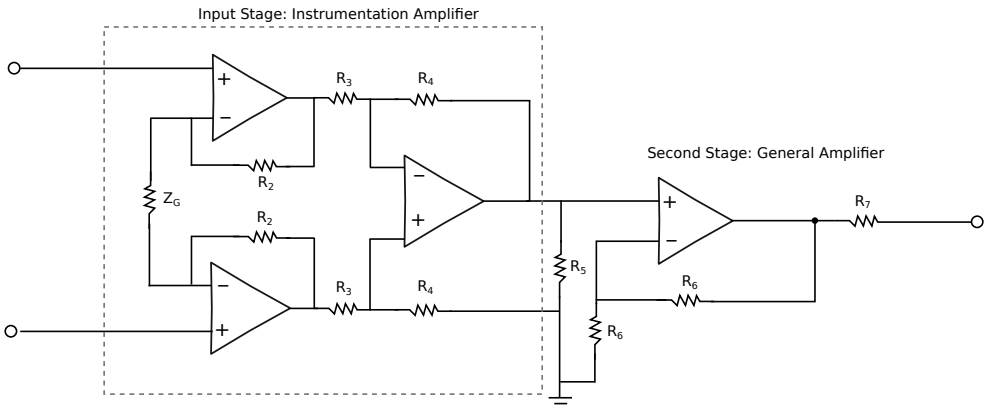

Figure 4.1. Generic input stage and second stage architecture.

This type of structure includes an input stage consisting of an instrumentation amplifier (inside dashed box), which provides high input impedance and good common-mode rejection. It also has a second stage amplifier that provides additional overall gain. The gain of only the instrumentation amplifier is given below in Equation 4.1.

$$\frac{V_A'}{V_2 - V_1} = \left(1 + \frac{2R_2}{Z_G}\right)\frac{R_4}{R_3} \tag{4.1}$$

By setting R_3 and R_4 to be the same value, the gain of the instrumentation amplifier is then only set by R_2 and Z_G. By allow Z_G to contain a frequency dependent component then the gain will be dependent on the frequencies of the signal being recorded. The gain of the second stage amplifier is set to a constant by the balance of resistors labeled R_6 and is:

$$\frac{V_{out}}{V_A\prime} = \left(1 + \frac{R_6}{R_6}\right) = G \tag{4.2}$$

When these two stages are combined using the concept of superposition, the overall system transfer function turns out to be:

$$\frac{V_{out}}{V_2 - V_1} = G\left(1 + \frac{2R_2}{Z_G}\right) \tag{4.3}$$

4.2 Analog Amplification Scheme

Again, it is important that the IUA amplify bioelectric signals based on their relative amplitudes and corresponding frequency bandwidths so that (1) higher frequency biosignals, specifically ENG, can be more easily monitored relative to other biosignals during recording and so that (2) a frequency band from DC to beyond 20 kHz could be digitally recorded for digital on- or off-line processing. As presented earlier in the background information, the magnitude of bioelectric signals and electro-potentials have a low-pass filter characteristic, which may be compensated for with an amplifier that has a high-pass filter characteristic. However, as presented previously a simple high-pass filter will cause the problem of losing the DC content of the signal. In the use case of universal observing and recording of bioelectric signals the IUA must allow for acquisition of the DC information without saturation of the amplifier or recording equipment. Since it is desirable to amplify the higher frequency signals more due to their smaller amplitudes, for bioelectric signal observation and recording, the pattern shown in Figure 2.1 is considered as well as the bioelectric signal characteristics in Figure 4.2. From these, it is logical to choose a high cutoff frequency between 10^2 and 10^3 Hz and a low-frequency cutoff between 10^{-1} and 10^0 Hz. Plus, a second stage amplifier will be used to provide an additional gain for all frequencies. Thus, the magnitude plot for the IUA in relation to the amplitude-frequency magnitude of bioelectric signals looks like that shown with a red line in Figure 4.2 below.

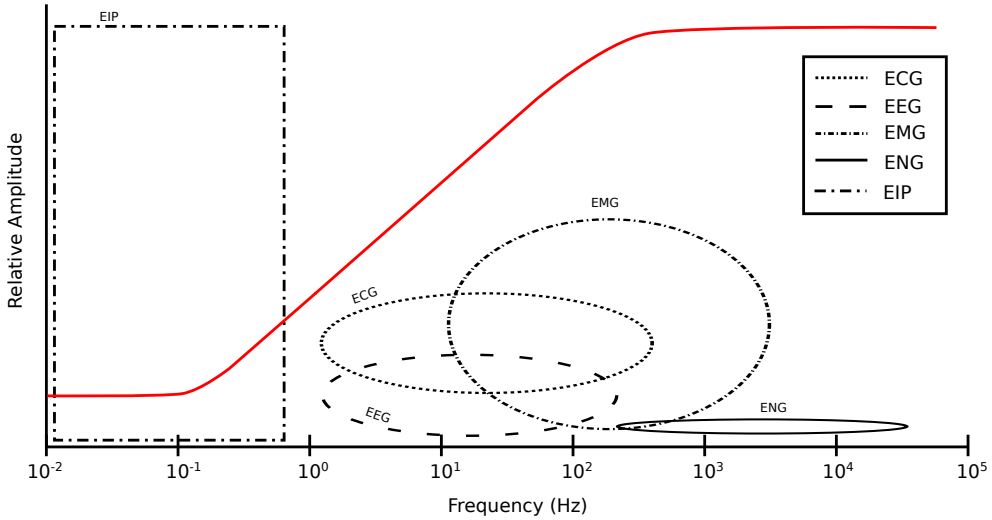

Figure 4.2. The relationship of bioelectric signal magnitudes and variable amplification.

With this profile in mind, if in Equation 4.3 Z_G is equal to the sum of a resistance and an impedance due to a capacitor then

$$Z_G = R_1 + Z_C = R_1 + \frac{1}{sC} \tag{4.4}$$

Now, according to Equation 4.4, the transfer function in Equation 4.3 at high frequencies shows that the gain becomes a gain of $2\left(1 + \frac{2R_2}{R_1}\right)$. While at DC the gain will become 2. The gain transitions at a rate of 20 dB/decade between these two gain plateaus.

4.3 Digital System Identification of the IUA

Since the DC gain of the amplifier is no longer zero, all information down to DC will be retained, which could possibly cause an issue with the design requirement that the transfer function of the amplifier be invertible. Yet, since it is a linear system it is most likely stable. Moreover, since it is a linear system a digital filter can be used to describe its transfer function and invert it to create a compensator to restore the gain profile from that of the variable gain of the IUA to a flat gain. The ability to digitally characterize and invert the transfer function will require the use of system theory and powerful computational tools.

4.3.1 The Digital Characterization and Determination of the Digital Filter

In order to achieve the second requirement of this new proposed approach for biosignal acquisition the system must be fully characterized so that the amplifier parameters may be used to construct a restoration filter to reverse any distortion first caused by the variable gain profile. Unfortunately, the final analog components that will be selected to create the amplifier of the IUA system will not be known perfectly and therefore the system may be best characterized by digital means. When it comes to digital characterization the goal is to determine the system h(t) by using a de-convolution with the time-domain captured signals $y(t)$ and $x(t)$ according to the Equation 4.5 [28]:

$$y(t) = k \times h(t) * x(t) \tag{4.5}$$

According to system analysis theory, when using the Laplace Transform in Equation 4.6 the causal continuous signals $y(t)$ and $x(t)$ can be converted to the frequency domain using the Equation 4.6 in order to move away from determining the system transfer function using convolution-related techniques [28]:

$$X(s) = \int_0^\infty x(t)e^{-st}dt \tag{4.6}$$

Thus, according to the Laplace Transform in Equation 4.6 the transfer function of the amplifier would be found using the following Equation 4.7:

$$Y(s) = kH(s)X(s) \tag{4.7}$$

where $kH(s)$ is the transfer function of the system $H(s)$ times a constant k. If a compensator, $C(s)$, can be found that is equal to the inverse of this product $kH(s)$ such that Equation 4.8 is true:

$$C(s) = \frac{1}{kH(s)} \tag{4.8}$$

then for any given output signal Y(s),

$$Y(s)C(s) = X(s) \tag{4.9}$$

$X(s)$ may be found according to Equation 4.9, where $X(s)$ is the original input signal in the frequency-domain. In the implementation of the IUA, the time-domain signal $y(t)$ will be captured by the ADC, which applies the sampling theorem resulting in a signal in the discrete domain known as $y(n)$ rather than a continuous signal. Then rather than using the Laplace Transform, its counterpart in the digital-domain, the unilateral z-transform shown in Equation 4.10 will be utilized [28]:

$$X(z) = \sum_{n=0}^{\infty} x[n]z^{-n} \tag{4.10}$$

This will allow for the identification of a digital filter $C(z)$ equivalent to $C(s)$ to allow the ultimate and accurate estimation of the original input signal $x(n)$, which is simply the sampled version of $x(t)$.

4.3.2 The Output-Error Method

Presuming at this point that the amplifier system will be stable, it may be characterized by estimating the coefficients of the transfer function if the input and output are known. In this case, a known analog input may be given to the amplifier and simultaneously sampled along with the output. With the discrete input and output data, one of the most common methods for determining the discrete parameters of a system is known as the output-error method. The output-error (OE) method estimates model parameters and corresponding covariances using the input-output data using the general structure below [29]:

$$y(k) = \frac{B(q)}{A(q)}x(k) + w(k) \tag{4.11}$$

where

$$\begin{aligned} A(q) &= 1 + a_1 q^{-1} + ... + a_{n_a} q^{-n_a} \\ B(q) &= b_1 q^{-1} + ... + b_{n_b} q^{-n_b} \end{aligned} \tag{4.12}$$

where $x(k)$ and $y(k)$ are the input and output of the system and $w(k)$ represents a noise in the measured output [28, 29]. The noise-free system can be expressed as described in [29]. In summary, the output can be rewritten in regression form:

$$\begin{aligned} y_0(k) &= \theta_0^T \psi_0(k) \\ \theta_0 &= [a_1, ..., a_{n_a}, b_1, ..., b_{n_b}]^T \\ \psi_0(k) &= [-y_0(k-1), ..., -y_0(k-n_a), x(k-1), ..., x(k-n_b)]^T \end{aligned} \tag{4.13}$$

The model based on the estimation of parameters at the ith iteration is described by

$$y_M(k, \hat{\theta}_i) = \hat{\theta}_i^T \psi_M(k, \hat{\theta}_i) \tag{4.14}$$

where

$$\begin{aligned} \hat{\theta}_i &= [\hat{a}_i, ..., \hat{a}_{n_a}, \hat{b}_1, ..., \hat{b}_{n_b}]^T \\ \psi_M(k) &= [-y_M(k-1, \hat{\theta}_i), ..., -y_M(k-n_a, \hat{\theta}_i), u(k-1), ..., u(k-n_b)]^T \end{aligned} \tag{4.15}$$

The off-line OE method uses several optimization algorithms to determine the best estimate. The different optimization algorithms are the Gauss-Newton approach, an adaptive Gauss-Newton approach and the Levenberg-Marquardt method. Each of these optimization algorithms are described in more detail in the literature and in computational tools documentation such as Matlab® [30]. Mathematical and computational tools like Matlab® may also be used to implement the OE method. Specifically, the OE method in Matlab concludes by selecting the best estimates from the available optimization algorithms and returns the parameter estimates, making running these estimates very simple. With the computational determination of these parameters, the digital filter $C(z)$ that is equivalent to the analog filter $C(s)$ will have been determined and one only has to multiply it by $Y(z)$ to accurately estimate the original digital signal $X(z)$. With the general selection of where the cutoff frequencies should be, with an identified amplifier architectural layout, and the theory in place for digital system characterization and signal restoration, the next step is to implement and tune these components to a working IUA system setup.

5. INITIAL IMPLEMENTATION AND TUNING OF THE IUA SYSTEM

The optimal amplifier architectural layout of the IUA has been previously provided and the idea of how to implement and realize it has been theorized, yet the vital steps of actually implementing the theory and making the implementation work well are yet to come. The specific resistor and capacitor components of the amplifier still need to be determined, the transfer function characterized, identification of restoration parameters, and optimizing of the process to identify the restoration coefficients. These topics will be presented in this chapter and the results of optimizing the process for identifying the inversion coefficients will be discussed.

5.1 Invertible Universal Amplifier Architecture

The IUA was constructed using a high impedance input stage op-amp and a second amplifier stage. A Burr-Brown INA111AP high-speed FET input instrumentation amplifier [31] was used as the input stage because it offers very high input impedance due to its internal instrumentation op-amp design, high common-mode rejection ratio (106 dB minimum), and excellent DC accuracy due to laser trimmed internal resistors. As already discussed in Chapter 4 the impedance component on the instrumentation input stage allows for the variable gain configuration to be set through the use of a resistor and capacitor. Based on the bioelectric signal profiles discussed in Chapter 2 through Chapter 4, the low-frequency corner was set at 0.32 Hz and the high-frequency corner was set at 159 Hz. With a resistor and capacitor combination the instrumentation input stage according to Equation 4.1 incorporates the low-frequency corner set at 0.32 Hz with unity gain for frequencies below this, the high-frequency corner set at 159 Hz with a gain of nearly 500

for frequencies above this, and a variable gain between these two frequencies. The second stage of the IUA consisted of a Texas Instruments OP27GP low-noise operational amplifier and was used for additional constant gain of 2 across all frequencies [32]. Thus at frequencies well below 0.32 Hz a total gain of 2 is expected and at frequencies much higher than 159 Hz a gain of 1000 is expected. The circuit diagram for the implemented IUA is found below in Figure 5.1.

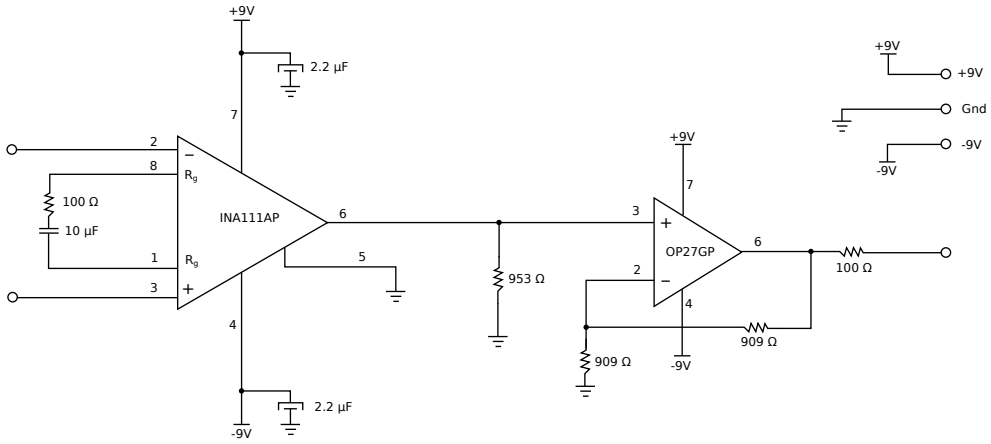

Figure 5.1. Final architecture of one channel of an invertible universal amplifier (IUA).

5.2 Invertible Universal Amplifier Transfer Function

With the architecture for the IUA fully laid out the nominal transfer function may easily be identified using system analysis discussed in Chapter 4. The equation for the transfer function of the circuit shown above in Figure 5.1 is given in Equation 5.1 below.

$$TF = 2\left(\frac{j\omega C\left(R_1 + R_2\right) + 1}{j\omega C R_1 + 1}\right) \tag{5.1}$$

where C is 10 µF, R_1 is 100 Ω, and R_2 is 25 $k\Omega$, which is set internally in the INA111AP. The gain of 2 is created through a non-inverting amplifier configuration with the OP27GP. Plugging in the resistor and capacitor values gives the complete transfer function of the IUA system shown below in Equation 5.2.

$$TF = 2\left(\frac{j\omega + 1.885}{0.000995\,j\omega + 1}\right) \tag{5.2}$$

A plot of the nominal transfer function of the system is shown below in Figure 5.2. The nominal transfer function has the zero at approximately 0.32 Hz and the pole at approximately 159 Hz. There is also an approximately 6 dB magnitude (2 times gain) at frequencies lower than 0.1 Hz and approximately 60 dB magnitude (1000 times gain) at frequencies greater than 200 Hz.

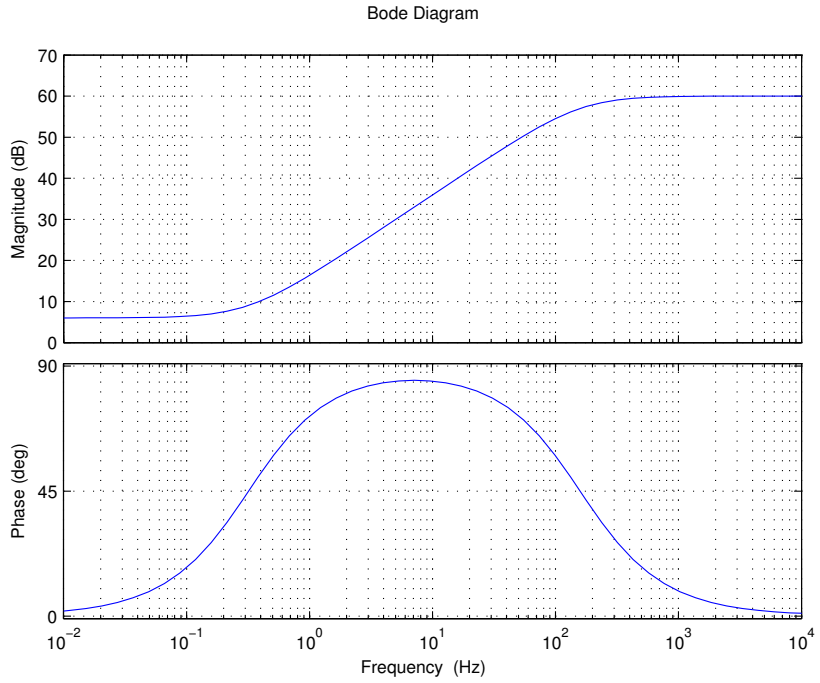

Figure 5.2. The nominal transfer function of the invertible universal amplifier based on the nominal values of the resistors and capacitors.

It should be noted that there is only one zero and one pole with this transfer function. The zero is at approximately $s = 1.885$ in the left-half s-plane (LHP) and is far from the imaginary axis of the Nyquist plot. The pole is located in the LHP at approximately $s = 1005.25$, which is important because stability of the original transfer function is determined by the location of the poles of the system in the LHP. Since the transfer function is stable, it

may be mathematically inverted. It is also important to note that the IUA transfer function when inverted will be still stable because the original zero, when it becomes a pole in the restoration transfer function, will still be in the left-hand *s*-plane, albeit close to the imaginary axis.

5.3 Multi-channel Development of the Invertible Universal Amplifier

The architecture of the invertible universal amplifier was used to create 12 separate channels in one amplifier to be used in multi-channel recordings. This 12 channel IUA was used for all other testing and results to be described and discussed.

5.4 Restoration Filter:Inversion from Variable Gain to Flat Gain

Since the transfer function in Equation 5.2 of the constructed IUA is stable it may be mathematically inverted in order to restore the signals to their original ratios and return a stable signal. The inversion process for the transfer function began with a one-time process of accurately digitally characterizing the original system in Figure 5.2 above. This was first achieved by initially passing a known, very small arbitrary amplitude 1 Hz square wave with no intended DC offset (i.e. ideally zero offset) generated by a function generator (GW Instek SFG-2110) through the amplifier that maximized the amplifier output yet without reaching saturation. These signals were sampled using a 12-bit data acquisition board (National Instruments® PCI-6024E) sampling at 48 kHz/ch in a standard PC using the Mr. Kick II (Knud Larsen, Aalborg Univ) data acquisition software. Two caveats arose during this situation. The first caveat was that due to the need for a small input amplitude and associated SNR issues related to recording this input signal, the 1 Hz square wave was separately amplified using an external bioamplifier (Axon Instruments, CyberAmp 320) using a 20 times gain in order to increase the SNR before digitization. The second caveat was that large errors in the restoration process might occur if there were a mismatch in the small amplitude DC component of the signal. Initial attempts to identify the system was done by taking the recorded input and output and estimating the transfer function by creating a rep-

resentative digital filter using the OE method in the custom Matlab script where the order of coefficients $A(q)$ and $B(q)$ in Equation 4.12 are first order and second order, respectively. However, the initial estimation of the system parameters using the digital filter created by the OE method also had issues as shown in Figure 5.3. It shows the original (red) and estimated (blue) output (left) and the input (right) signals for the first channel of the IUA. In this figure it can be seen that the amplifier output and calculated output estimate appear to match, but the original input and the input estimate have a difference in their final offset values.

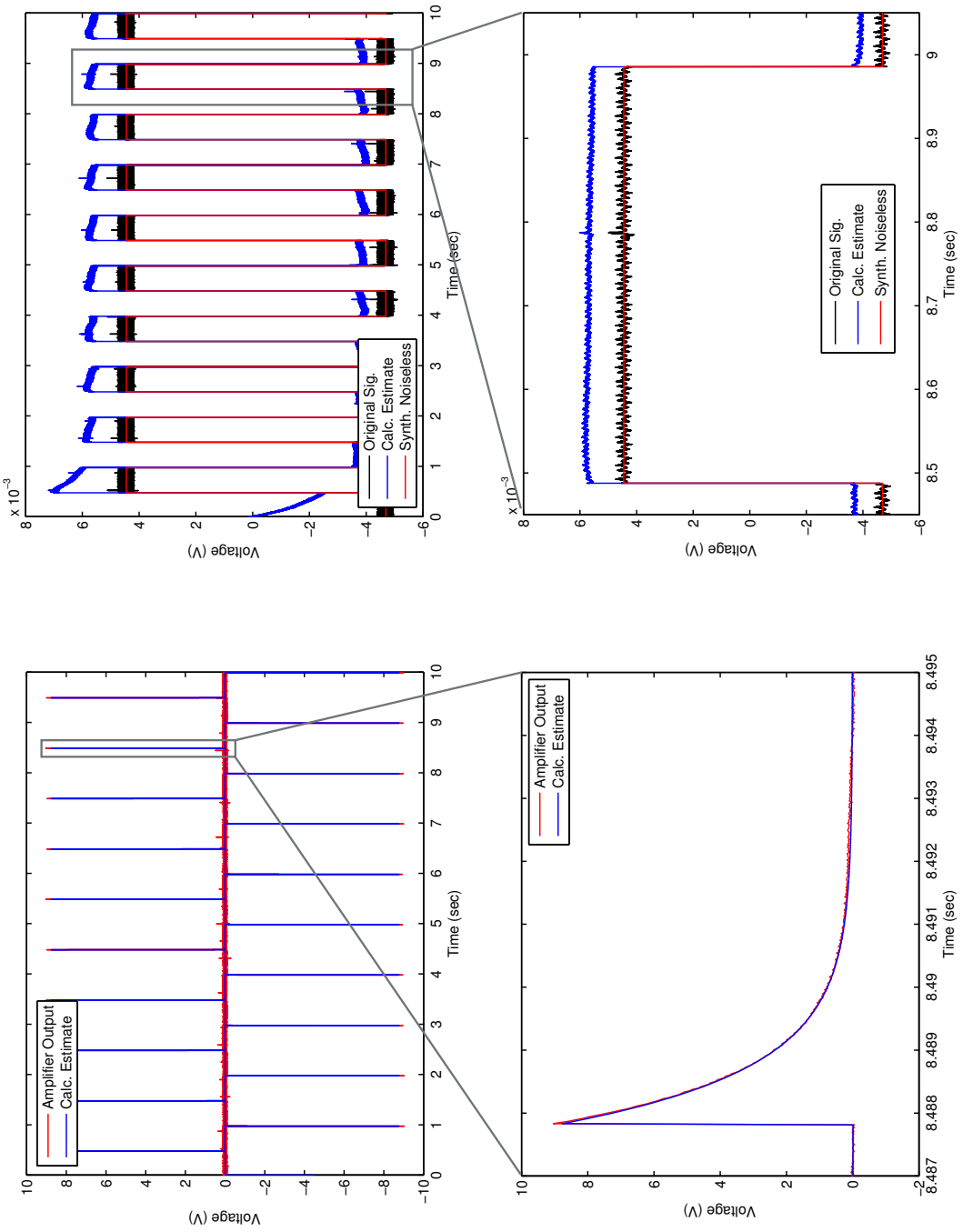

Figure 5.3. Output and input estimates based on output-error based parameters.

These results were also seen when a 16-bit NI USB 6251 analog-to-digital converter was used. While this might have been due to small DC potentials being introduced into the output signal as it goes through the IUA possibly due to an improper DC trim, it was found that the the process of amplifying the input signal with the CyberAmp could also result in varying offsets being added to the signal. Thus, when the output was used to estimate the input the estimated input would not match the original input in its DC component. The offset created by the CyberAmp was found to vary depending on the frequency of the signal as well how the amplifier was setup prior to use. Unfortunately, these observations were not until much later in the process of system identification and so other forms of compensation were initiated.

The first method for compensating for the results and observations in Figure 5.3 was a modified form of signal preparation prior to system identification with the OE method. For this method ten seconds of the arbitrary amplitude, 20 times amplified 1 Hz square wave and the amplifier output were digitally recorded using the the 12-bit data acquisition board (National Instruments® PCI-6024E) sampling at 48 kHz/ch in a standard PC using the Mr. Kick II (Knud Larsen, Aalborg Univ) data acquisition software. The amplified 1 Hz square wave input was digitally de-amplified using the calibrated gain of the CyberAmp, then filtered using a first-order HPF with a -3dB point at 0.15 Hz in order to remove any offset differences, and was then used to establish a noiseless estimate of the 1 Hz amplifier input square wave. The amplifier output was also filtered using the same high-pass filter as not to create problems during system identification and to maintain a linear system. After this the conditioned input and the original output were ready to use to determine the transfer function of the system using the OE method using the custom Matlab script and the system identification toolbox (Matlab R2009b, the Mathworks, Natick MA) [30].

5.5 Output-error Optimization and Input-error Optimization

After using the conditioned input and output signals with the OE method the second set of parameter estimates were obtained. In Figure 5.4 below, the OE method and was

used to digitally estimate the analog system transfer function, create a restoration filter by inverting the transfer function, and to estimate both the input signal and the output signal with the estimated restoration and original filters, respectively. As all twelve channels of the IUA were built using similar components and produce similar results, Figure 5.4 shows the original (red) and the estimated (blue) output (left) and the input (right) signals for the first channel of the IUA, which is a good a representation of the other 11 channels. In this figure it can be seen that the amplifier output and the calculated output estimate match closely and this is likely due to the OE method estimating the transfer function based on error-minimization of the output.

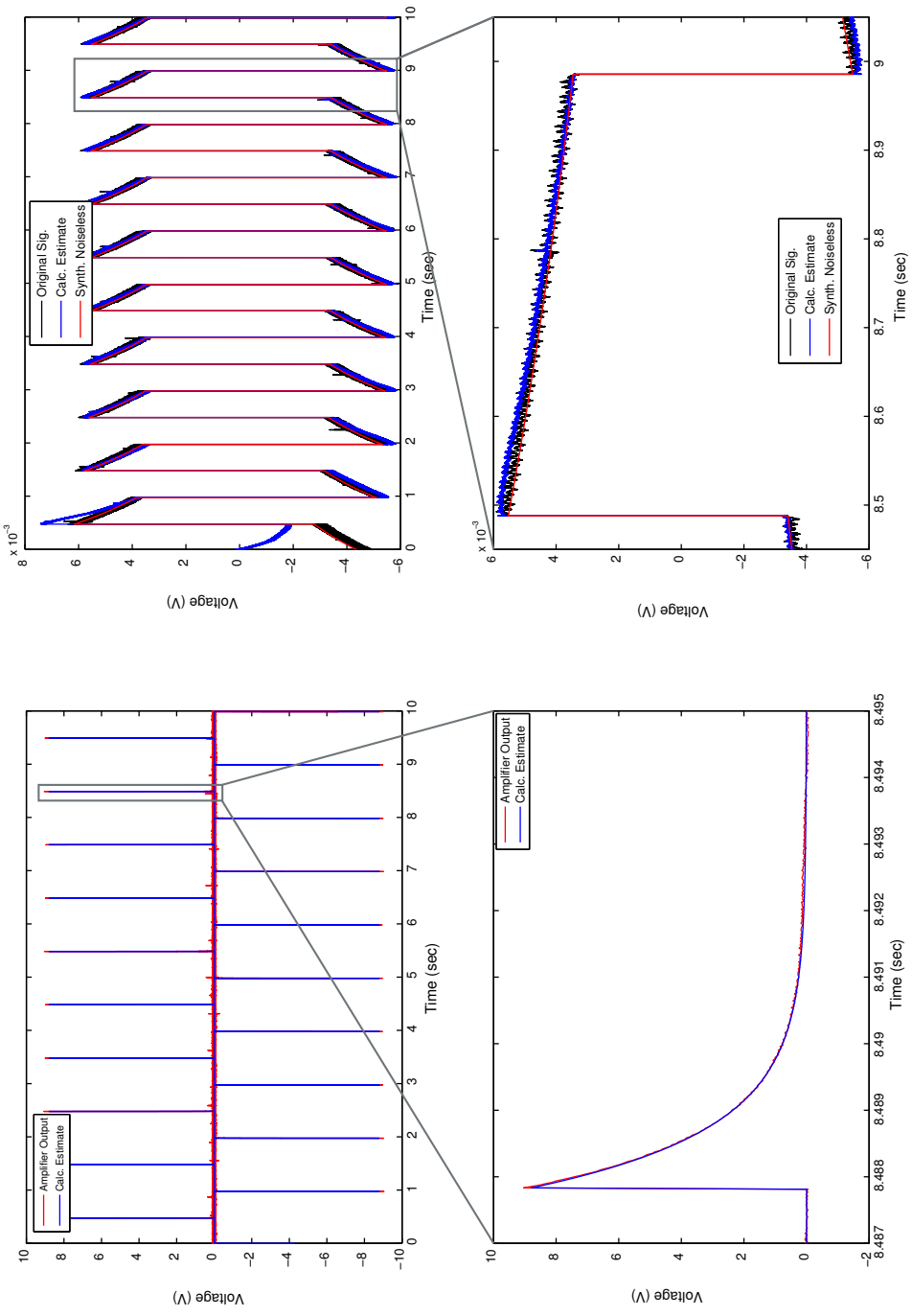

Figure 5.4. Output and input estimates based on output-error based parameters but also with high-pass filtering.

However, it was important to consider that the OE method provides a discrete transfer function estimate of the system by minimizing the error of the output. Furthermore, it is importance to remember that this type of optimization may lead to error-minimization issues when inverting the transfer function and using an output signal to estimate the input as was seen in Figure 5.4. Moreover, with a perfect transfer function estimate, it should be able to be inverted and the input should be perfectly predicted using the output. Yet, in Figure 5.4 above the deviations between the input estimate and the original input signal are specifically noticed at the beginning of the step up or step down where the estimated input arches above the original signal. From these observations, it was concluded that minimizing the error on the output does not necessarily minimize the error of the input signal and that it is important to use techniques to minimize the error of the input signal after minimizing the error of the output with the OE method. The techniques for minimizing the input error, and thus identifying a better transfer function estimate, included (1) converting the parameter estimates from the discrete-time domain produced by the OE method to the continuous-time domain and (2) minimizing the error of the input estimate through estimating only specific analog components in the continue-time domain.

These two techniques were crucial in the error minimization process because any attempts to simply swap the input for the output while running the OE method failed due to the lack of excitability of the then input signal. Therefore, these techniques laid out had to be followed as no shortcut was achievable. Thus, the first technique for minimizing the input error involved the Matlab® function *d2c* (discrete-to-continuous) after the discrete-time parameter estimates are returned with the OE method. This *d2c* function may be used to transform the transfer function from the z-domain back to the s-domain similar to the techniques discussed in Chapter 2, which is to effectively applying the bilinear transform. For this purpose, the *d2c* function was used with a zero-order hold and applied the bilinear transform on the inputs. However, the *d2c* function when used with a zero-order hold cannot adequately transform systems with poles at $z = 0$. If the pole is close to $z = 0$ then the *d2c* conversion in Matlab may fail. Thus, a key design requirement of the IUA is to keep the pole as close to zero as possible but to ensure that the *d2c* function will not fail.

Staying several tenths of Hertz above 0 Hz would ensure that the *d2c* function will not fail and keeps the pole sufficiently low. The pole at 0.32 Hz for the IUA was sufficiently low to include low-frequency bioelectric data but not so low as to allow the *d2c* function to work correctly.

After the successful conversion of the transfer function with *d2c* and once the parameters are in the continuous-time domain then, according to the second technique for input error-minimization, the parameters may be used to estimate the values of analog components used in the circuit, which may or may not be directly measured or known. The estimation of the analog components may then be adjusted to produced an input signal estimate that minimizes the error of the input. The equations and program used for output error, input error (OEIE) minimization are discussed next.

5.6 Matlab Script Development and IUA Tuning

As previously discussed, the OE method helped with initially identifying parameters through the development of a discrete digital filter but failed to optimize the input estimate from the inverse transfer function. From this point, the filter was converted from a discrete to a continuous filter in order to further optimize the transfer function parameters. In order to implement the output-error, input-error (OEIE) minimization, it was ideal to implement an automated method for improving both the output and the input estimates. This effect was conducted in three steps. The first step was to understand the practical effects on the system of the different factors which included the gain (G), the resistor (R_1), the capacitor (C), and the op-amp-integrated resistor (R_2). The second step was to create a single-correction algorithm based on understanding gleaned from the first step. The third step was to create a corrective algorithm that corrected the values of components that fell outside their stated tolerance ranges.

The first step was an attempt to understand the practical effects of the how the analog components affected the results. During calibration the gain (G) effected the overall gain of the signal. The R_1 effected the nature of the descent of the output signal from its peak

when a square wave input signal was given. The capacitor value (C) also affected the lower part of the descent to during the transient part and the op-amp integrated resistor (R_2) also affected this transient descent section. Both G and R_2 had an affect on the amplitude of the signal as well where as R_1 had less an effect on the signal amplitude. This understanding was used in attempts at improving the input estimate after the use of the OE method through manual iteration and adjustment of the G and R_2 values and visual inspection of the output estimates and the input estimates. Due to the crude procedure, at best the input estimate was only slightly improved by visually inspection of the input estimate and adjusting the R_2 parameter to achieve a better RMS error value between the original input and the input estimate. However, there were inconsistent improvements with the output estimate.

As a next step, a computational process was then implemented to arrive at a one-time R_2 adjustment depending on whether the value of C was above or below a threshold. In the Matlab calibration script for each channel of the IUA the value of C would instruct whether to and how to adjust the value of R_2. The value of R_2 was selected since it could not be directly measured unlike the other components. Unfortunately, there was no conclusive trend in which way or how much to adjust R_2 and so manual inspection and input was required on certain channels. The combination of this computational and manual process was possible because of the small number of channels needing to be calibrated for this IUA system implementation. However, if the number of channels were to increase, manually determining how the op-amp-integrated resistor value should change in order to improve the input estimate would become tedious and prove to be unreliable.

In a final effort an automated optimization was crafted and conducted. The automated optimization utilized the equations derived from the transfer function provided in Chapter 4. The transfer function may be viewed in two similar ways as shown below, where the set of Equations 5.3 below treats the gain (G) value as a known value of 2 and the set of Equations 5.4 treat the gain (G) as an unknown parameter:

$$TF = 2\left(\frac{j\omega C(R_1+R_2)+1}{j\omega CR_1+1}\right) = 2\left(\frac{j\omega k_1+1}{j\omega k_2+1}\right)$$

$$\begin{aligned} k_1 &= C(R_1 + R_2) \\ k_2 &= \frac{C}{R_1} \end{aligned} \tag{5.3}$$

$$\begin{aligned} C &= \frac{k_2}{R_1} \\ R_2 &= \frac{k_1-k_2}{C} \end{aligned}$$

$$TF = \left(\frac{j\omega GC(R_1+R_2)+G}{j\omega CR_1+1}\right) = G\left(\frac{j\omega k_1+k_0}{j\omega k_2+1}\right)$$

$$\begin{aligned} k_0 &= \frac{k_{oo}}{k_{eo}} = G \\ k_1' &= k_0 C(R_1 + R_2) \end{aligned} \tag{5.4}$$

$$\begin{aligned} C &= \frac{k_1'}{k_0}(R_1 + R_2) = \frac{k_2}{R_1} \\ R_1 &= \frac{k_1-k_0CR_2}{k_0C} \\ R_2 &= \frac{k_1-k_2}{C} \end{aligned}$$

Using Equations 5.3 and setting the gain value to the expected value of 2, an estimate of the values of C, the capacitor, and R_2, the resistor in the op-amp, may be determined. The initial estimates of the capacitor and the op-amp resistor will then allow further improved estimations of these values using the set of Equations 5.4. It is important to note that the second set of equations shows the gain value (G) being the quotient of two other constants. These other constants are based on the amplitude determined through a computational process in Matlab of the original output signal and the estimated output signal respectively. Once the gain value have been updated the values of the capacitor and the resistor (R_1) in the second equation set will also be updated since they are dependent on the adjusted gain value. The op-amp-integrated resistor (R_2) is also update as it relies on the capacitor. Once all the components are updated, a new restoration parameters are determined and the input signal is estimated and compared to the original input signal again. In this fashion an iterative process may be used to update the component values and then to stop adjusting

the values after a given number of iterations. The Matlab code that was developed ran the iterative process for one hundred iterations as this was found to be both fast enough and but also allow for enough iterations for the values to stabilize.

After the iterative process, it was found that the value of the capacitor was usually more than 10% lower than the nominal value, which violated the tolerance of the capacitor. However, the values of the gain and of the resistors were acceptable or were within the accepted tolerances when compared to the nominal component values. In order to ensure that the returned capacitance also fell within its stated tolerances, a third iterative process was conducted that focused on incrementally increasing the capacitor value until the RMS voltage of the difference of the original input signal and the estimated input signal over the last 6 seconds was less than 1×10^{-5} V_{RMS}. For this proces the op-amp-integrated resistor (R_2) was fixed at the value given in the INA111AP datasheet, which was 25 $k\Omega$, as the resistors in the op-amp are precision laser trimmed. Specifically, this sequence involved:

1. The capacitor value was increased incrementally by a small value.
2. The gain and resistor values were left alone.
3. The transfer function was determined and restoration parameters identified.
4. The input signal was estimated.
5. The RMS voltage difference of the original input and the estimated input over the last 6 seconds of the signals was determined.
6. The sequence was repeated as long as the RMS voltage difference over the last 6 seconds was less than 1×10^{-5} V_{RMS}.

After the conclusion of this sequence, the final values of the capacitor and the resistors were reported along with the original and restoration transfer function parameters and both the capacitors and the resistors were within their accepted tolerance ranges. Although a minimization point was found, it was not determined whether or not the RMS voltage minimization was actually the minimum given the unknown amount of computation time this would require. Error analysis was conducted as described later on in Section 5.8.

5.7 Method for Optimization of System Identification with Matlab Script

With the improved method of how to minimize the input error, data for system identification optimization was collected for twelve (12) different channels of the IUA using the methods described in Section 5.4. Altogether, collecting the data involved again passing a small arbitrary amplitude 1 Hz square wave through the IUA without saturation and digitally acquiring both the input and the output using a 16-bit National Instruments NI-USB 6251 data acquisition device and Mr. Kick II custom-acquisition software with a sampling rate of 48 kHz. The input signal was amplified 20 times prior to acquisition using the CyberAmp with calibrated gain and then rescaled to its original amplitudes inside the computer. The acquired input and output signal were conditioned using a first-order digital high-pass filter with a 0.15 Hz cutoff frequency. The Matlab® script was updated in order to implement the OEIE optimization previously described to optimized the transfer function based on the output signal using the OE method, convert the transfer function from the discrete to the continuous domain, and then adjusted the parameters in the continuous domain in order to improve the input estimate as previously discussed in Section 5.6.

During these efforts, the aim of leveraging the power of digital signal processing to invert the amplifier transfer function and restore the recorded signal to an accurate representation of the original signal was achieved by the refining of the Matlab® script that provided better system identification. Initial implementation of the updated Matlab® script showed noticeable improvements as shown in Figure 5.5. Figure 5.5 shows the first channel of the IUA as a representation of all 11 remaining channels of the 12 channel IUA. The outputs are shown on the left and the original signal is red and the estimated signal after the OEIE method is blue. The inputs are shown on the right and the original signal is black, the noiseless input estimate is red, and the estimated input after the OEIE method is blue.

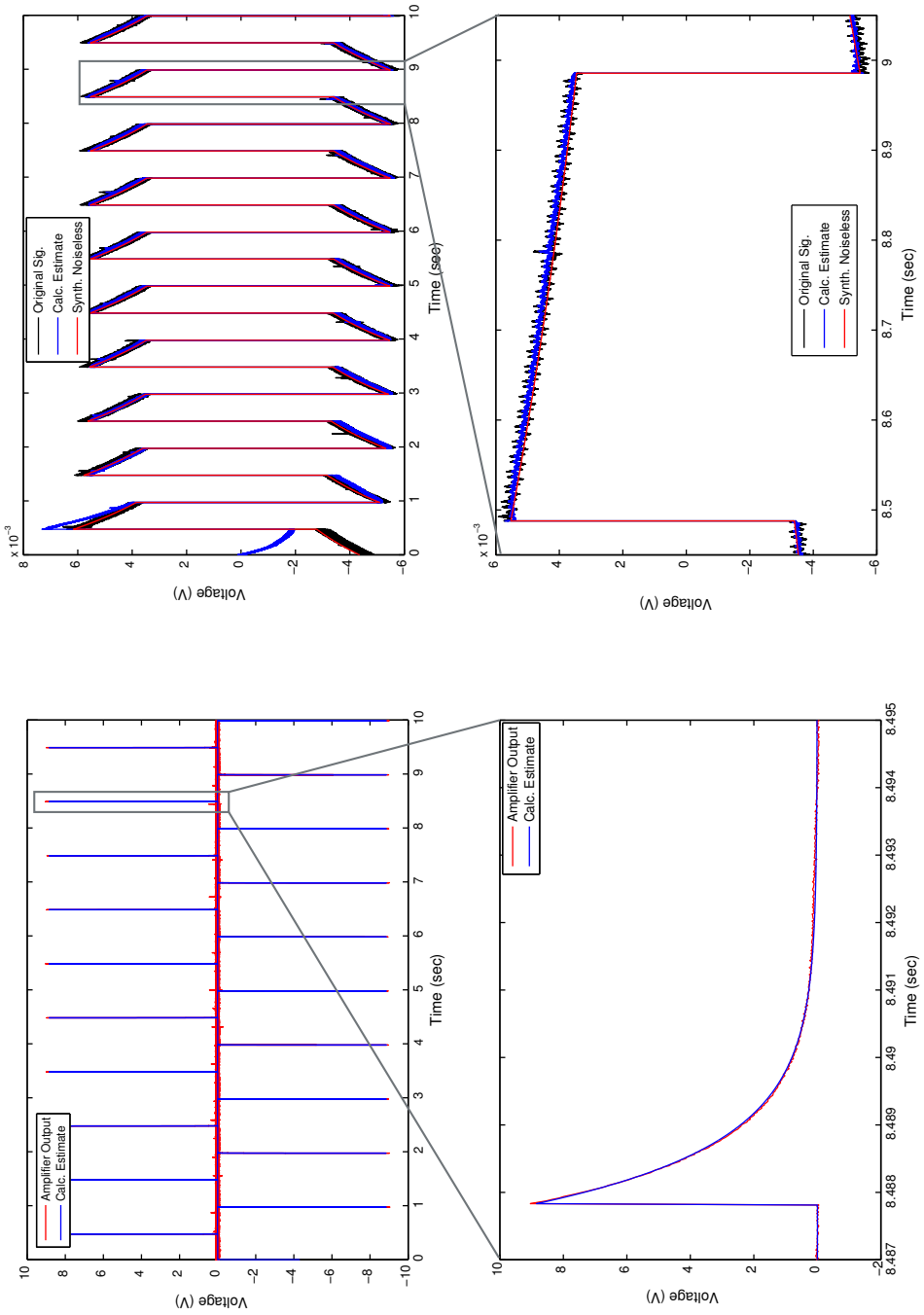

Figure 5.5. Improved output and input estimation results.

In Figure 5.5 above, it can be seen that the original and estimated output signal (left) still match very closely but now the original and estimated input signals match even closer. There is no arching deviation on the estimated signal was there was before immediately after using the OE method. These improvements in the output and input estimates are naturally reflected in better system identification. When compared the transfer function estimated by the OEIE method had a closer fit to the nominal transfer function than if the OE method has been used solely. There is little difference between the transfer function determined using only the OE method and the transfer function determined using the OEIE method in the magnitude, except the OEIE method determined transfer function is slightly closer to the nominal magnitude. The same trend is true for the phase plot of the two transfer functions. These results were seen across all channels built using the IUA configuration but are not shown here.

5.8 Comparison of the OE and OEIE methods

For the error analysis, the voltage difference between the original input, V_{in}, and estimated input signals, $V_{in_{est}}$, using the OE method and the developed output-error, input-error (OEIE) method was calculated and displayed. The RMS value of the last 6 seconds of this voltage difference, $V_{diff_{RMS}}$ was calculated using Equation 5.5:

$$V_{diff_{RMS}} = \left(\frac{1}{N}\right)\sqrt{\sum(V_{in} - V_{in_{est}})^2} \tag{5.5}$$

The RMS value of the original input signal, $V_{in_{RMS}}$, was also calculated and used along with $V_{diff_{RMS}}$ to calculated the percent error of the estimated input signal to the original input signal using the Equation 5.6:

$$\%Error = 1 - \left(\frac{V_{in_{RMS}} - V_{diff_{RMS}}}{V_{in_{RMS}}}\right) \tag{5.6}$$

The percent error of the input signal estimate was computed for each channel of the constructed IUA for both the OE methods and the OEIE method and is reported in Figure 5.6 as verification that the OEIE method is better across multiple channels than just the

OE method alone. The red bars are the percent error for the input estimate with reference to the original input using the OE method originally. The blue bars are the percent error of the input estimate with reference to the original input using the developed OEIE script.

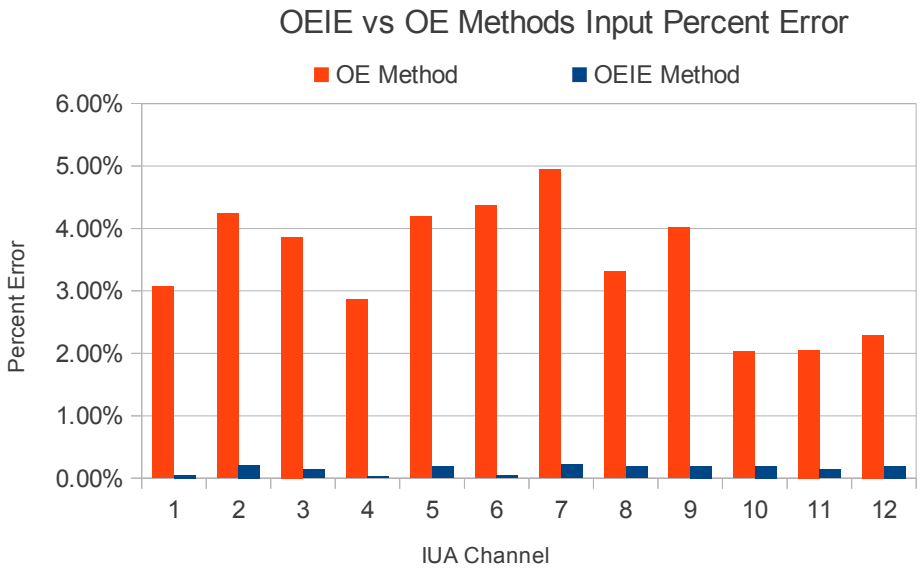

Figure 5.6. Input percent error comparisons between the two optimization methods based on the last 6 seconds of the signal.

Figure 5.6 shows that through the development and use of the OEIE method that the precent error is observable reduced. With the OE method the average percent error was 3.44%±0.98% while with the OEIE method the average percent error was only 0.15%±0.07%. Since it is difficult to see the actual distribution of the OEIE method percent error values, these values are show apart from the OE method in Figure 5.7.

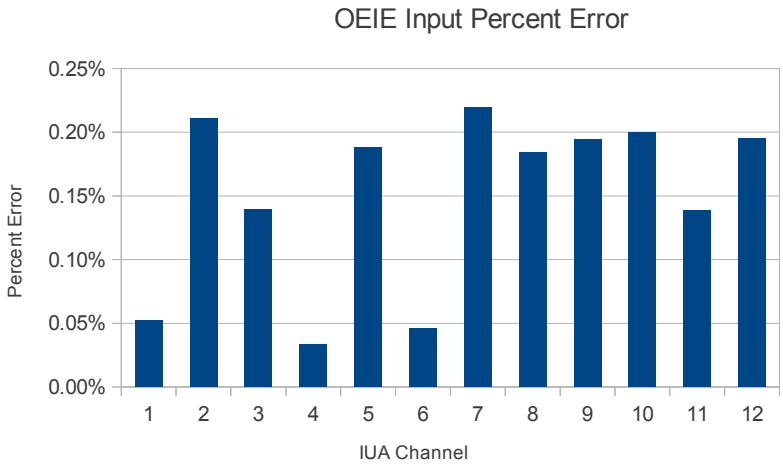

Figure 5.7. Input percent error for the OEIE optimization method based on the last 6 seconds of the signal.

Figure 5.7 shows that for the twelve different channels of the IUA, the OEIE method allows for error minimization of less than 0.25%. Thus, the system may be optimally identified using the developed OEIE method.

5.9 Final Characterization and Restoration Transfer Functions

The verification of the improved OEIE method enabled the final characterization the twelve channels of the IUA. In this section the transfer functions, both original and restoration, from the OEIE method previously described are presented and discussed.

5.9.1 Restoration Transfer Functions

The original and restoration transfer function of the nominal component values used in the circuit and the predicted original and restoration transfer function are shown together in Figure 5.8. The original transfer functions of the nominal component values are noted by the black circles while the restoration transfer function of the nominal component values is noted by the black asterisks. The predicted original transfer is in blue while the red traces show the restoration transfer function.

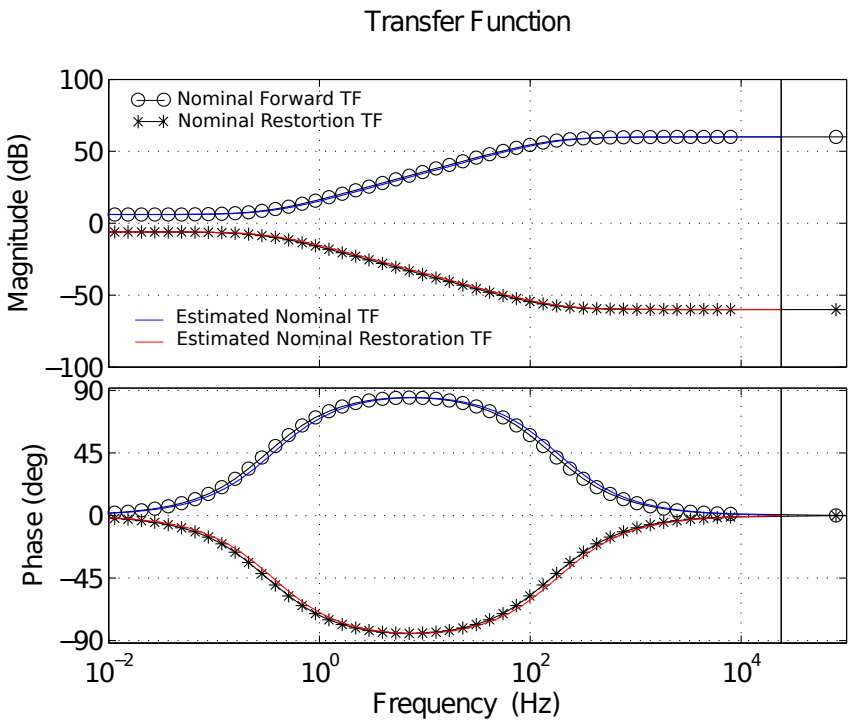

Figure 5.8. Typical original and restoration transfer functions for the IUA.

5.9.2 Restoration Transfer Functions Comparisons

There appears to be little differences in the magnitude across the frequency range when viewing it across a while spectrum. There are, however, noticeable magnitude differences and phase shifts of the estimated and restoration systems compared to the nominal system when viewing over a smaller frequency range. While these differences are noticeable, the error of the estimated transfer function has been minimized and it is being compared to a nominal transfer function, which may also contain its own inaccuracies. Some of these differences, particularly at the edges of the transfer functions, are shown below in Figure 5.9 and Figure 5.10.

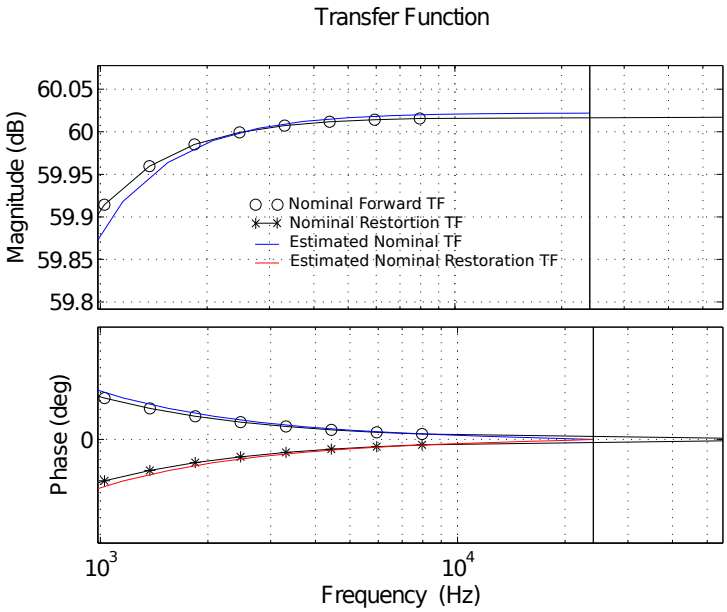

Figure 5.9. Inaccuracies at the low-frequency spectrum of the transfer functions.

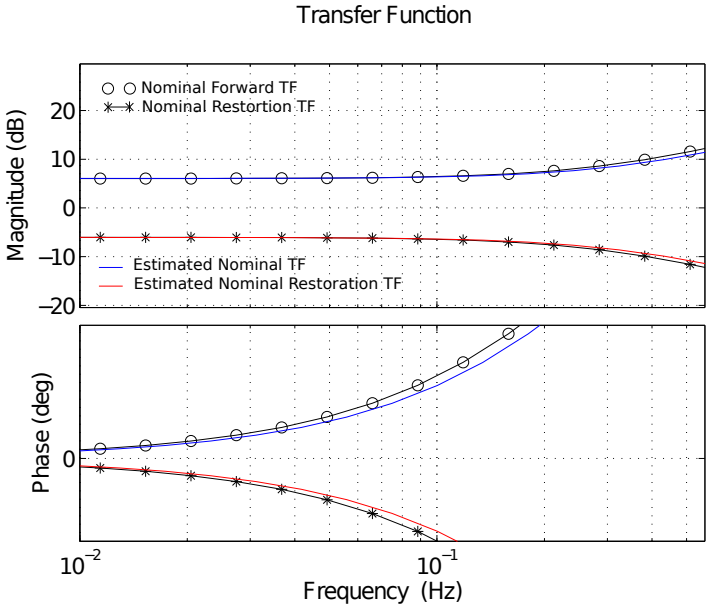

Figure 5.10. Inaccuracies at the high-frequency spectrum of the transfer functions.

Because of these subtle differences in the transfer functions, it is possible that the use of the estimated restoration transfer function will introduce additional error in the input estimate so that both magnitude and phase differ significantly when compared to the original input signal. Therefore, it is vitally important to fully verify and validate the IUA. These are discussed in the following chapters. Specifically, the verification implementation and verification results of using the IUA system are presented and discussed in the next chapter.

6. POTENTIAL CAVEATS OF THE IUA SYSTEM

It would be amiss to leave out particular work that was done or knowledge about the IUA system that gives more insight into particular aspects of this work or attempts to address any limitations or shortcomings that such a system may have. These aspects are grouped together in this chapter but do not necessarily related directly to one another. This section will discuss three possible caveats of the IUA system either because of the IUA or because of the digital restoration.

6.1 Amplifier Usage Over Time

The first potential caveat with using the IUA system could be caused by any changes in the amplifier due to long term use and temperature. As the amplifier is used over a extended periods of time, it could possibly heat up and cause the pole and zero to slightly change. Should the IUA begin to be used in long-term, chronic experiments as a universal amplifier this issue would need to be investigated further. If this were to truly be an issue, one potential solution would be to create a digital adaptive, compensation filter that corrects the DC values based on the DC values from the recorded output signal of the amplifier. The IUA was used only for acute experiments in this work and there was no concern of this issue and the development of such an adaptive/corrective filter was not the concentration of this work.

6.2 Restoration After Amplifier Saturation

The second potential caveat is a result of the fast time-constant of the amplifier and saturation of the signal. The time-constant of the amplifier is 0.0063 seconds and so the system responds very quickly to all frequencies. This is an important characteristic for observa-

tion and recording of bioelectric signals so that frequency content of signals is properly viewed or recorded; however, this feature proves to be a possible limitation of the entire schema because the fast time-constant becomes a slow time-constant, that is approximately 3.14 second long, after the amplifier transfer function is digitally inverted. The slow time-constant of the inverted transfer function will have the greatest affect on low-frequency components of the signals that are being recorded, such as the DC component of the signal. If the signal being recorded should ever become saturated then the DC information (and all signal information that is saturated) is lost forever and the restored signal would not be accurate again until approximately 3.14 seconds after the original amplifier output returns from saturation. The actual verification of this is difficult to show because any saturation of the amplifier will be masked by saturation of the recording system since the dynamic range of the amplifier is greater than the dynamic range of the acquisition equipment used; however, the central point that saturation causes signal loss during digital inversion and restoration may still be displayed. The input signal was also saturated because the same CyberAmp settings were used that had been used during the tuning of the system and so the input was amplified to a magnitude greater than the dynamic range of the acquisition equipment.

Several samples of bench data of sine and square waves of different offsets and different frequencies were collected during which the amplitude content of the signal fluctuated through points of system saturation. Below in Figure 6.1 is one example of a 167 Hz sine wave signal that saturated during acquisition and that shows the inability for the restoration process to recapture or correctly restore the signal due to signal loss during acquisition. Figure 6.1 is the original output of the amplifier. It is clear from this Figure 6.1 that the output collected into the computer was saturated because there is a visible plateau just above the 10 V and below the -10 V amplitudes.

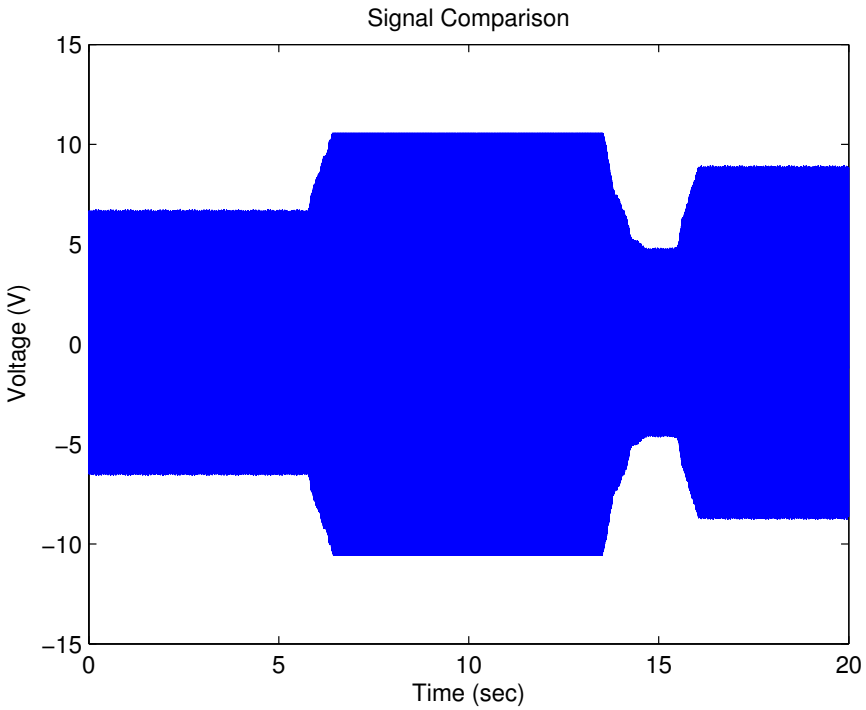

Figure 6.1. 167 Hz sine output wave with saturation.

In Figure 6.2 the original input signal that was acquired is shown (in black) along with the restored signal (in red) for comparison. It is interesting to see that the restored signal reaches the same DC level as the original signal and tracks the signal up until the point that the output signal (blue) in Figure 6.1 becomes saturated.

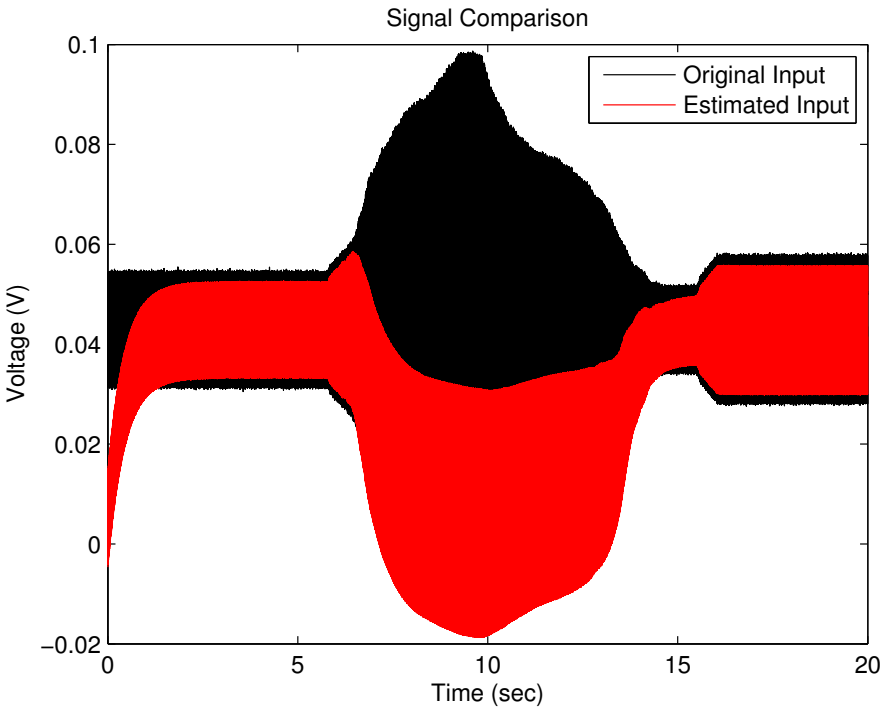

Figure 6.2. 167 Hz input estimate from IUA output with saturated input.

At the point prior to saturation the restored signal follows the path of the original signal and also appears to match the correct DC offset. This can be seen in the zoomed-in view in Figure 6.3.

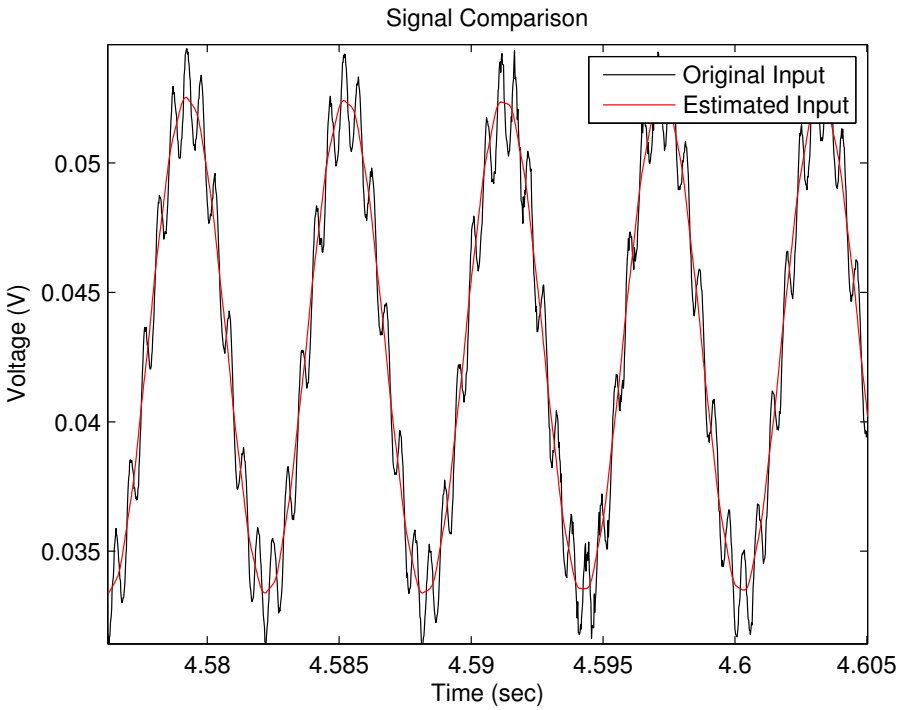

Figure 6.3. Zoomed view of Figure 6.2 prior to saturation showing the accuracy of the estimation.

At the point of saturation the restored signal begins to deflect downward in the opposite direction. At a closer, zoomed-in view in Figure 6.4, it is evident that the representation of the sine wave by the restored signal is also inadequate and begins to look more like a triangle wave.

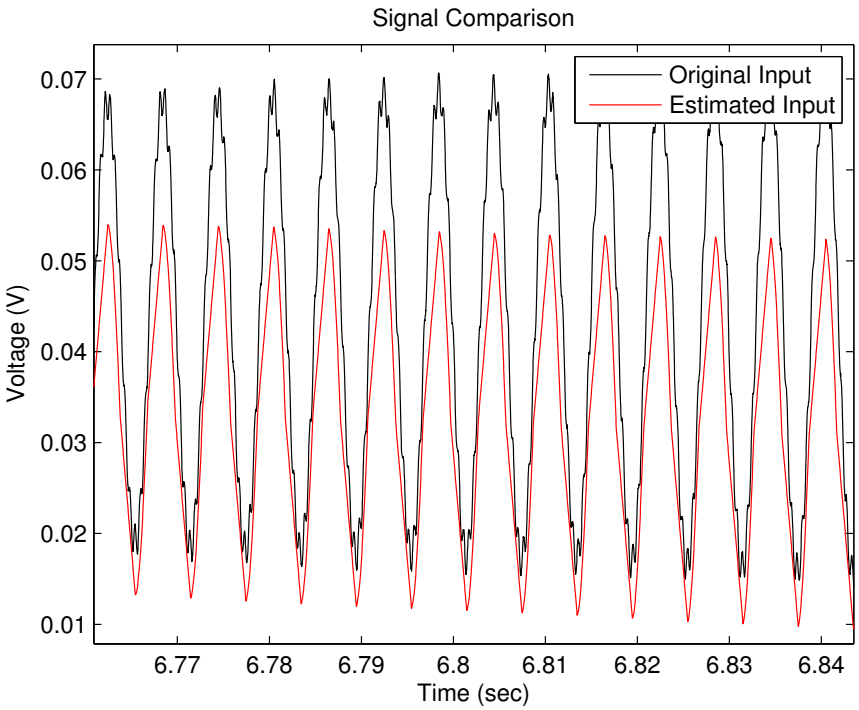

Figure 6.4. Zoomed view of Figure 6.2 showing the effect on signal estimation during the region of saturation.

While this first example with the sine wave and amplitude modulation showed the effect of the amplitude of the signal saturating the amplifier and/or the data acquisition system, the next examples shows the effect of passing an already saturated signal through the amplifier. The input signal now has a much greater offset value and when the amplitude is modulated the signal saturates in the function generator before entering the IUA. By looking at Figure 6.5 below the output signal is only slightly clipped for the first fifteen seconds and then the signal drops into a amplitude that is within the dynamic range of the system.

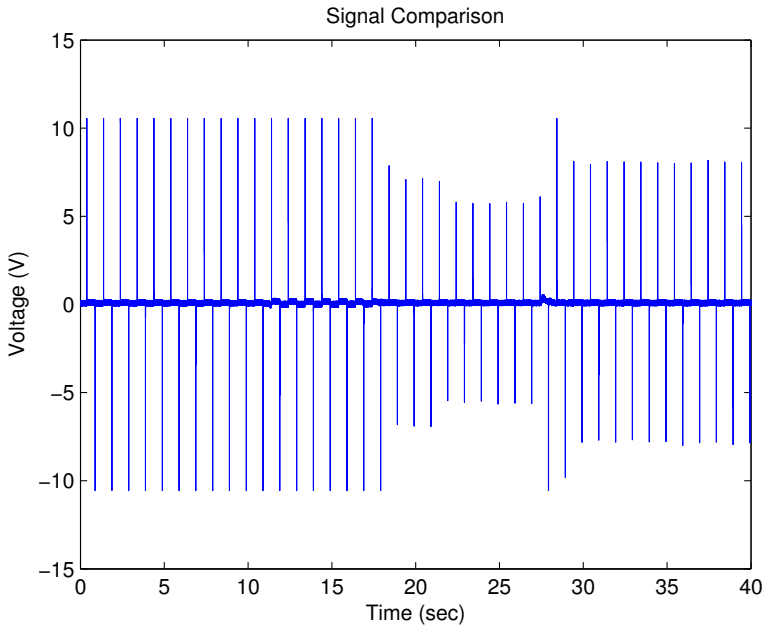

Figure 6.5. IUA output from input of 167 Hz sine wave with saturation.

In Figure 6.6 below, the original input signal is seen in black and the restored signal is shown in red. There is the usual period of the startup transient (green region) while the DC component is matched. The restored signal for the first 10 seconds almost matches the input signal but a careful observation showed that the signal is not completely corresponding to the original input signal due to the slightly clipped output signal. Then after this point the DC offset was increased and the function generator saturated the signal. The input signal becomes saturated shortly after 10 seconds during the large region shown in gray and returns just before 20 seconds has passed. The overall result is that the restored signal is negatively affected during the regions of saturation due to the data that was lost when both the output and the input signal saturated but it is able to correctly represent the original input signal in regions were saturation has not occurred between the time point of 20 seconds to a little after 25 seconds. When returning from saturation, the restored input estimate does end up representing the signal after the effect of the time-constant has passed and the output and input signal are within the smallest dynamic range of the entire acquisition chain.

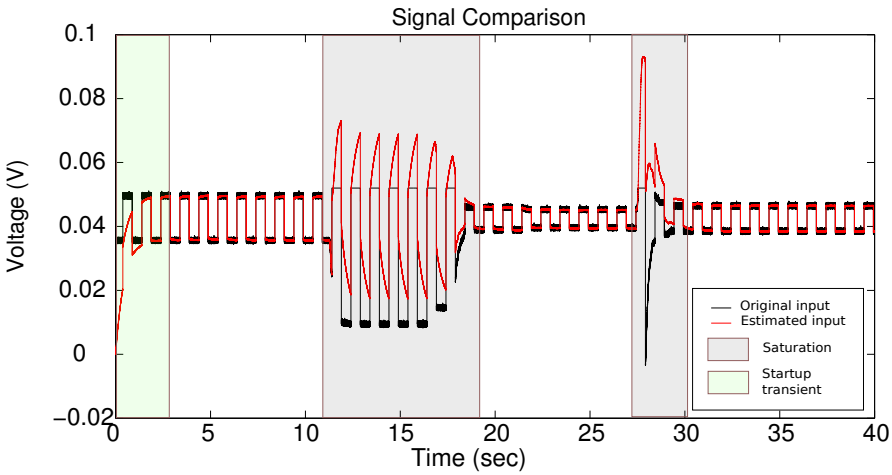

Figure 6.6. Original saturated input and input estimate. The startup transient is shown in green. The regions of saturation of are shaded gray. The signal matches in the regions without saturation.

6.3 Variable Bit Weight of the IUA

The third caveat is caused by the variable bit weight of the IUA. The issue is best described by a comparison between the a standard flat amplifier and the IUA. With a completely flat amplifier with ideal infinite bandwidth and infinite range and a gain of 1000x, for example, that this is sampled by a 12 bit ADC, which has an input range of -10 V to +10 V, the bit weight of the whole amplifier and ADC chain is $\frac{1}{1000}\left(\frac{20}{2^{12}}\right)$. Then the quantization error of the flat amplifier is $\pm\frac{1}{2}$ the bit weight, which is constant over all frequencies in this case. In the case of the IUA, the gain is variable and so one can see that the bit weight and also the quantization error will also be variable. At high frequencies the quantization error is $\pm\frac{1}{2}\left(\frac{1}{1000}\right)\left(\frac{20}{2^{12}}\right)$. At low frequencies, it is $\pm\frac{1}{2}\left(\frac{1}{2}\right)\left(\frac{20}{2^{12}}\right)$, and in the transition zone, it is something in between. Thus, during analysis one will be able to resolve signals at high frequencies at the greatest resolution with a decrease in resolution when decreasing in frequency.

These differences in bit weight and quantization error between a flat amplifier and the IUA can also have an impact on the noise in the amplifier and data acquisition chain. For

example, if the noise peak-to-peak voltage is around 100 nV across the 20 kHz bandwidth of the system, then it would be scaled by the gain of the IUA depending upon the frequency, which will result in the signal being recorded differently until the it goes through the restoration process at which time the noise will have the same amplitude as it did before it was recorded but will be bandwidth-limited. This is also true, if for example, the noise floor is dominated by thermal sources at the electrode interface and these thermal sources are basically white and Gaussian distributed and have a peak-to-peak voltage of about ±10 μV for 20 kHz bandwidth, then it will also be shaped by the amplifier and recorded that way. After recording it will be apparently smaller at higher frequencies and lower at lower frequencies until the signal is restored. In the case where noise or signal is introduced into the amplifier-ADC chain before the amplifier, then the it will be shaped by the amplifier and will be restored during the digital inversion. The other case to consider is when signal or noise is injected into the chain after the amplifier, in which case the noise will not be shaped by the IUA and so the noise will be recorded normally. The issue then is when the signals recorded from the amplifier-ADC chain are restored in the computer that the noise injected post-amplifier will be shaped by the restoration process.

7. BENCH VERIFICATION TESTING OF THE IUA SYSTEM

With the development of the IUA so far described and discussed, the progress has been made toward completing the aims to (Aim 1) design and implement a new high-impedance input, low-noise, low-bias current amplifier that provides an invertible universal amplifier for bioelectric recordings with appropriate bioelectric-oriented analog filtering that is easily and accurately estimated and inverted through digital processing, and (Aim 2) leverage the power of digital signal processing to invert the amplifier transfer function and restore the recorded signal to an accurate representation of the original signal, which may then be digitally processed in ways that minimize distortion of morphological characteristics. However, these aims cannot be called successful without testing the amplifier and the restoration process and both verifying that it is working has theorized and that it works in real-world application. The first steps of verifying its function is described in this chapter.

7.1 Bench Restoration Verification Set Generation and Collection

Verification-sets were generated using a GW Instek SFG-2110 function generator. A total of 45 verification sets were created divided into three different waveform groups. The waveform groups were square, sine, and triangle waves. There were thus a total of fifteen (15) waveforms in each group. Offsets of varying magnitudes divided into 5 groups in the range from 0 to 2 volts (classified as none, small, medium, large, and very large) were pseudo-randomly added to the fifteen (15) waveforms in each group so that there was at least one type of each offset classification in the group. The selected frequencies of the signals in each group were 13, 60, 159, 500, and 1616 Hz. The verification-set data were collected using the IUA and the 16-bit NI USB-6251 data acquisition system and were sampled at 48 kHz. A standard PC and the Mr. Kick II data acquisition software was used. The output from the IUA was then filtered with the restoration coefficients from the

system identification and restored to its original ratios using the developed Matlab analysis code. Error analysis was conducted on the IUA as the means of comparing the result of restoration to the original input to the IUA system and to determine the accuracy of the restored signal as described in Section 5.8.

7.2 Bench Restoration Verification Analysis and Results

The RMS voltage of the difference of the original signal and the restored signal estimate was computed over approximately the last 6 seconds of the data sets because this is in the region during which effect of restoration had settled. The RMS value of the original input signal was computed and then the percent error for each data set was calculated with these RMS values. The mean percent error after convergence of all forty-five verification sets was 4.7821%±6.0406%. The largest portion of the error is concentrated around the data sets with no offsets and will be discussed. It is important to view an enlarged region after the restoration filter has converged to the DC value and determine the percent error in the region after DC convergence because as there is a period of time that the restored signal has an incorrect DC value.

7.2.1 Verification Sets with Negative Offsets

The first verification sets to be analyzed where the sets that had negative offsets. In Figure 7.1 below, an example of the case of a negative DC offset is shown.

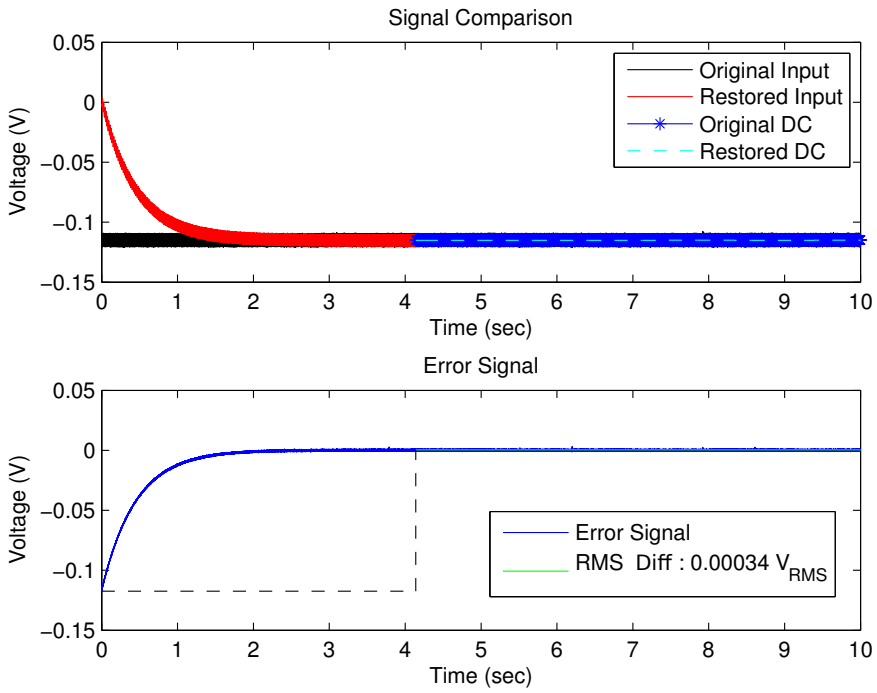

Figure 7.1. Example of a negative offset verification set showing the original and restored estimated input signal and DC values. The difference was labeled as the error signal and the RMS voltage of the error signal (RMS Diff) was calculated over the last 6 seconds.

It is observed that initially there is an incorrect prediction of the offset. While it appears that this region is only over a period of 3.14 seconds in accordance with the restoration time-constant, the region is extended to ensure consistent analysis across all data sets and is identified by the black dashed line in the error signal. Below in Figure 7.2 is a view of the region in which the signal is beginning to settle.

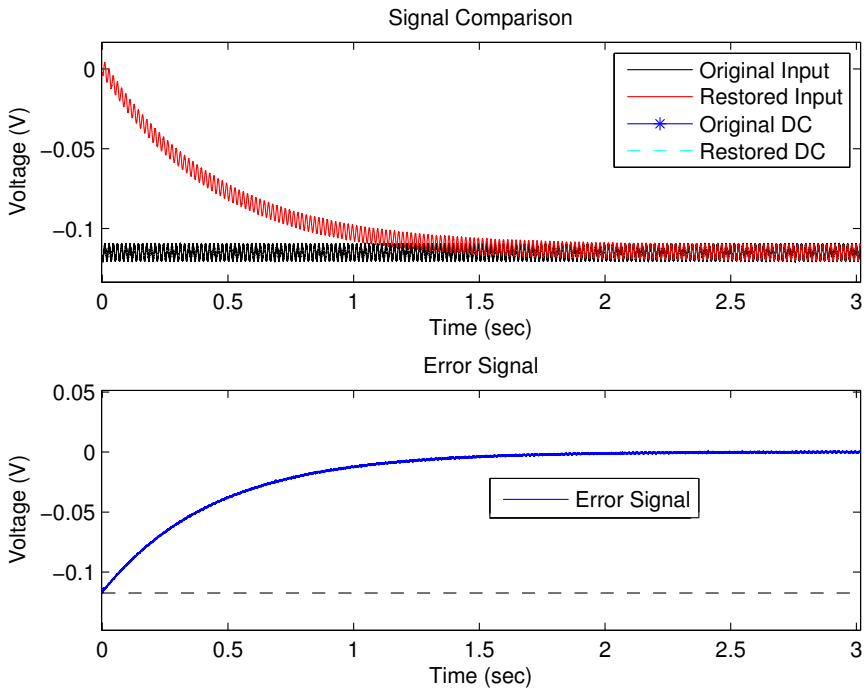

Figure 7.2. Enlarged view of Figure 7.1 in the region before convergence.

Once the DC value has converged there is close resemblance in between and will be at the state that closely matches the signal. Below in Figure 7.3 is a zoomed view of the same signal in the region after convergence of the DC values. It is clear that in this region the DC values and the time-varying waveforms match very closely.

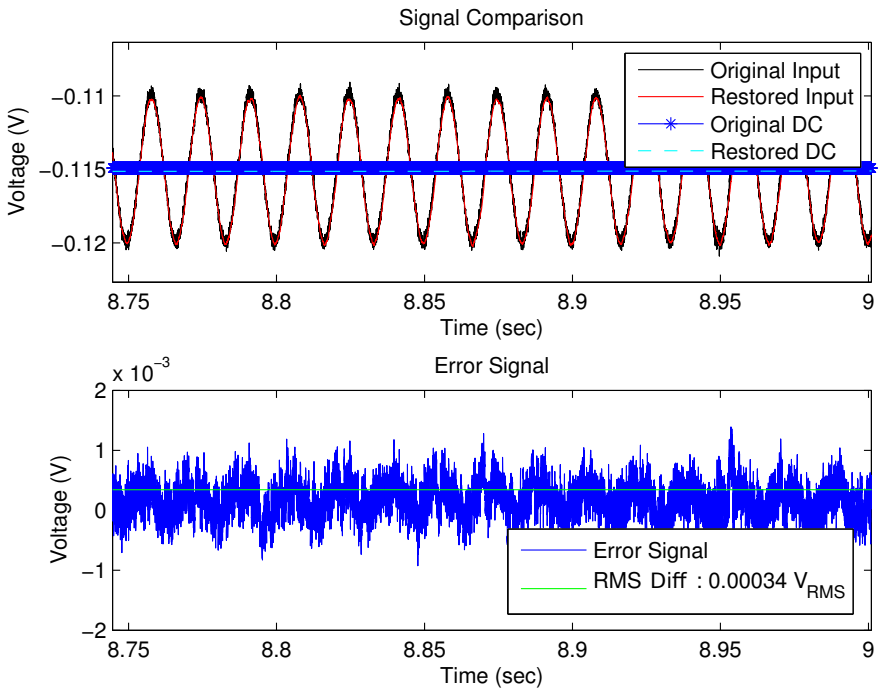

Figure 7.3. Enlarged view of Figure 7.1 in the region of after convergence showing the original and restored estimated input signal and DC values. The difference was labeled as the error signal and the RMS voltage of the error signal (RMS Diff) was calculated over the last 6 seconds.

In this case above the percent error between the restored input signal and the original input signal with their DC components was 0.30% while without their DC components it was 1.71%. The percent error without the DC component was computed to analyze the effect that a non-zero offset had on the signal. A total of 15 verification sets with negative DC potentials at different frequencies were tested and had a mean percent error of 1.35%±1.00%. The percent error for each verification set with a negative offset is shown in Figure 7.4 below with their DC components as well as without their DC components. It may be seen that the estimated input is more accurate with its DC components. It is thought that this evidence of the reality of the variable bit weight of the IUA at work in which case the DC component is more difficult to resolve, but especially when its amplitude is very small.

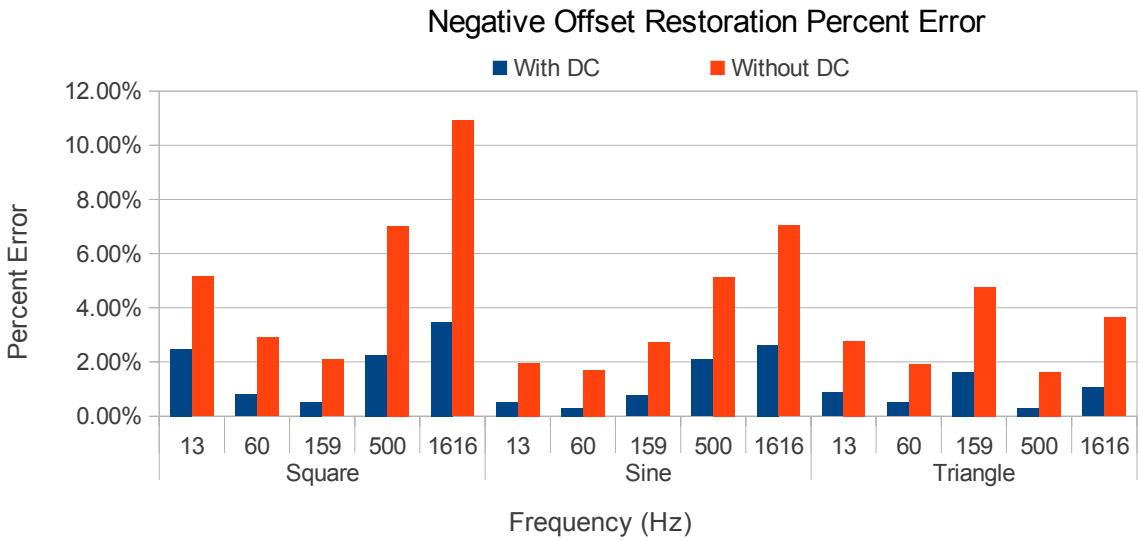

Figure 7.4. Restoration percent error for all negative offset verification sets. The percent error is based on the RMS voltage of the last 6 seconds of the original input signal and the error signal.

7.2.2 Verification Sets with Positive Offsets

Besides a negative offset, the other two cases to evaluate are a positive DC potential and no DC potential. Figure 7.5 below shows a restoration signal with a positive DC potential. It can be seen in this figure that there is the previously mentioned DC error over the first few seconds of the waveform. This signal is a triangle wave at 1616 Hz.

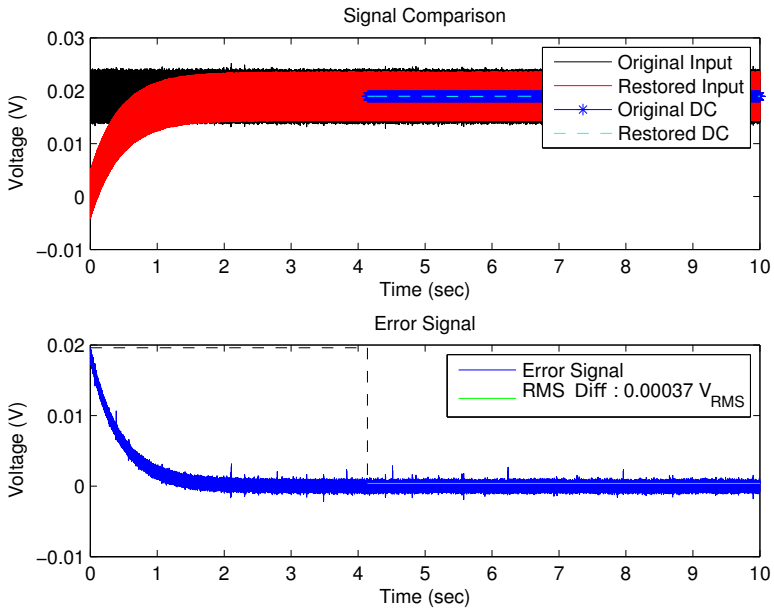

Figure 7.5. Example of a positive offset verification set showing the original and restored estimated input signal and DC values. The difference was labeled as the error signal and the RMS voltage of the error signal (RMS Diff) was calculated over the last 6 seconds.

For the case above, the percent error between the restored input signal and the original input signal with their DC components was 1.92% while without their DC components it was 5.93%.

In the Figure 7.6 it is seen that the DC component is held steady and the original signal is matched closely the the restored input signal estimate.

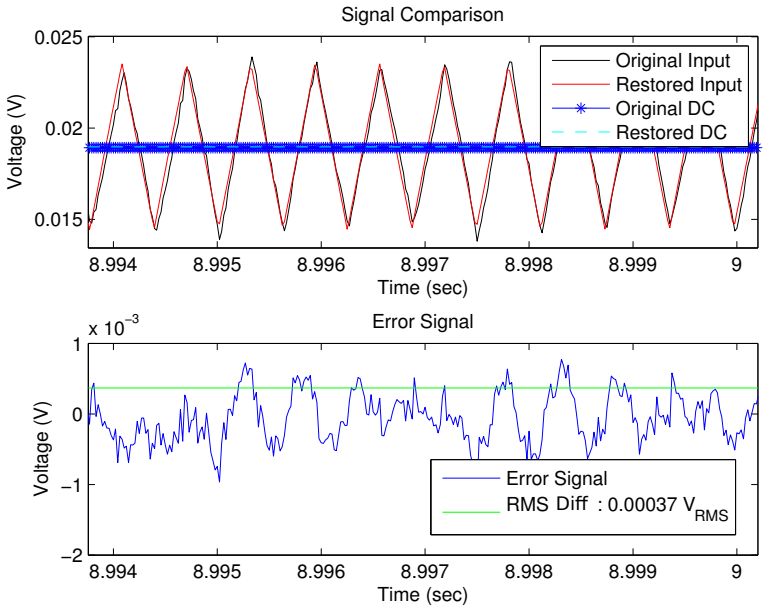

Figure 7.6. Enlarged view of Figure 7.5 in the region of after convergence showing the original and restored estimated input signal and DC values. The difference was labeled as the error signal and the RMS voltage of the error signal (RMS Diff) was calculated over the last 6 seconds.

The restored signal matches both the DC component and the original signal very well. A total of 15 verification sets with a positive DC potential at different frequencies were tested and had a mean percent error of 1.02%±0.89%. The percent error for each verification set with a positive offset is shown in Figure 7.7 below. There does not appear to be any evidence of a trend in the percent errors over the different frequencies and waveforms.

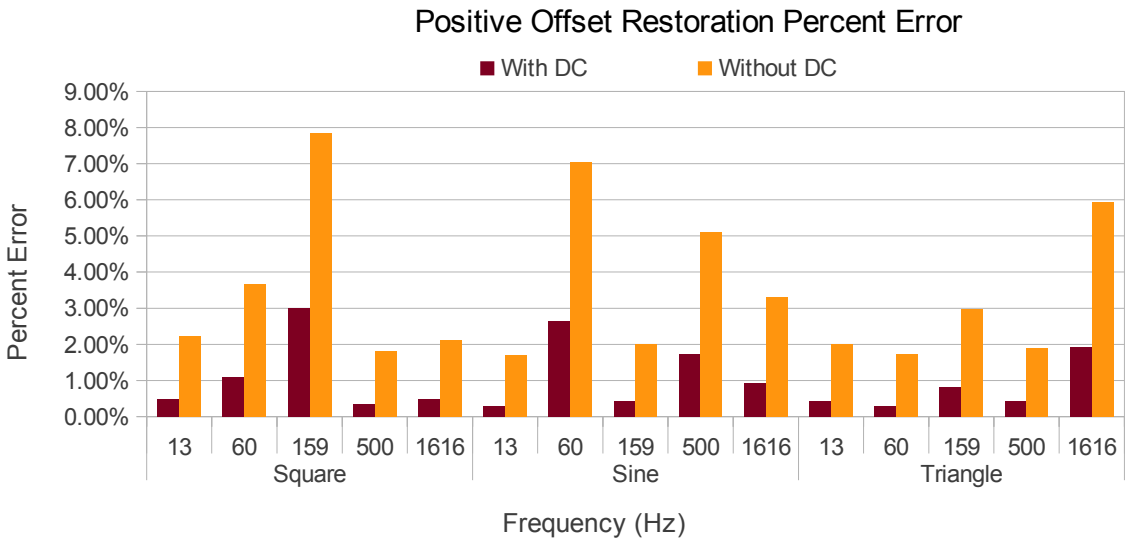

Figure 7.7. Restoration percent error for all positive offset verification sets. The percent error is based on the RMS voltage of the last 6 seconds of the original input signal and the error signal.

7.2.3 Verification Sets with No Offset

The analysis of the final offset case is the case of no offset. An example of the results of the analysis from the no-offset verification sets is below in Figure 7.8. However, no DC potential was impossible to achieve and so there is always a small offset due to the errors of the function generator.

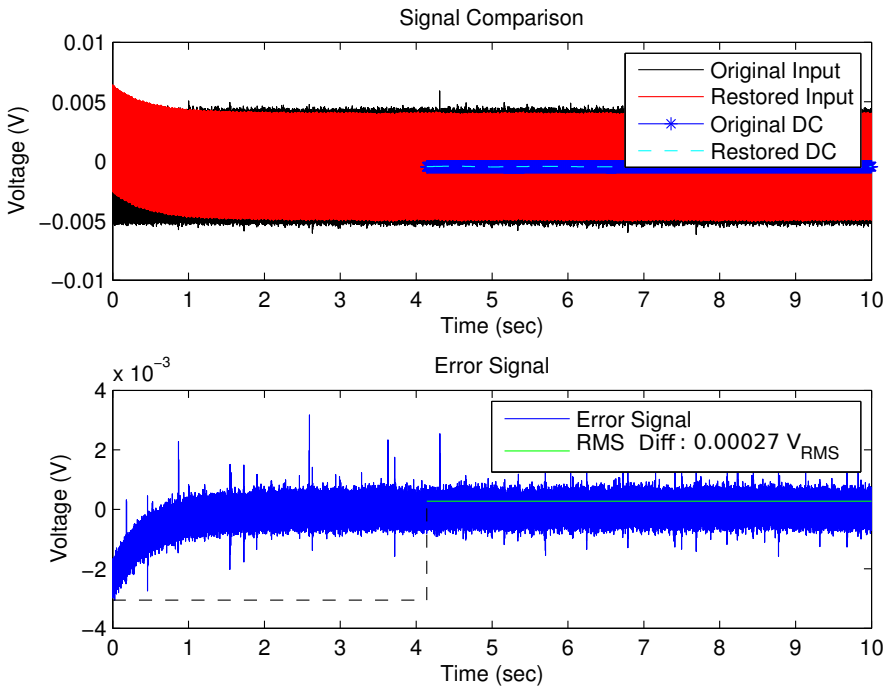

Figure 7.8. Example of a no-offset verification set showing the original and restored estimated input signal. The difference was labeled as the error signal and the RMS voltage of the error signal (RMS Diff) was calculated over the last 6 seconds.

The frequency of the signal shown above is 159 Hz and yet again it should be observed that there is a DC error at the beginning of the restored signal; however, it is less significant than the the negative and positive DC cases.

To follow the convention of showing a region after convergence, Figure 7.9 is shown. Figure 7.9 shows that the time-varying aspect of the signals match closely and that the DC potential of the restoration signal closely meets the zero-offset.

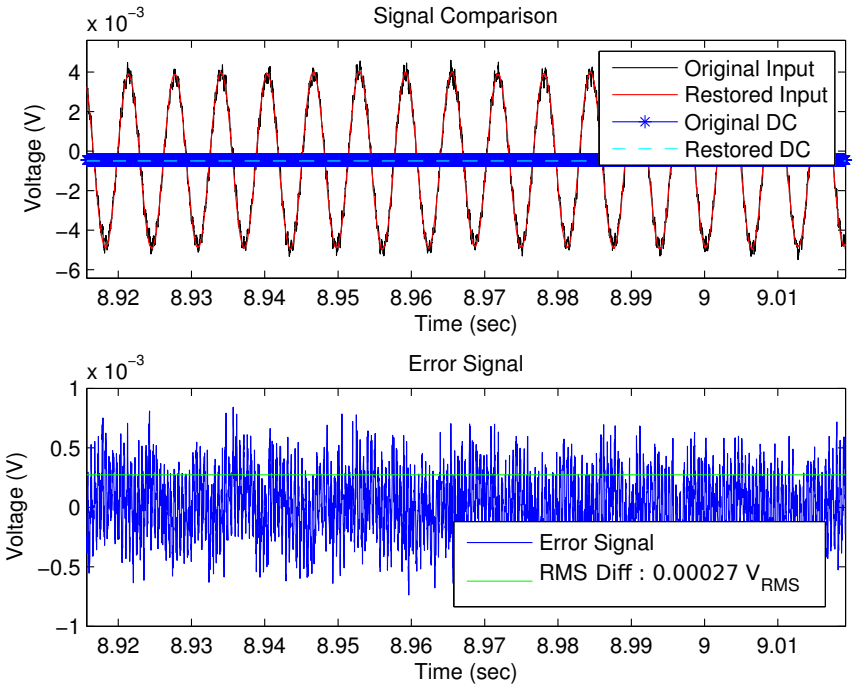

Figure 7.9. Enlarged view of Figure 7.8 in the region of after convergence showing the original and restored estimated input signal. The difference was labeled as the error signal and the RMS voltage of the error signal (RMS Diff) was calculated over the last 6 seconds.

Once the signal as settled at the DC value it continues to track the original input as has been shown before. The percent error between the restored input signal and the original input signal was 8.73%. In total, 15 verification sets with no DC potentials were tested and had a mean RMS error of 11.79%±5.52%. The percent error for each verification set with no potential is show in Figure 7.10 below.

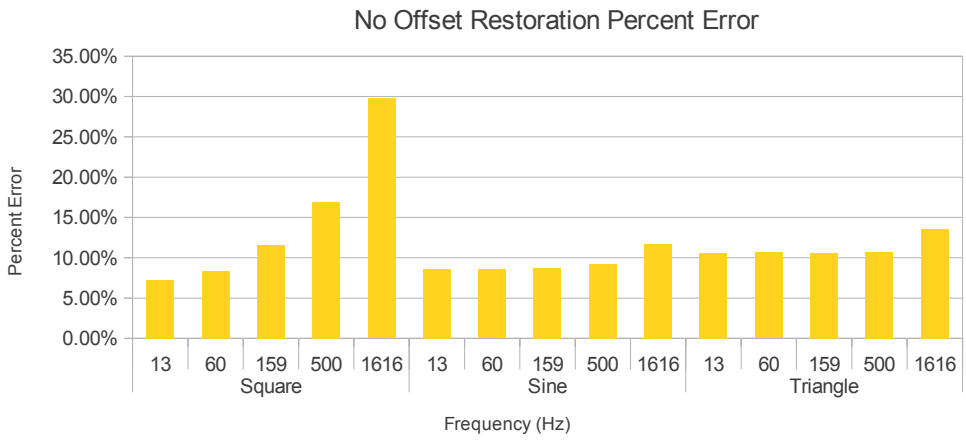

Figure 7.10. Restoration percent error for all no-offset verification sets. The percent error is based on the RMS voltage of the last 6 seconds of the original input signal and the error signal.

From Figure 7.10 above, it is clearly seen again that the square wave at the high-frequencies has the highest percent error for all the no-offset verification sets. Although this was investigated it was thought that perhaps it was a limitation of the function generator while producing a -40 dB magnitude square wave (TTL) signal at high frequencies. Even at the same frequencies (500 Hz or 1616 Hz) when the waveform is changed to sinusoidal or triangle the function generator is able to correctly output the signal. Another reason that the percent errors for these zero-offset data sets are higher than the negative and positive offset data sets without their DC components may be attributed to errors introduced into the DC component when amplifying the original input signal with the CyberAmp and then rescaling it within the computer. The CyberAmp was discovered to introduce various offsets into the amplified original input signal depending on how it was setup; however, it was identified post-analysis and could only be corrected for by subtracting off residual error between the DC values of the original input and the restoration signal. Despite this the percent error was still considerably higher then the sets with offsets and this is most likely because not all error due to the external amplifier was removed or accounted for.

8. IN-VIVO VALIDATION TESTING OF THE IUA SYSTEM

The next part of ensuring that the IUA system works as theorized and verified is to validate it through in-vivo use cases. The validation of the IUA system involved using it in two in-vivo cases using thin-film multi-site electrodes meanwhile comparing it to another standard amplifier in order to test and compare the restoration and post-acquisition digital signal processing on the signal. The first case was primarily recording ECG. The aim of the second case was to record neural activity in the hope of recording single-fiber action potentials along with some EMG. For the remainder of this chapter, the methods and procedures for these in-vivo cases will be described and the results of the data analysis presented and discussed.

8.1 In-Vivo Amplifier Implementation

With a low percent error for restoration on the bench the next test of the IUA was to use the IUA along with a second amplifier that had similar input and secondary stages in-vivo and compare the post-processed IUA signal to a custom amplifier. The difference between the two amplifiers was that the second amplifier was a standard flat bandwidth preamplifier configuration with a 3-dB point at approximately 72 Hz. This flat-bandwidth amplifier would served as a reference for evaluating the accuracy of restoring the in-vivo data. For this the IUA and the standard flat bandwidth pre-amplifiers were used during the recording of bioelectric signals containing primarily ECG from Sprague Dawley rats and and ENG and EMG from New Zealand rabbits.

8.2 Animal Preparation for Each In-Vivo Case

The experimental procedures for the in-vivo use case with the rabbits were conducted under IACUC approved protocols by the IUPUI School of Science Animal Resource Center (SARC). The experimental procedures for the in-vivo use case with the rabbits were conducted under IACUC approved protocols by the Indiana University School of Medicine Laboratory Animal Resource Center (LARC). The following sub-sections will detail the methods and procedures used during the recording sessions with each animal.

8.2.1 Preparation for Recording ECG From the Sprague Dawley Rats

The first use case for recording the ECG using the thin-film multi-site electrodes involved the Sprague Dawley rats. The rats were anesthetized using 0.2 mL of a Ketamine/Xylazine cocktail (87.7 mg/mL Ketamine, 12.3 mg/mL Xylazine). The underside of the neck of the rat and its left side of the chest were shaved. The rat was placed on its back and secured to the table using tape. An incision was made along the underside of the neck and access to the trachea was gained. Three 10-0 – 8-0 sutures of two to three inch lengths were placed underneath the trachea and esophagus. The trachea was lifted slightly using small forceps and a small incision was made on the trachea in order to create an opening to insert the silicon tubing for the respirator. The respirator was turned on and the silicon tubing was inserted into the trachea. The sutures were used to secure the silicon tubing to the trachea without constricting the air passage. The silicon tube was temporary held in place by packing the surrounding space with cotton dots and securing a gauze over the opening in the neck. The rat was then placed on its right side and was checked to make sure that it was breathing with the respirator. A left thoracatomy was then performed. An incision was made between the fourth and five rib and access into the chest was gained. The lungs were held out of the way using gauze and the left atrial appendage (LAA) was identified. The pericardical sac was opened slightly to allow the atrial appendage to be manipulated and to expose the area where the Ligament of Marshall (LOM) should be located (above the LAA and adjacent to the left superior pulmonary vein (LSPV)). The rat was given 0.1 mL

intramuscular injections of the Ketamine/Xylazine cocktail as needed when non-breathing movement or movement to the tail-pinch reflex were observed.

8.2.2 Preparation for Recording ENG and EMG from the New Zealand Rabbits

The rabbits were anesthetized using a Rompun cocktail be prepared from stock solutions of Ketamine (50 mg/ml), Xylazine (20 mg/ml) and Acepromazine (10 mg/ml) in the relative ratio of Ketamine:Xylazine:Acepromazine of 20:2.5:1.Anaesthesia was induced with an intramuscular dose of the Rompun cocktail using an initial dosage of 1.25 ml/kg. This dosage corresponds to 25 mg/kg Ketamine, 0.125 mg/kg Xylazine and 0.125 mg/kg Acepromazine. The experimental and contralateral hind limb were shaved to the hip. The skin on the experimental leg was treated with a topical applicaton of lidocaine spray for at least 5 minutes. The lidocaine treatment helps to maintain the level of anaesthesia during surgical handling and manipulation of the skin. Following the treatment period, the skin will be rinsed using saline and sponged dry before an incision was made. Periodic hourly intramuscular injections of 0.625 ml/kg was used to maintain anaesthesia.

The depth of anaesthesia was monitored by testing reflex responses to the cornea, ear, and paw withdrawal. Additional intramuscular injections of 0.625 ml/kg were administered as needed in case of non breathing related movement or obvious reflex responses. Rectal body temperature, and heart rate were monitored to assess the depth of anaesthesia, and the health of the preparation. During the entire experiment, the rabbit was be placed with its upper body on its side. The lower body below the hips was be placed approximately in the prone position or on the same side as the upper body, with the experimental leg on top.

An incision on the lateral side of the upper leg near the knee to expose the femur near its distal epiphysis. An incision on the lateral side near the ankle to expose the distal epiphysis of the tibia. Holes were drilled through distal epiphyses of the experimental legs tibia and femur to enable anchor pins to be attached to the bone. Anchor screws (3mm dia. x 1.5cm Stainless Steel screws) were placed through the holes in the tibia and femur with the head of the screw on the medial side, and into stainless steel anchor rods. The Achilles tendon

and cancaneous were exposed and freed from the fascia and connective tissue between the tendon and the tibia.

Peripheral nerve electrodes implanted consisted of two types: 1) a control electrode, the circumferential cuff electrode or hook electrode, and 2) test electrodes: LIFE, tfLIFE or TIME. Cuff electrodes are silicon tubes with multiple electrode contact rings embedded on its inner surface, and a slit cut longitudinally down one side to enable implantation. They are typically implanted by sliding the nerve into the silicon tube through the slit, and secured closed by carefully tying sutures around the silicon tube. LIFE, tfLIFE and TIME served as the test electrode and are penetrating electrodes implanted into the body of the peripheral nerve fascicle. They are ribbon like structures that are sewn into the nerve with the aid of a 80 – 120 m diameter needle. The needle is discarded after implantation. The structures are anchored by tying the structure to the nerve trunks epineurium using 10-0 – 8-0 sutures.

The test and control electrodes were displaced from one another along the nerve to enable nerve conduction tests. Two access points to the sciatic nerve or branches of the sciatic nerve were created in order to place the electrode structures into the endoneural space. The proximal access point will be at the level of the thigh. A lateral incision will be made to access the sciatic nerve between the sciatic notch and the popleteal fossa. A set of peripheral nerve electrodes will be implanted at this site. The access to the sciatic nerve was temporarily closed using stainless steel staples or towel clamps. A second access to the nerve was created at the level of the popleteal fossa. Following an incision through the skin, the popleteal fat pad will be removed to enable visualization of the branching of the sciatic nerve. The lateral gastrocnemius and soleus (LG/S) nerve, the myasthenis gravis (MG) nerve, the common peroneal (CP) nerve and deep tibial nerve branches were identified. Electrodes were implanted at this level into one or more of these branches of the sciatic nerve. The distance between the electrodes at the distal access and proximal access points will be measured. The skin overlying the implant sites was temporarily closed using stainless steel staples or towel clamps to prevent drying of the tissues, and periodically moistened using normal saline (0.9% NaCl).

8.3 In-Vivo Recordings

The methods for recording in each in-vivo case is described below. The first case is the recording setup with the rats and the second section covers the methods used when recording from the nerves in the rabbits.

8.3.1 Recording Methods for the Rat In-Vivo Validation

For recording from the rats, a third generation transverse intrafasicular multi-channel electrode (TIME V3) electrode structure [18] was placed in the space between the LSPV and the LAA and packed into place using cotton dots. A TIME V3 electrode was separately connected to each implemented amplifier in two different recording experiments. Bioelectric signals were recorded from the area between the LAA and the LSPV over a period of approximately one minute repeatedly during each experiment. The data collected during these experiments was collected at a sampling rate of 48 kHz using a 16 channel DSP, 16-bit simultaneously sampled Innovative Integration M67 with AD16 omnicard DAC that sampled from DC to Nyquist rate.

8.3.2 Recording Methods for the Rabbit In-Vivo Validation

For recording from the rabbits, a tfLIFE electrode was placed in the tibial nerve. The tfLIFE electrode was separately connected to each implemented amplifier during each recording experiment. A cuff electrode was placed farther dorsal along the tibial nerve as per the animal preparation. The first type of recording experiment involved stimulating the nerve using the cuff electrode with a stimulus amplitude of 50, 75, 100, 125, or 150 μA at 1 Hz rate with a pulse delay of 100 μsec while recording from the tfLIFE. The type of second recording experiment involved manually manipulating the left leg while recording from the tfLIFE. The data collected during these experiments was also collected at a sampling rate of 48 kHz using the same 16 channel DSP, 16-bit simultaneously sampled

Innovative Integration M67 with AD16 omnicard DAC system used while recording from the rats.

8.4 In-Vivo Data Signal Processing, Results, and Discussion

As with the bench verification data, the in-vivo bioelectric signals collected using the IUA system were returned to the prerecorded state by filtering the signal in Matlab using the restoration parameters. Then in order to compare the IUA system system and digital signal processing with that of analog signal processing, the restored data was further filtered using the same characteristics of the flat bandwidth amplifier (i.e. 1st order, 72 Hz, high-pass filter). The amplitude of the restored data was amplified to match the amplification of the signal from the flat bandwidth amplifier. The flat-bandwidth amplifier and the scaled restored data were QRS-triggered averaged and compared through a RMS voltage difference leading to the calculation of a percent error, which allows analysis to determine the accuracy of digital filtering of restored bioelectric signals. This type of analysis was necessary because in the case of in-vivo validation the original input signal is not known but by comparing the post processed signal to another filtering amplifier, the accuracy of the restoration may be in some way assessed.

8.4.1 Results and Discussion of the ECG Data

The comparison of the restored, post-processed ECG signals from the IUA to ECG signals from the flat-bandwidth amplifier is shown in Figure 8.1 and Figure 8.2. Figure 8.1 and Figure 8.2 show two different sequential instances of normalized ECG recordings, which have been QRS-triggered averaged. The data was detrended in Matlab so that percent error analysis could be conducted and represent the error only in the shape of the waveform without additional error due to amplification differences.

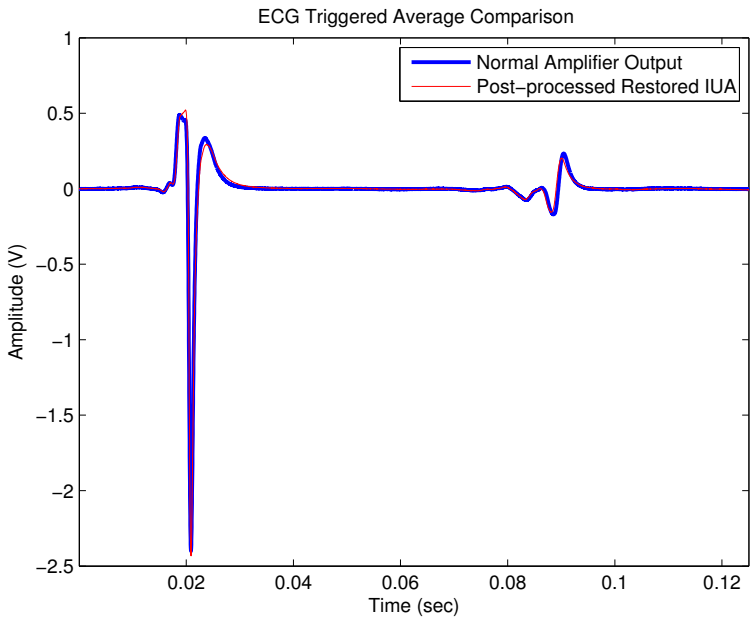

Figure 8.1. The first QRS-averaged ECG example. The percent error was 13.66%.

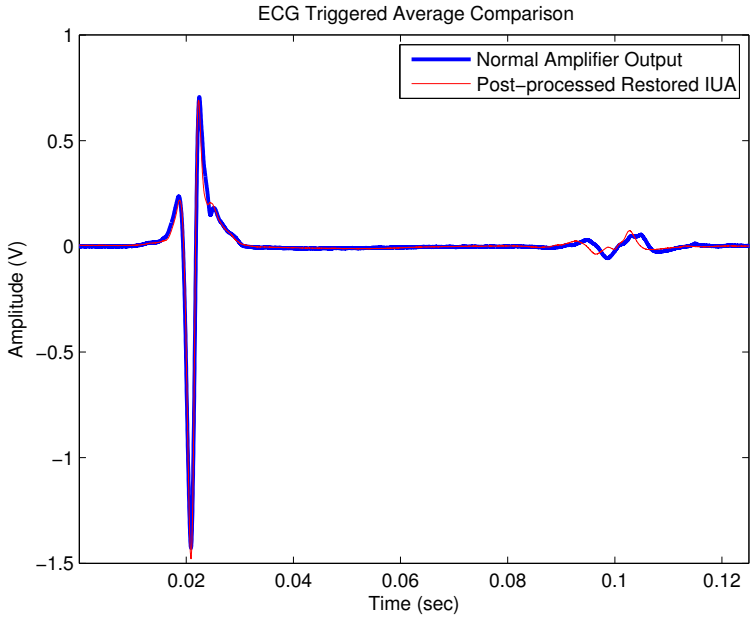

Figure 8.2. The second QRS-averaged ECG example. The percent error was 15.63%.

The time between recording was approximately twenty minutes and the electrode position and packing was adjusted. The IUA system data was initially restored using the previously described methods and then post-processed using the nominal characteristics of the normal amplifier. Although the two signals in Figure 8.1 have noticeable difference in their details, percent error for the QRS-triggered average shown in each figure was found to be 13.66% and 15.63% for Figure 8.1 and Figure 8.2 respectively. The signals being compared were not collected simultaneously. Since the electrode was merely packed into place using cotton dots, differences between them may be due to possible electrode movement, since it resides in between two parts of the beating heart, or may be due to normal physiological changes between sequential recording times leading to possible changes in heart rate. The spectral distribution of these signals was also plotted for comparison. A Hamming window was applied to the QRS-triggered averaged signal and then the FFT was computed using Matlab. In addition, the spectral distribution of the restored IUA system data for each set was included. The spectral distributions relating to the signals in Figure 8.1 and Figure 8.2 are shown in Figure 8.3 and Figure 8.4 respectively. In Figure 8.3, it can be seen that the normal amplifier output has a different magnitude-frequency relationship than the post-processed IUA system output. This is attributed to the differences in recording time and setup, because in Figure 8.4, there does not seem to be this difference.

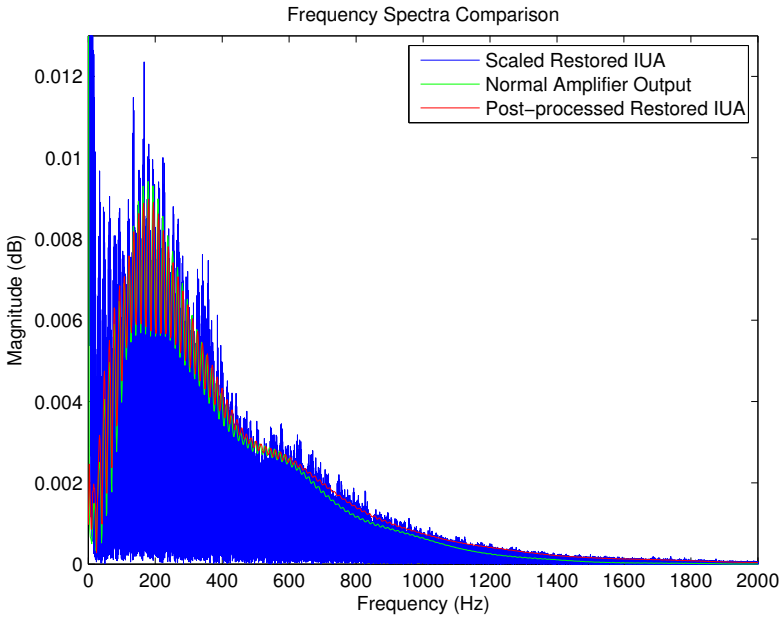

Figure 8.3. The FFT comparisons for the first QRS-averaged ECG example.

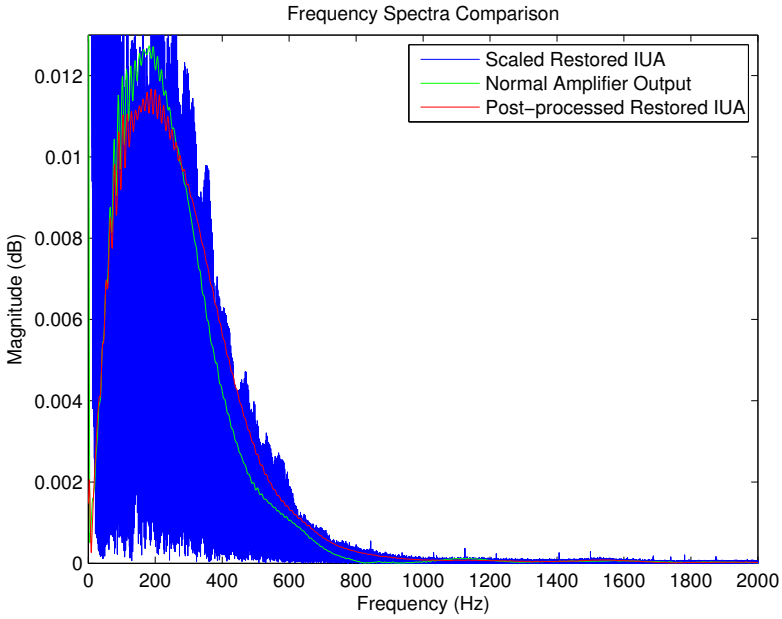

Figure 8.4. The FFT comparisons for the second QRS-averaged ECG example.

In either Figure 8.3 or Figure 8.4 it should be noted that the spectral distribution of the normal amplifier and the post-processed IUA system have the same general magnitude-frequency characteristics. It should also be noted that the scaled spectral distribution of the restored IUA system data also has the same general magnitude-frequency characteristics except for frequencies around and below 72 Hz, which was the corner frequency of the normal amplifier. These observations of the spectral distributions confirm that spontaneous bioelectric data collected with the IUA system is able to be restored, digitally post-process and produce waveforms that are similar in both time and frequency characteristics as a specific analog amplifier would.

8.4.2 Results and Discussion of the ENG and EMG Data

The second case of the in-vivo work involved stimulation and recording compound ENG and EMG. Two instances of the compound ENG and EMG that was collected and processed is shown below in Figure 8.5 and Figure 8.6. The data in these figures was spike-triggered averaged over at least 40 spike-trains.

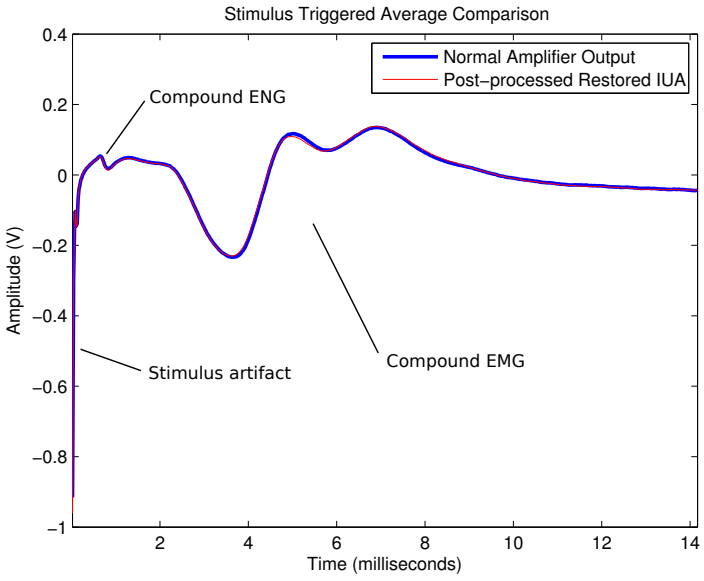

Figure 8.5. The first stimulus-triggered averaged compound ENG and compound EMG example. The percent error was 4.84%.

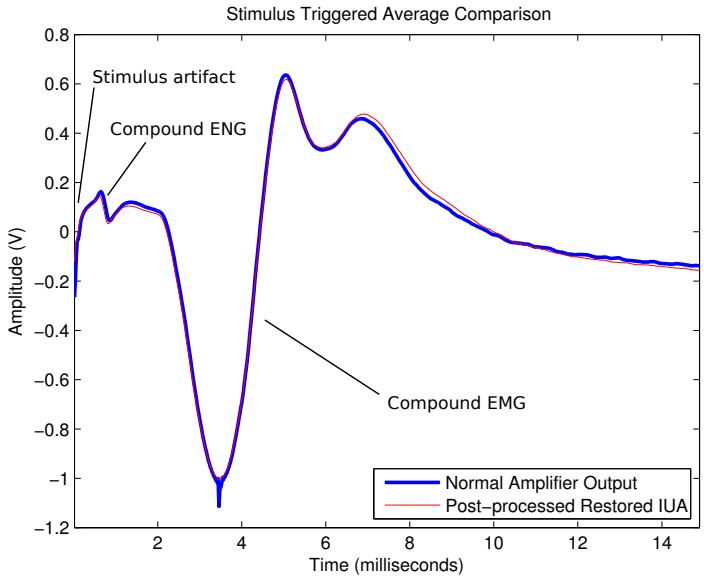

Figure 8.6. The second stimulus-triggered averaged compound ENG and compound EMG example. The percent error was 5.94%.

Since the bioelectric events were driven by the stimulus the waveforms were much more repeatable and in both Figure 8.5 and Figure 8.6 there seems to be a high degree of similarity between the normal amplifier output and the post-processed, restored output. The FFT of the spike-triggered average signals in Figure 8.5 and Figure 8.6 was computed using Matlab and is displayed in Figure 8.7 and Figure 8.8, respectively. A Hamming window was applied to the averaged signal before the FFT was computed. In Figure 8.8 and Figure 8.8 the scaled FFT of the restored IUA system data for Figure 8.5 and Figure 8.6, respectively, was also included.

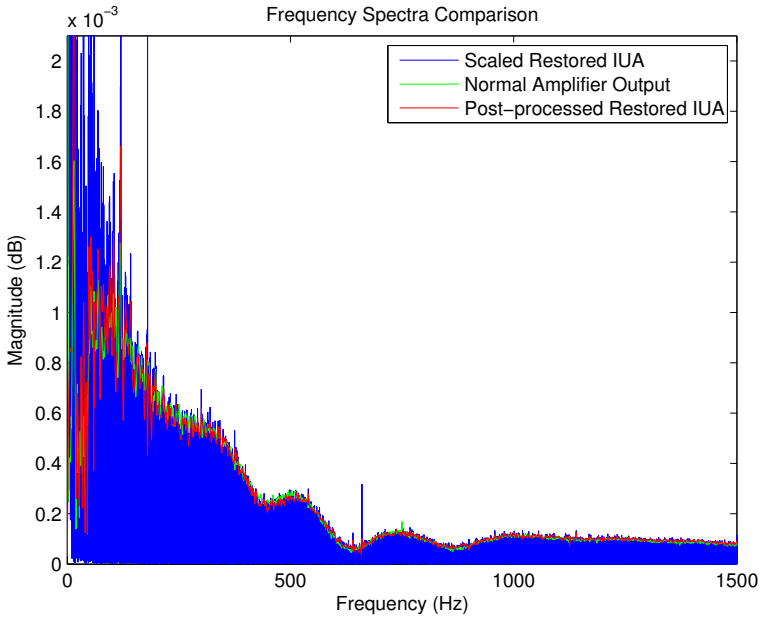

Figure 8.7. The FFT comparisons for the first stimulus-averaged ENG/EMG example.

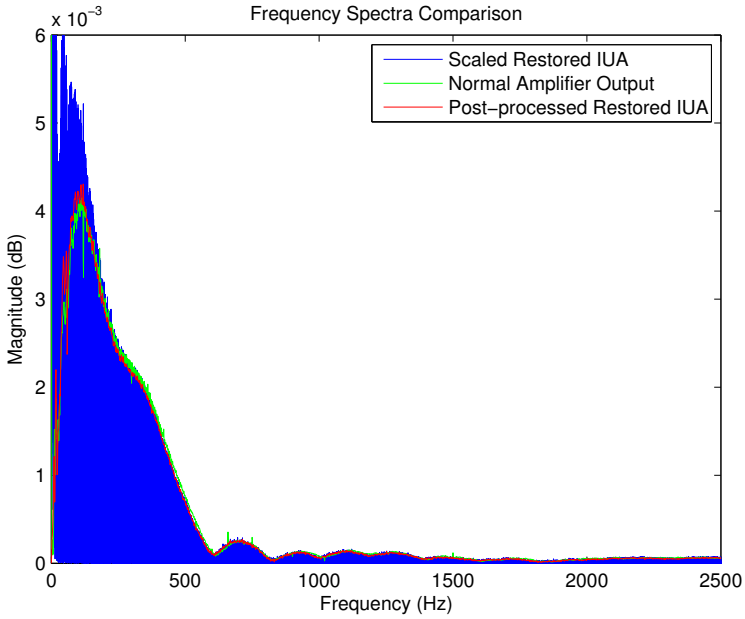

Figure 8.8. The FFT comparisons for the second stimulus-averaged ENG/EMG example.

In both Figure 8.7 and Figure 8.8 it should be noted that the spectral distribution of the normal amplifier and the post-processed, restored IUA have the same general magnitude-frequency characteristics. It should also be noted that the scaled spectral distribution of the restored IUA system data also has the same general magnitude-frequency characteristics except for frequencies around and below 72 Hz, which was the corner frequency of the normal amplifier. The spectral distribution of the restored IUA system clearly shows that the DC content (truncated by the figure windowing) and low-frequency content is retained in the restored IUA system signal. These observations of the spectral distributions confirm that stimulus-driven bioelectric data collected with the IUA system is able to be restored and digitally post-processed to produce waveforms that are similar in both time and frequency characteristics as a specific analog amplifier would.

8.5 Post-verification and Post-validation Discussions

The results from the bench verification tests and the in-vivo validation tests and comparisons give evidence that the IUA is able to capture and accurately restore signals for preservation of the original signal and or digital post-processing. In order to sufficiently demonstrate the IUA system the reported tests for the verification used numerous different waveforms, amplitudes, and offsets and the in-vivo cases with several different types of bioelectric signals that included ECG, compound ENG, and compound EMG. In the case of the verification the analog-to-digital converters used a multiplexed sampling method rather than a simultaneous sampling, which may also be a source of error. In the case of the in-vivo validation, the signals were not collected simultaneously and so there may be more difference between the signals than if they had been collected at the same time. Nevertheless, these demonstrations showed that this IUA architecture may be used as a universal bioamplifier thus eliminating the need for special, custom bioelectric amplifiers while also bringing more power and versatility to digital signal processing. In the analysis of neural signals this power and versatility may have a significant impact where distortion

of the spectral distribution of the units due to typical bioelectric amplifiers could distort the analysis of fiber distance and conduction velocity.

9. SUMMARY AND CONCLUSION

The bioelectric signal is recorded from the body using amplifiers and electrodes. These bioelectric signals are generated in excitable tissues in the body due to the movement of sodium ions into and potassium ions out of the cells. The method of recording these bioelectric signals has led to the development of specialized amplifiers with certain filtering characteristics to match the frequency content of the signal. Thus there are amplifiers for ECG, ENG, EMG, and EEG signals. Yet, these amplifiers fall short when it comes to capturing a wider bandwidth or they rely on additional methods to accomplish that. These amplifiers also distort the signal and cause permanent signal loss due to their filtering characteristics. This permanent signal loss is unfortunate because advances in digital signal processing provide more powerful analysis techniques that may be done off-line or digital filtering options similar to analog filter that may allow for better noise reduction or signal separation. However, signals that have lost large portions of their frequency content may not be fully analyzed using such techniques or may not be analyzed in other ways once they are permanently distorted. Through the development of a new amplifier and new digitial processing scheme, the issues of present amplifier may be overcome. This thesis presented the work of an invertible universal amplifier that was developed around the frequency distribution and magnitude of common bioelectric signals as well as a means to digitally characterize the amplifier and use this characterization to create a way to restore the recorded signal back to the original signal with frequency content from DC to high-frequencies. Specifically, the aims of this work were to (Aim 1) design and implement a new high-impedance input, low-noise, low-bias current amplifier that provided a universal analog frontend for bioelectric recordings with appropriate bioelectric-oriented analog filtering that was easily and accurately estimated and inverted through digital processing, and (Aim 2) leverage the power of digital signal processing to invert the amplifier transfer

function and restore the recorded signal to an accurate representation of the original signal, which may then be digitally processed in ways that minimize distortion of morphological characteristics.

The work to achieve these aims first involved developing the architecture and filtering characteristics of the amplifier. The low-frequency corner was set at 0.32 Hz and the high-frequency corner at 159 Hz. Secondly, a computational script in Matlab was written that initially characterized the system by using collected input and output signals of the amplifier and using the output-error method in Matlab to produce a system transfer function. However, other refinements to the system identification process through an output-error, input-error process, referred to as OEIE, resulted in reductions of percent error on system identification down to below 0.25%. Also, during the tuning process several caveats of the IUA were discussed, such as amplifier usage over time, amplifier saturation, and variable bit weight. In most cases the identified caveats with the IUA system have a solution that can easily be implemented thus reduce the shortcomings of the device and increase the overall useful performance of the IUA system. In this respect, there are also two primary advantages of the IUA as a universal amplifier over the use of creating specialized amplifiers for recording bioelectric signals. The advantage of the IUA system is as discussed in this work: not only can it still be used to appropriately amplify the frequencies in which bioelectric signals operate so that there may be real-time observation and confirmation that the desired signals are being correctly acquired, but it can also be inverted and used to restore the data back to the pre-recorded state once in the computer. This allows the undistorted signal to undergo any desired processing technique. This advantage in signal processing could lead to new technologies or diagnostics not previously possible due to permanent distortion of signal and frequency content by standard amplifiers.

Before the IUA could make the leap to be a tool for more powerful analysis, it had to be fully verified and validated. The verification of the IUA system on the bench showed that waveforms with negative offsets had a percent error of 1.35%±1.00%, waveforms with positive offsets had a percent error of 1.02%±0.89%, and waveforms without any offset had a percent error of 11.79%±5.52%. The errors with the data with no offset was attributed

to errors with the function generator at small amplitudes as well as the external equipment used to separately amplify the original input prior to acquisition and the act of rescaling it within the computer. These percent error results showed that the tuning of the IUA system was very accurate and that the system would be able to accurately record and restore signals. The validation of the IUA system through the recording, restoration, and post-processing of averaged bioelectric signals boasted results of percent error of only 13.66% and 15.63% for ECG data and only 4.85% and 5.94% for ENG/EMG data. These results came from comparing the averaged post-processed restored input of the bioelectric signals to the averaged output of a traditional flat-gain amplifier with a high-pass cut-off at 72 Hz. These signals were not simultaneously recorded and also relied on the estimation of the flat-bandwidth amplifier transfer function characteristics.

Through the development and demonstrated use of the IUA the conclusion is that it is possible to shape the bandwidth amplification characteristics of the amplifier to scale and capture all the signals from DC to approximately 20 kHz through modern data acquisition equipment. Moreover, with the determination of the transfer function of the IUA, the system parameters may be used to exploit the modern advancements of digital signal processing, it is possible to digitally capture the entire signal from the IUA. Then the signal can be rescaled to their original ratios by first digitally determining and inverting the amplifier system. Once the signal is inside the computer, digital filters may be used to filter the original full bandwidth recording, effectively moving the needed filtering from the analog to the digital domain and thus improving the signal to noise ratio of the specific signal. This not only accomplishes the two aims originally set out but it also opens the door to the possibilities of testing and optimizing filtering and signal processing of the original undistorted signal with a myriad of possible digital signal processing tools either on- or off-line.

LIST OF REFERENCES

LIST OF REFERENCES

[1] W. F. Boron and E. L. Boulpaep, *Medical Physiological: A Cellular And Molecular Approach*. Saunders Elsevier, 2009.

[2] J. Malmivuo, *Bioelectromagnetism - Principles and Applications of Bioelectric and Biomagnetic Fields*. Oxford University Press, New York, 1995.

[3] G. E. Loeb and C. Gans, *Electromyography for Experimentalists*. The University of Chicago, 1986.

[4] H. Reuter, "Ion channels in cardiac cell membranes," *Annu. Rev. Physiol.*, vol. 46, pp. 473–84, 1984.

[5] D. DiFrancesco, "Pacemaker mechanisms in cardiac tissue," *Annu. Rev. Physiol.*, vol. 55, pp. 455–72, 1993.

[6] K. Yoshida and J. Strujik, *Neuroprosthetics*, ch. The Theory of Peripheral Nerve Recordings. World Scientific Publishing Co., 2004.

[7] "The axon cns guide: a guide to electrophysiology & biophysics laboratory techniques."

[8] A. Metting van Rijn, A. Peper, and C. Grimbergen, "High-quality recording of bioelectric events: Part 1. interference reduction, theory and practice," *Medical & biological engineering & computing*, vol. 5, pp. 389–97, Sept. 1990.

[9] H. W. Ott, *Noise reduction techniques in electronic systems*. Wiley, 1988.

[10] S. Qiao and K. Yoshida, "Influence of unit distance and conduction velocity on the spectra of extracellular action potentials recorded with intrafascicular electrodes," *Medical Engineering & Physics*, no. 0, 2012.

[11] K. Yoshida and R. Stein, "Development of chronic longitudinal intrafascicular electrodes," in *Engineering in Medicine and Biology Society, 1996. Bridging Disciplines for Biomedicine. Proceedings of the 18th Annual International Conference of the IEEE*, vol. 1, pp. 373–374, Oct. 1996.

[12] A. Metting van Rijn, A. Peper, and C. Grimbergen, "High-quality recording of bioelectric events: Part 2 low-noise, low-power multichannel amplifier design," *Medical & biological engineering & computing*, vol. 29, pp. 433–440, 1991.

[13] F. Censi, G. Calcagnini, P. Bartolini, E. Cervi, I. Diemberger, I. Corazza, and G. Boriani, "Effect of ecg filtering on time domain analysis of the p-wave," in *Computers in Cardiology, 2008*, pp. 1077–1080, Sept. 2008.

[14] S. Qiao, M. Torkamani-Azar, P. Salama, and K. Yoshida, "Stationary wavelet transform and higher order statistical analyses of intrafascicular nerve recordings," *Journal of Neural Engineering*, vol. 9, no. 5, p. 056014, 2012.

[15] G. Urban, J. Ganglberger, F. Olcaytug, F. Kohl, R. Schallauer, M. Trimmel, H. Schmid, and O. Prohaska, "Development of a multiple thin-film semimicro dc-probe for intracerebral recordings (during surgery)," *Biomedical Engineering, IEEE Transactions on*, vol. 37, pp. 913–918, Oct. 1990.

[16] I. Triantis, A. Demosthenous, M. Rahal, H. Hong, and R. Bayford, "A multi-frequency bioimpedance measurement asic for electrical impedance tomography," in *ESSCIRC (ESSCIRC), 2011 Proceedings of the*, pp. 331–334, Sept. 2011.

[17] A. Garrett, D. Heibert, and B. Lithgow, "Electrovestibulography: The "dc" potential used to separate meniere's disease and benign paroxysmal positional vertigo," in *Engineering in Medicine and Biology Society, 2007. EMBS 2007. 29th Annual International Conference of the IEEE*, pp. 2381–2384, Aug. 2007.

[18] Y. Moghe and T. Lehmann, "A novel safety system concept and implementation for implantable stimulators: A universal dc tissue leakage current detector," in *Circuits and Systems, 2008. ISCAS 2008. IEEE International Symposium on*, pp. 2498–2501, May 2008.

[19] P. Laguna, R. Jane, O. Meste, P. Poon, P. Caminal, H. Rix, and N. Thakor, "Adaptive filter for event-related bioelectric signals using an impulse correlated reference input: comparison with signal averaging techniques," *Biomedical Engineering, IEEE Transactions on*, vol. 39, pp. 1032–1044, Oct. 1992.

[20] M. Malboubi, F. Razzazi, and S. Aliyari, "Elimination of power line noise from emg signals using an efficient adaptive laguerre filter," in *Signals and Electronic Systems (ICSES), 2010 International Conference on*, pp. 49–52, Sept. 2010.

[21] S. Hu, M. Stead, and G. Worrell, "Removal of scalp reference signal and line noise for intracranial eegs," in *Networking, Sensing and Control, 2008. ICNSC 2008. IEEE International Conference on*, pp. 1486–1491, April 2008.

[22] C. Grimbergen, A. MettingVanRijn, A. Kuiper, R. Honsbeek, K. Speijer, and A. Peper, "Dc rejection and deblocking in multichannel bioelectric recordings," in *Engineering in Medicine and Biology Society, 1995., IEEE 17th Annual Conference*, vol. 2, pp. 1665–1666, Sept. 1995.

[23] M. Chae, J. Kim, and W. Liu, "Fully-differential self-biased bio-potential amplifier," *Electronics Letters*, vol. 44, pp. 1390–1391, 20 2008.

[24] C. Sevcencu, C. P. Pennisi, K. Yoshida, and H. Gregersen, "Simultaneous monitoring of cellular depolarization and contraction: a new method to investigate excitability and contractility in isolated smooth muscle cells," *Am J Physiol Gastrointest Liver Physiol*, vol. 294, pp. G648–G654, 2008.

[25] T. Boretius, K. Yoshida, J. Badia, K. Harreby, A. Kundu, X. Navarro, W. Jensen, and T. Stieglitz, "A transverse intrafascicular multichannel electrode (time) to treat phantom limb pain; towards human clinical trials," in *Biomedical Robotics and Biomechatronics (BioRob), 2012 4th IEEE RAS EMBS International Conference on*, pp. 282–287, June 2012.

[26] L. Citi, J. Carpaneto, K. Yoshida, K. Hoffmann, K. Koch, P. Dario, and S. Micera, "Characterization of tflife neural response for the control of a cybernetic hand," in *Biomedical Robotics and Biomechatronics, 2006. BioRob 2006. The First IEEE/RAS-EMBS International Conference on*, pp. 477–482, Feb. 2006.

[27] X. Navarro, N. Lago, M. Vivo, K. Yoshida, K. Koch, W. Poppendieck, and S. Micera, "Neurobiological evaluation of thin-film longitudinal intrafascicular electrodes as a peripheral nerve interface," in *Rehabilitation Robotics, 2007. ICORR 2007. IEEE 10th International Conference on*, pp. 643–649, June 2007.

[28] B. Lathi, *Linear Systems and Signals*. Oxford University Press, 2 ed., 2005.

[29] E. Tohme, *Initialization of Output Error Identification Algorithms*. PhD thesis, Laboratoire dAutomatique et dInformatique Industrielle of Poitiers, 2008.

[30] MATLAB, *version 7.9.0 (R2009b)*. Natick, Massachusetts: The MathWorks Inc., 2009.

[31] Burr-Brown Corporation, *High Speed FET-Input INSTRUMENTATION AMPLIFIER*, 1992.

[32] Texas Instruments, Post Office Box 655303 Dallas, TX 75265, *OP27A, OP27C, OP27E, OP27G, OP37A, OP37C, OP37E, OP37G LOW-NOISE HIGH-SPEED PRECISION OPERATIONAL AMPLIFIERS*, 1994.

APPENDICES

A. CALIBRATION AND TUNING CODE

```
function [fn,bbd,aad,gain,C,R2,R,sys]=calibrate(channels,...
    ExtAmpGain,method,HPF,¬)
format long
%For analysis and calibration of the Variable Gain Amplifier. The ...
    insig
%signal should be a 1 Hz square wave and the output amplitude ...
    should not
%be clipped.  The suggested acquition time length is 10 second. ...
    The
%data for IFDA calibration was sampled at 48 kHz.
%
%The script expects that the calibration data, both insig and ...
    output will
%be within a single .mat file.  All calibration data files should ...
    have
%standard names and should end with a three digit code ...
    representing the
%channel number (i.e. 001,002,etc). The data should be in a ...
    variable
%called dath001. In this variable the insig should be the first ...
    column and
%the output should be the second column.
%
%The parameters that are passed to this function are:
%(1) the channel number: this can be either 1-12 or the string '...
    all'.
%(2) the value of additional amplification used on the input ...
    signal
%before acquisition.
%(3) the preferred method for determing the amplifier
%coefficients: this is either (i) 'rc' for determining the ...
    transfer function
%based on estimates of the resistor and capacitor in the circuit ...
    or (ii)
%'oe' for taking the output of just the ouput-error method.
%(4) the data variable that the function should use if already ...
    loaded in
%the base workspace
%
%The variable ChannelCoeff stores coefficients of the inverted ...
    transfer
```

```
%function for each channel.  Each row represents a channel and the...
    columns
%contain the coefficients b1, b2, a1, and a2 for creating a ...
   transfer
%function.

clc; close all;
number=channels; rms=[];

%% Initial Setup
for m=1:1
    if channels~='all'
    if nargin < 5
        [fn,pn]=uigetfile('*.mat','Select the calibration data ...
           file');
        if isequal(fn,0)||isequal(pn,0)
            return;
        else
            clc; %close all;
            cd(pn);
            load(fn);
        end
        channels=1; %do not process all 12 channels; only process ...
           one channel
    end
    else
    if nargin < 5
        [fn,pn]=uigetfile('*.mat','Select the calibration data ...
           file for Channel 01');
        prefix=fn(1:end-6);
        if isequal(fn,0)||isequal(pn,0)
            return;
        else
            clc; %close all;
            cd(pn);
            load(fn);
        end
        channels=12; %process all 12 channels at once
    end
    end

    if method=='oe'
        method='y';
        gain=1;
    else
        method='n';
    end
end

%% Main Section
n=1; AmpCoeff=[];

```

```
74 while n≤channels;
75     close all;
76
77     %% Setup save names, etc.
78     for m=1:1
79         if channels==12
80             if n<10
81                 fn=[prefix '0' num2str(n) '.mat'];
82                 savename=['ifda_channel0' num2str(n)];
83                 zipname=['ifda_channel0' num2str(n) '_cal'];
84             else
85                 fn=[prefix num2str(n) '.mat'];
86                 savename=['ifda_channel' num2str(n)];
87                 zipname=['ifda_channel' num2str(n) '_cal'];
88             end
89             load(fn);
90             fprintf('filename: %s\nsavename: %s\n\n',fn,savename);
91         else
92             if number < 10
93                 savename=['ifda_channel0' num2str(n)];
94                 zipname=['ifda_channel0' num2str(n) '_cal'];
95             else
96                 savename=['ifda_channel' num2str(n)];
97                 zipname=['ifda_channel' num2str(n) '_cal'];
98             end
99         end
100    end
101
102    %% Load sampling rate and data;
103    for m=1:1
104        div=1;
105        sr=DaqSettings(3);
106        insig=((dath001(1:round(length(dath001)/div),1))/...
               ExtAmpGain); output=dath001(1:round(length(dath001)/div...
               ),2);
107
108        %% method 3: DC correction using highpass filtering
109        if strcmp(HPF,'y')
110            [bh,ah]=butter(1,0.15/(sr/2),'high');
111            output=filter(bh,ah,output);
112            insig=filter(bh,ah,insig);
113        end
114    end
115
116    %% Generate the noiseless input signal
117
118    for m=1:1
119        %Determine the upper and lower bounds of the insig signal.
120        uind=find(insig≥mean(insig));
121        lind=find(insig<mean(insig));
122        utmp=zeros(length(uind),1);
123        ltmp=zeros(length(lind),1);
```

```
124
125         for k=1:length(uind);
126             utmp(k)=insig(uind(k));
127         end
128         um=mean(utmp);
129
130         for k=1:length(lind);
131             ltmp(k)=insig(lind(k));
132         end
133         lm=mean(ltmp);
134
135         %Synthesize noise-free square insig waveform
136         nonoise=insig;
137         nonoise(nonoise≥mean(insig))=um;
138         nonoise(nonoise<mean(insig))=lm;
139     end
140     nonoise_max=max(nonoise);
141     nonoise_min=min(nonoise);
142     nonoise_adjust=(nonoise_max+nonoise_min)/2;
143     nonoise(nonoise≥mean(nonoise))=nonoise_max-nonoise_adjust;
144     nonoise(nonoise<mean(nonoise))=nonoise_min-nonoise_adjust;
145     for m=1:1
146         %Determine the upper and lower bounds of the insig signal.
147         uind=find(insig≥mean(insig));
148         lind=find(insig<mean(insig));
149         utmp=zeros(length(uind),1);
150         ltmp=zeros(length(lind),1);
151
152         for k=1:length(uind);
153             utmp(k)=insig(uind(k));
154         end
155         um=mean(utmp);
156
157         for k=1:length(lind);
158             ltmp(k)=insig(lind(k));
159         end
160         lm=mean(ltmp);
161
162         %Synthesize noise-free square insig waveform
163         nonoise=insig;
164         nonoise(nonoise≥mean(insig))=um;
165         nonoise(nonoise<mean(insig))=lm;
166     end
167
168     nonoise=filter(bh,ah,nonoise(1:length(insig)));
169     oe_input=nonoise;
170     output=(output(1:length(insig)));
171
172
173     %% Determine the original transfer function coefficients
174     %Paramater estimataton using SID toolbox.
175     adat=iddata(output,oe_input,1/sr);
```

```
176     for l=1:1
177         %Output error method
178         Md=oe(adat,[2,1,0],'Focus','Stability','Init','Zero');
179         ad=Md.f;
180         bd=Md.b;
181 
182         %Continuous time idpoly model
183         Mc=d2c(Md);
184         bc=Mc.b;
185         ac=Mc.f;
186 
187         k1=bc(1)/ac(2);
188         k2=ac(1)/ac(2);
189 
190         % original system
191         CO=10e-6; R1O=100; R2O=50e3;
192         originalsys=tf(2.*[CO*(R1O+R2O) 1],[CO*R1O 1]);
193         [high_mag]=bode(originalsys,{10^4.1,10^5.2});
194         high_gain=max(high_mag);
195         [low_mag]=bode(originalsys,{10^-10,10^-9});
196         low_gain=min(low_mag);
197 
198         if method=='n'
199             R=100;
200             G=2;
201             C=k2/R;
202             R2=(k1-k2)/(2*C);
203 
204             b=G.*[C*(R+R2) 1]; a=[C*R 1];
205             sys0=tf(b,a); sys=c2d(sys0,1/sr);
206             [low_mag]=bode(sys,{10^-10,10^-9});
207             gain=min(low_mag);
208             [bbd,aad]=tfdata(sys,'v');
209 
210         else
211             bbd=bd; aad=ad; G=2; C=CO; R2=R2O; R=R1O;
212             sys=tf(bbd,aad,1/sr);
213             [mag]=bode(sys,{10^-10,10^-9});
214             gain=min(mag);
215         end
216     end
217 
218     %% Invert the ouput and adjust the gain, op-amp resistor, and ...
        capacitor to improve the match
219     if method == 'n'
220         for l=1:100
221              out_est=filter(bbd,aad,oe_input);
222              [high_mag]=bode(sys,{10^4.1,10^5.2});
223              high_gain2=max(high_mag);
224              high_gain_adjust=high_gain/high_gain2;
225              gain_adjust=high_gain_adjust;
226 
```

```
227                 G=G*gain_adjust;
228                 C=k1/(G*(R2+R));
229                 R=(k1-(R2*G*C))/(G*C);
230                 R2=(k1-k2)/(2*C);
231
232              b=G.*[C*(R+R2) 1]; a=[C*R 1];
233              sys0=tf(b,a); sys=c2d(sys0,1/sr);
234              [mag]=bode(sys,{10^-10,10^-9});
235              gain=min(mag);
236              [bbd,aad]=tfdata(sys,'v');
237          end
238
239          loop=1; loop4=1; prev_rms_volt4=1; curr_rms_volt=1; ...
                tripped=0; prev_rms_volt=[]; error=[]; prev_C=[];
240
241              while curr_rms_volt ≥ 1e-5  %0.00012946
242                  C=C+1e-10; R2=50e3;
243                  b=G.*[C*(R+R2) 1]; a=[C*R 1];
244                  sys0=tf(b,a); sys=c2d(sys0,1/sr);
245                  [mag]=bode(sys,{10^-10,10^-9});
246                  gain=min(mag);
247                  [bbd,aad]=tfdata(sys,'v');
248
249                   %% Invert the output and the input
250                  in_est=filter(aad,bbd,output);
251                  error=[error (insig(1.98720e+05:end))-(in_est(1...
                        .98720e+05:end))];
252                  prev_rms_volt=[prev_rms_volt curr_rms_volt];
253                  prev_C = [prev_C C];
254                  curr_rms_volt=norm(error(loop4))/sqrt(length(error...
                        (loop4)));
255                  loop4 = loop4 + 1;
256              end
257               prev_rms_volt=[prev_rms_volt curr_rms_volt];
258               prev_C = [prev_C C];
259               min_rms_volt=min(prev_rms_volt);
260               ind_rms_volt=find(prev_rms_volt==min(prev_rms_volt))...
                     -1;
261               C=prev_C(ind_rms_volt);
262               error=error(ind_rms_volt)
263               b=G.*[C*(R+R2) 1]; a=[C*R 1];
264               sys0=tf(b,a); sys=c2d(sys0,1/sr);
265               [mag]=bode(sys,{10^-10,10^-9});
266               gain=min(mag);
267               [bbd,aad]=tfdata(sys,'v');
268               in_est=filter(aad,bbd,output);
269               out_est=filter(bbd,aad,oe_input);
270      else
271           %% Invert the output and the input
272          in_est=filter(aad,bbd,output);
273          error=(insig(1.98720e+05:end))-(in_est(1.98720e+05:end));
274          out_est=filter(bbd,aad,oe_input);
```

```
275     end
276     curr_rms_volt=norm(error)/sqrt(length(error));
277     rms_input = norm(insig(1.98720e+05:end))/sqrt(length(insig(1...
            .98720e+05:end)));
278     rms_error = 1-(rms_input-curr_rms_volt)/rms_input;
279     rms=[rms; curr_rms_volt rms_input rms_error];
280
281     time=((1:length(insig))/sr)';
282     sys=tf(bbd,aad,1/sr);
283     %% Generate the first three plots
284     for l=1:1
285         h1=figure;
286         hold off; plot(time,output,'r'); hold on; plot(time,...
                out_est);
287         legend('Amplifier Output','Calc. Estimate','Location','...
                Northeast');
288         xlabel('Time (sec)');
289         ylabel('Voltage (V)');
290
291         h2=figure;
292         hold off; plot(time(4.07376e5:4.0776e5),output(4.07376e5:4...
                .0776e5),'r'); hold on; plot(time(4.07376e5:4.0776e5),...
                out_est(4.07376e5:4.0776e5));
293         legend('Amplifier Output','Calc. Estimate','Location','...
                Northeast');
294         xlabel('Time (sec)');
295         ylabel('Voltage (V)');
296         xlim([time(4.07376e5) time(4.0776e5)]);
297
298         h3=figure;
299         hold off; plot(time,insig,'k'); hold on; plot(time,in_est)...
                ;
300         hold on; plot(time,nonoise,'r');
301         legend('Original Sig.','Calc. Estimate','Synth. Noiseless'...
                ,'Location','Southeast');
302         xlabel('Time (sec)');
303         ylabel('Voltage (V)');
304
305         h4=figure;
306         hold off; plot(time(4.056e5:4.344e5),insig(4.056e5:4.344e5...
                ),'k'); hold on; plot(time(4.056e5:4.344e5),in_est(4...
                .056e5:4.344e5));
307         hold on; plot(time(4.056e5:4.344e5),nonoise(4.056e5:4...
                .344e5),'r');
308         legend('Original Sig.','Calc. Estimate','Synth. Noiseless'...
                ,'Location','Southeast');
309         xlabel('Time (sec)');
310         ylabel('Voltage (V)');
311         xlim([time(4.056e5) time(4.344e5)]);
312
313         h5=figure;
314         ax=axes;
```

```
315         P=bodeoptions;
316         P.FreqUnits='Hz';
317         P.Title.FontSize=12;
318         P.XLabel.FontSize=12;
319         P.YLabel.FontSize=12;
320         P.TickLabel.FontSize=12;
321         P.FreqScale = 'log';
322         P.Grid='on';
323 
324         bode(originalsys,'ko-',P);
325         hold on;
326         bode(1/originalsys,'k*-',P);
327         bode(sys,P);
328         bode(1/sys,'r',P);
329         title('Transfer Function')
330         linkaxes(ax,'x');
331 
332     end
333 
334     %% Store the coefficients for each channel
335     for m=1:1
336         save(savename,'bbd','aad','gain','C','R2','R');
337          if number=='all'
338             AmpCoeff=[AmpCoeff; aad, bbd, gain, G, C, R2, R;];
339         else
340             if size(AmpCoeff,1)≥1
341                 AmpCoeff(str2num(number),:)=[aad, bbd, gain, G, C,...
                        R2, R];
342             else
343                 AmpCoeff=[AmpCoeff; aad, bbd, gain, G, C, R2, R;];
344             end
345          end
346     end
347 
348     %% Save all five plots
349     for m=1:1
350         hgsave(h1,'Outputs');
351         hgsave(h2,'Zoomed Outputs');
352         hgsave(h3,'Inputs');
353         hgsave(h4,'Zoomed Inputs');
354         hgsave(h5,'Transfer Functions');
355         zip(zipname,{'Outputs.fig','Zoomed Outputs.fig','...
                Inputs.fig','Zoomed Inputs.fig','Transfer Functions.fig...
                ',...
356              [savename '.mat']});
357         delete('Outputs.fig','Zoomed Outputs.fig','Inputs.fig','...
                Zoomed Inputs.fig','Transfer Functions.fig',...
358              [savename '.mat']);
359     end
360 
361     n=n+1;
362 end
```

```
363
364 %% Ending Section
365 save('ChannelCoeff-noHPF','AmpCoeff');
366 if method =='n'
367     xlswrite('rc_rms_calibrate_20121202.csv',rms);
368 else
369     xlswrite('oe_rms_calibrate_20121202.csv',rms);
370 end
371 cd '/home/kmauser/Documents/2009_IUPUI-VarGainAmp/05_Software/...
      Calibration/Current Configuration/'
372 end
```

B. RESTORATION CODE

```
function [time,invdata,data,sr,fn,pn,wd] = invert(channel,...
    ExtAmpGain,wd,plots,closeplots,saveplots,data)
% invert.m outputs a time array, an inverted data array (invdata),
% the original data (data), the sampling rate (sr), the file name ...
    analyzed
% (fn), the path name for that file (pn), and the working ...
    directory (wd).

% invert.m requires as the (1) first input the channel number to ...
    invert.
% You may type an integer value from 1 to 12 to invert the ...
    individual
% channel specified or type the string 'all' to invert all twelve ...
    channels
% in one run of the function.

% IMPORTANT: The remaining inputs you must specify in the order ...
    described.
% You can specify as few parameters as you wish, but any preceding
% parameters must be provided. For example, if plots should be ...
    saved, then
% you will specify 'y' for saveplots but you must specify all the
% preceding parameters. This is were the function is dumb with it'...
    s
% inputs. Failure to do this will most likely result in errors. If...
    times
% allows I will make the function smarter.

% The (2) second input is the value of external amplification (...
    ExtAmpGain)
% used. If additional amplification was used it should be recorded...
    in the
% experimental notes. The (3) third input is the working directory...
    from
% which this script is run. The (4) fourth input is for specifying...
    whether
% or not you want to display plots of the inverted data.  This is ...
    a string
% parameter that accepts either 'y' or 'n'. The (5) fift input is ...
    for
% specifying whether or not you want to save the generated plots.
```

```
% It is also a 'y' or 'n' parameter.  If you opt to not generate ...
    plots,
% then this input defaults to 'n' even if you put 'y'. The (6) ...
    sixth input
% is the data variable.  If you have previously run readBin or ...
    already
% have data loaded in the workspace that needs to be inverted you ...
    can
% give the variable here and not have to run readBin again.  You ...
    MUST
% ensure that the variable name for your data in the workspace is ...
    "data".

if closeplots=='y'
    close all;
end

    if nargin == 7
        fs=evalin('base','sr');
        data=evalin('base','data');
        fn=evalin('base','fn');
        pn=evalin('base','pn');
    elseif nargin == 6
        readBin
    elseif nargin == 5
        saveplots='n'; readBin;
    elseif nargin == 4
        closeplots='y'; saveplots='n'; readBin;
    elseif nargin == 2
        wd=pwd; plots='n'; saveplots='n'; readBin;
    elseif nargin == 1
        ExtAmpGain=1; wd=pwd; plots='n'; saveplots='n'; readBin;
    elseif nargin == 0
        channel='all'; ExtAmpGain=1; wd=pwd; plots='n'; saveplots=...
            'n'; readBin;
    end

    % Must change the directory again after calling readBin
    cd(wd);

    if channel ~= 'all';
        channels=channel;
    else
        channels='all';
    end

    load('ChannelCoeff.mat');
    cd(wd);

    sr=fs;

    if channels=='all'
```

```
71          n=1;
72          m=min(size(data));
73          if m>12, m=12; end
74      else
75          n=channel;
76          m=n;
77      end
78
79      try
80          tmp=min(size(invdata));
81      catch
82          tmp=channels;
83          invdata=[];
84          data_v2=data';
85          for k=n:m
86              output=data_v2(:,k);
87              output=output/ExtAmpGain;
88
89              aad=[AmpCoeff(k,1) AmpCoeff(k,2)];
90              bbd=[AmpCoeff(k,3) AmpCoeff(k,4)];
91              in_est_tmp=filter(aad,bbd,output);
92              invdata = [invdata; in_est_tmp'];
93          end
94          time=(1:length(invdata))/sr;
95      end
96
97
98  if plots=='y'
99      if channels~='all'
100         h0=figure;
101
102         if tmp==12
103             plot(time,invdata(channels,:));
104         else
105             plot(time,invdata);
106         end
107         title(['Inverted from ' fn]);
108         xlabel('Time (sec)');
109         ylabel('Voltage (V)');
110         legend(['Channel ' num2str(channels)]);
111     else
112         h1=figure(1);
113         ax(1)=subplot(2,1,1);
114         plot(time,invdata([1:7],:),'Parent',ax(1));
115         legend('Channel 1','Channel 2', 'Channel 3', ...
116             'Channel 4','Channel 5', 'Channel 6', ...
117             'Channel 7');
118         ax(2)=subplot(2,1,2);
119         plot(time,invdata([8:12],:),'Parent',ax(2));
120         legend('Channel 8', 'Channel 9', ...
121             'Channel 10','Channel 11', 'Channel 12');
122         linkaxes(ax,'x');
```

```
123
124         h2=figure(2); col=2;
125         for k=n:m
126             ak(k)=subplot(6,2,k);
127             plot(time,invdata(k,:),'Parent',ak(k));
128             title(['Channel ' num2str(k)]);
129         end
130         linkaxes(ak,'x');
131         cd(pn)
132         if saveplots=='y'
133             hgsave(h1,[fn '_AllChannels.fig']);
134             hgsave(h2,[fn '_Subplots.fig']);
135             print('-f1','-dpsc',[fn '.ps']);
136             print('-f2','-dpsc','-append',[fn '.ps']);
137         end
138         cd(wd);
139     end
140 end
141
142 % The lines below are here so that I could change directories and ...
      save the
143 % output as a MAT file.  Uncomment and change the directory as ...
      apporpriate
144 % if you want to save all the output.
145 % Warning: it takes a long time to do this.
146 %     cd '/media/Bioellab/00_Lab/03_Projects/2010_IUPUI-Shield/02...
      _Experiments/110405 - rabbit/Inverted Data'
147 %     cd(pn)
148 %     save([fn(1:end-4) '.mat'],'time','wd','pn','invdata','fs','...
      fn','data');
149 %     cd(wd);
150 end
```